Experimental Study on Effect of hydrophobicity on Polymer Conformations, Rheology and Flow in Porous Media

by

Viralkumar Patel

A thesis submitted in partial fulfillment of the requirements for the degree of

Doctor of Philosophy

in

Petroleum Engineering

Department of Civil and Environmental Engineering
University of Alberta

Abstract

Typically, polymer screening for enhanced oil recovery operations is done based on viscosity, viscosity dependent molecular weight correlations, and concentration. However, direct measurement of molecular weight and Molecular Weight Distribution (MWD) along with the other conformational parameters can provide better insights into the molecular characteristics of polymer molecules. In this work, we emphasize the need for incorporating MWD, radius distributions, and conformational characteristics of polymer solutions over the conventional screening criteria or enhance oil recovery operations. In particular, the hydrophobicity and concentration-dependent polymer conformations affect the polymer network formations at the molecular level in the aqueous and salinity environments is studied, and how they relate to polymer flow in the porous media. Due to limitations of gel permeable chromatography, direct measurement of polymer molecular weight, MWD, radius distributions, and conformations are measured using fluid flow fractionation (FFF) method. The effect of hydrophobicity on the rheological properties, shear rheology, and extensional rheology is also explained. Furthermore, the flow behavior of the polymer solutions in the consolidated and unconsolidated porous media in terms of Resistance Factor (RF) and Residual Resistance Factor (RRF) is justified by using the viscoelastic properties and polymer conformation.

The results show that the average molecular weight increased with polymer concentration and hydrophobicity in both, aqueous and saline environments. However, narrow MWDs were observed for the polymer solutions with brine salinity. The average radius increased with the polymer concentration. However, these values decreased with hydrophobicity in aqueous media and increased with hydrophobicity in a saline environment due to the charge screening effect. The domination of intermolecular networks only seems to occur above the critical aggregation

concentration. The polymer conformations changed from randomly coiled Hookean to the compacted sphere Non-Hookean as the hydrophobicity, concentration, and salinity increased. This corresponded to the higher resistance and residual resistance factors. The MWDs along with different types of confirmations were not able to differentiate the shear rheological behavior at the identical polymer concentration. However, the higher apparent extensional viscosity justifies the formation of an intermolecular network eventually responsible for forming Hookean randomly coiled polymer conformations.

The polymer conformational properties measured using FFF and apparent viscosity profiles are used to explain how the hydrophobicity of polymer affects the polymer resistance and retention in the porous media, especially when shear and extensional rheology fails to explain the flow behavior in the porous media. The results showed that higher hydrophobic polymer was able to form non-Hookean rigid spherical structures that increase the hydrodynamic trapping. Whereas, at the low hydrophobicity, the formation of soft randomly coiled polymer conformations offers ease of injectivity even at the higher injection rates. Additionally, the proposed interaction mechanism of the coiled conformations on the rock surface is an important criterion for the prediction of polymer retention in the porous media. At the higher polymer concentration, the polymer retention in the porous media increased due to the domination of gel retention in the porous media. Combining concentration and hydrophobicity-dependent structure formations allow for optimizing the operation parameters like flow rate, pre-shearing, and filtration conditions.

Preface

The research presented in this dissertation benefited greatly from the oversight of Dr. Japan Trivedi, who contributed to the formulation of the research concept and provided valuable input during the review and editing of this document's initial draft.

A version of Chapter 2 has been published as "Patel, V, Dalsania, Y, Azad, MS, Sharma, T, Trivedi, J. Characterization of co- and post-hydrolyzed polyacrylamide molecular weight and radius distribution under saline environment. J Appl Polym Sci. 2021; 138:e50616. https://doi.org/10.1002/app.50616". I was responsible for conceptualization and characterizing polymer solutions for rheology, infrared spectroscopy, and fluid flow fractionation. Yogesh Dalsania has developed and validated the characterization technique to determine molecular weight and radius distributions by using the fluid flow fractionation principle. I wrote the manuscript and addressed the reviewer's queries. Dr. Japan Trivedi was responsible for the supervision and progressive feedback.

A version of Chapter 3 has been published as "Patel, V., Trivedi, J. & Sharma, T. Influence of hydrophobic association in the aqueous media on the rheology and polymer conformation of associative polymers. Polym. Bull. (2022). https://doi.org/10.1007/s00289-022-04484-9". I was responsible for performing all experiments associated to support the scope of the research, writing the manuscript, and addressing the reviewer's questions. Dr. Japan Trivedi and Dr. Tushar Sharma supervised the research.

A version of Chapter 4 has been accepted as "Patel, V., Chissonde, S. & Trivedi, J. Effect of Polymer Conformations on Rheology and the Flow of Polymer through Consolidated Porous Media. Geoenergy Science and Engineering" I was responsible for conceptualization and

characterizing polymer solutions for rheology, and fluid flow fractionation for determination of molecular weight and radius distributions. Chissonde Salomao and I performed the core flood experiments. The experimental results were interpreted by myself to establish the bulk properties correlations with the polymer injectivity experiments. Dr. Japan Trivedi was responsible for the supervision and progressive feedback.

Lord Swaminarayan

“મારી મરજી વિના રે, કોઈ થી તરણું ના તોડાય”

(Without my wish, not a blade of grass can be broken)

Acknowledgments

I would like to express my heartfelt gratitude to Lord Swaminarayan and Guru Hari Pramukh Swami Maharaj, who has been the source of all wisdom and knowledge throughout this academic journey. This thesis is not just the culmination of my efforts at the keyboard but also a significant milestone in over four years of work at the University of Alberta.

First and foremost, I would like to express my sincere appreciation and gratitude to my supervisor, Dr. Japan Trivedi, for their unwavering support and guidance throughout my Ph.D. journey. His extensive knowledge, expertise, and invaluable feedback have been instrumental in shaping my research and have helped me to achieve my goals. I am also grateful for his encouragement and belief in my abilities, which have motivated me to push beyond my limits and deliver the best possible work.

I would like to extend my heartfelt gratitude to my parents, Jagdishbhai (Papa) and Chhayaben (Mummy), for their constant support and guidance throughout my academic journey. Their belief in my abilities and unwavering support have kept me motivated and inspired, and I am forever grateful for their sacrifices and contributions to my success. This thesis is a testament to their love and support, and I am honored to have them in my life.

I must extend my heartfelt gratitude to my wife (Dixita) for her unwavering support and understanding as I navigated the rocky terrain of a Ph.D. program. And to my kids (Nirva, Divyata, and Parv), who were often collateral damage in my quest for academic glory - I promise to make it up to you with ice cream, pizza, and extra screen time. Their patience and understanding have been truly remarkable, and I promise to make it up to them with lots of quality time and vacations now that this thesis is behind me.

Contents

Chapter 1: Introduction and literature review 1
1.1 Introduction to oil recovery methods 1
1.2 Mechanisms 3
1.3 Polymer EOR 6
1.4 EOR polymers 13
1.4.1 Introduction to hydrolyzed polyacrylamide 13
1.4.2 Associative polymers for EOR 15
1.4.3 Effect of Mw of polymer on the solution viscosity 18
1.4.4 Limitations of solution viscosity on explaining flow behavior in the porous media 21
1.5 Mw, MWD, radius distribution and conformational characterization 22
1.5.1 Gel permeation chromatography 22
1.5.2 AF4-FFF characterization technique 23
1.6 Determining the polymer solution viscosity 30
1.6.1 Shear viscosity 30
1.6.2 Extensional viscosity 31
1.7 Problem Statement 32
1.8 Objectives of our research 34
Chapter 2: Characterization of Co and Post Hydrolyzed PAM molecular weight and radius distribution under saline environment 36
2.1 Abstract 36
2.2 Introduction 36
2.3 Materials and Methods 41
2.3.1 Chemicals 41
2.3.2 Polymer Solution Preparation 42
2.3.3 Measurements 43
2.4 Results and Discussion 46
2.4.1 AF4 measurements to determine structural changes in HPAM molecules 46
2.4.2 FTIR measurements to understand molecular interactions 59
2.4.3 Effect of structural changes on extensional viscosity measurements for HPAM saline solutions 60

2.5 Conclusion 65

Chapter 3: Influence of Hydrophobic Association in the aqueous media on the Rheology and Polymer Conformation of Associative Polymers 66

3.1 Abstract 66

3.2 Introduction 67

3.3 Materials and Methods 70

3.3.1 Reagents 70

3.3.2 Sample Preparation 71

3.3.3 Rheology Experiments 72

3.3.4 AF4-FFF Experiments 73

3.4 Results and Discussion 75

3.4.1 Rheological characterization 75

3.4.2 AF4-FFF characterization 83

3.5 Conclusions 90

Chapter 4: Effect of Polymer Conformations on Rheology and the Flow of Polymer through the Porous Media 92

4.1 Abstract 92

4.2 Introduction 92

4.3 Materials and Methods 95

4.3.1 Reagents 95

4.3.2 Sample Preparation 95

4.3.3 Rheology Experiments 96

4.3.4 AF4-FFF Experiments 98

4.3.5 Polymer injectivity Experiments 100

4.4 Results and Discussion 102

4.4.1 Rheological characterization 102

4.4.2 AF4-FFF characterization 110

4.4.3 Polymer Core floods with the consolidated cores 119

4.4.4 Molecular weight and radius distributions overcoming the limitations of rheology by explaining polymer flow in unconsolidated porous media 125

4.4.5 Application of AF4-FFF technique for field application 129

4.5 Conclusions 135

Chapter 5: Conclusion, Limitations, and recommendations 136
5.1 Conclusions 136
5.2 Limitations 138
5.3 Recommendations 139
References 140

List of Tables

Table 1.1 Successful field application of polymer EOR 7

Table 2.1. Specification of Polymers from SNF 42

Table 2.2 Average molar mass and radius of gyration for 2000 ppm post-hydrolyzed PAM under different salinity environment 46

Table 2.3 Average molar mass and radius of gyration for 2000 ppm co-hydrolyzed PAM under different salinity environment 52

Table 2.4 Relaxation time for 2000 ppm polymer solutions with varying salinity conditions 61

Table 3.1: Specifications of polymers from SNF Floerger 71

Table 3.2: Experimental break-up time, relaxation time, and maximum apparent extensional viscosity of polymer samples 78

Table 3.3: Effect of polymer concentration and hydrophobicity on the average molar mass and radius of gyration 84

Table 4.1: Specifications of polymers from SNF 96

Table 4.2: maximum apparent extensional viscosity, experimental break-up time, and relaxation time of polymer samples 105

Table 4.3. Average molar mass and radius of gyration for the polymer solutions 111

Table 4.4. Petrophysical Properties 120

Table 4.5 Fluid injection sequence for the injectivity experiments using unconsolidated porous media 125

Table 4.6 Polymer concentration in produced water 130

Table 4.7 Average Molar mass and radius for the produced water samples 130

List of Figures

Figure 1.1 Mechanism for the oil Recovery 3

Figure 1.2 Microscopic oil recovery by polymer flooding 5

Figure 1.3 An illustration of a lasting advantage associated with polymer EOR 6

Figure 1.4 Outline roadmap for polymer EOR 9

Figure 1.5 Polymer EOR Mechanism 10

Figure 1.6 Schematic of polymer retention mechanism 12

Figure 1.7 Hydrophobic molecular interactions between polymer chains 17

Figure 1.8 Schematic of AF4-FFF Principle 24

Figure 1.9 Light Scattering under MALS detector 25

Figure 1.10 AF4-FFF system set-up 27

Figure 1.11 AF4-FFF experimental steps to characterize the polymer samples 29

Figure 2.1 Interaction of HPAM molecule with cation 38

Figure 2.2 Mechanical Degradation of polymer subjected to high shear and elongational rates 39

Figure 2.3. Schematic of AF4 principle 45

Figure 2.4 Charges distribution around HPAM molecules under different salinity conditions 48

Figure 2.5 The cumulative molar mass of post-hydrolyzed PAM 49

Figure 2.6 The differential molar mass of post-hydrolyzed PAM 50

Figure 2.7. The cumulative radius of post-hydrolyzed PAM 50

Figure 2.8 The differential radius of post-hydrolyzed PAM 51

Figure 2.9 cation attachments with a different type of polymer molecules 53

Figure 2.10 The cumulative molar mass of co-hydrolyzed PAM 54

Figure 2.11 Differential molar mass of Co-hydrolyzed PAM 54

Figure 2.12 The cumulative radius of co-hydrolyzed PAM 55

Figure 2.13 Differential radius co-hydrolyzed PAM 55

Figure 2.14 The molecular weight of post-hydrolyzed PAM 57

Figure 2.15 The molecular weight of co-hydrolyzed PAM 57

Figure 2.16 Conformation plot for post-hydrolyzed PAM 58

Figure 2.17 Conformation plot for co-hydrolyzed PAM 58
Figure 2.18 Coordination structures of COO^{-} with metal ion 59
Figure 2.19 FTIR spectra of polymers under different brine concentrations 60
Figure 2.20 Normalized filament diameter vs time 62
Figure 2.21 Straining hardening of polymers under saline environments 63
Figure 3.1 Force domination during hydrophobic molecular interactions 68
Figure 3.2. Flow scheme of the channel (side view) while eluting 74
Figure 3.3: Influence of polymer concentration and hydrophobicity on the shear rheology 76
Figure 3.4: Uniaxial elongation and filament breaking for the polymer samples 79
Figure 3.5: Effect of hydrophobicity on the polymer conformations 80
Figure 3.6: Apparent extensional viscosity as a function of strain rate 81
Figure 3.7: Straining hardening for polymer samples 82
Figure 3.8: Conformational for the associative polymer samples 86
Figure 3.9: Molar mass distribution for the associative polymer samples 88
Figure 3.10: Radius distribution for the associative polymer samples 89
Figure 4.1 A summary of EOR projects performed worldwide including polymer flooding 93
Figure 4.2. Schematic of working principle of AF4-FFF 99
Figure 4.3 Schematic of polymer injectivity experiments 100
Figure 4.4: Influence of polymer concentration and hydrophobicity on the shear rheology 104
Figure 4.5 Uniaxial elongation and filament breaking for the polymer samples 106
Figure 4.6: Apparent extensional viscosity as a function of strain rate 108
Figure 4.7 Straining hardening for polymer samples 109
Figure 4.8 Mass distribution for the polymer solutions 114
Figure 4.9 Radius distribution for the polymer solutions 117
Figure 4.10 Conformational plots for the polymer solutions 119
Figure 4.11 RF as a function of flux rate for polymer solutions 121
Figure 4.12 RRF as a function of flux rate for polymer solutions 122
Figure 4.13 Adsorption mechanism of polymer on the rock surface 123
Figure 4.14 Resistance factors for the polymer solutions in unconsolidated sand-pack 126

Figure 4.15 Residual resistance factors for the polymer solutions in unconsolidated sand-pack 127

Figure 4.16 Samples received from polymer EOR field 129

Figure 4.17 Comparing the distributions of sample 1 with injecting fluid 131

Figure 4.18 Comparing the distributions of sample 2 with injecting fluid 132

Figure 4.19 Comparing the distributions of A-079 samples with injecting fluid 133

Chapter 1: Introduction and literature review

1.1 Introduction to oil recovery methods

Crude, natural gas and Coal are the most valuable non-renewable energy sources and essential feedstock for many processes as well. Among them, oil plays the foremost role in the world of increasing energy demand. Once the current crisis situation gets stabilized, the global oil demand could be boosted by 0.5 million barrels/day to reach about 0.170 million barrels and 0.210 million barrels daily by end of 2021 and 2022 respectively[1]. Additionally, the recent sharp drop in oil prices compelled the oil corporations to revise their production strategies and optimize their production cost based on the current oil price scenario. To satisfy the oil demand with the traded oil prices, the implementation of Enhanced Oil Recovery (EOR) techniques have been gaining more and more attention as the formation and exploration of new oil reserves continues[2].

Generally, a lifetime of a reservoir comprises three spans. Initially, primary oil recovery with natural drive mechanisms like gravity drainage, solution gas drive, supporting aquifers and, gas cap drive. Once this mechanism is depleted, the reservoir pressure can be maintained either by water or gas injection, also called a secondary oil recovery process. The tertiary oil recovery processes, also known as the enhanced oil recovery processes, consist of an extensive assortment of specific advanced techniques that are put into action as a third stage to improve the lifetime of a reservoir. When a new oil reservoir is drilled, only 20-40% of the potential oil can be extracted through a combined endeavor from the primary and secondary recovery processes[3]. Nearly 7.0×10^{12} barrels of conventional and heavy oil persist in reservoirs worldwide after the conventional, primary and secondary oil recovery methods have been exhausted[4], [5].

Application of the EOR processes gives an additional opportunity to extract up to 20% of its original oil reserve so much of this remaining oil can be recovered by a variety of EOR techniques that guarantee a long-term supply of oil in the future. The typical EOR methods include chemical flooding, gas injection, and thermal processes. In thermal processes the advantage of heat transfer is considered as a major advantage for oil recovery. Whereas, in the displacement methods, chemical and gas injection, the addition of the chemical species along with a carrier fluid into the reservoir helps to displace the remaining oil through various mechanisms like IFT and/or viscosity enhancement, and mass transfer. The majority of chemical flooding includes the addition of surfactants and/or polymers in water to enhance the oil displacement ability. The following terminologies can be useful to understand the mechanism of polymer flooding.

1. Polymers ultimately contribute to increasing the viscosity of injected water and enhance the fractional flow of oil defined in the equation below:

$$f_0 = \frac{q_0}{q_0 + q_w} = \frac{1}{1+M} \tag{1.1}$$

where, f_0 is fractional flow of oil, q_0 is the volumetric flow of oil, q_w is the volumetric flow of water, and M is the Mobility ratio

2. The sweep efficiency E, can be measured as,

$$E = E_D \, E_{AS} \, E_{VS} \tag{1.2}$$

where, E_D is displacement efficiency, E_{AS} is aerial sweep efficiency, and E_{VS} is vertical sweep efficiency.

E_D can be measured as,

$$E_D = \frac{\text{Volume of oil at start of flood} - \text{Remaining oil volume}}{\text{Volume of oil at start of flood}} \tag{1.3}$$

1.2 Mechanisms

The Improved volumetric sweep efficiency is governed by a combined effect of the microscopic (pore level) and macroscopic (areal and vertical sweep) recovery efficiencies as shown in Figure 1.1. The macroscopic recovery implies the extent of enhanced oil that displacing agent can sweep. Whereas microscopic recovery refers to the effectiveness of displacing agents that mobilize the enhanced oil ensnared in the reservoir pores by resultant capillary forces[6]. In general, two major factors that affect the residual oil mobilizations are the Mobility Ratio (M) and the Capillary Number (N_c). The N_c represents the relative effect of viscous forces versus the surface tension across the interface between oil and the displacement fluid as shown in Eq. 1.4.

$$N_c = \frac{v\,\mu}{\sigma} \qquad 1.4$$

where v is the Darcy velocity (m/s), μ is the displacing fluid viscosity (Pa·s), and σ is the interfacial tension between displacing fluid and oil (N/m)

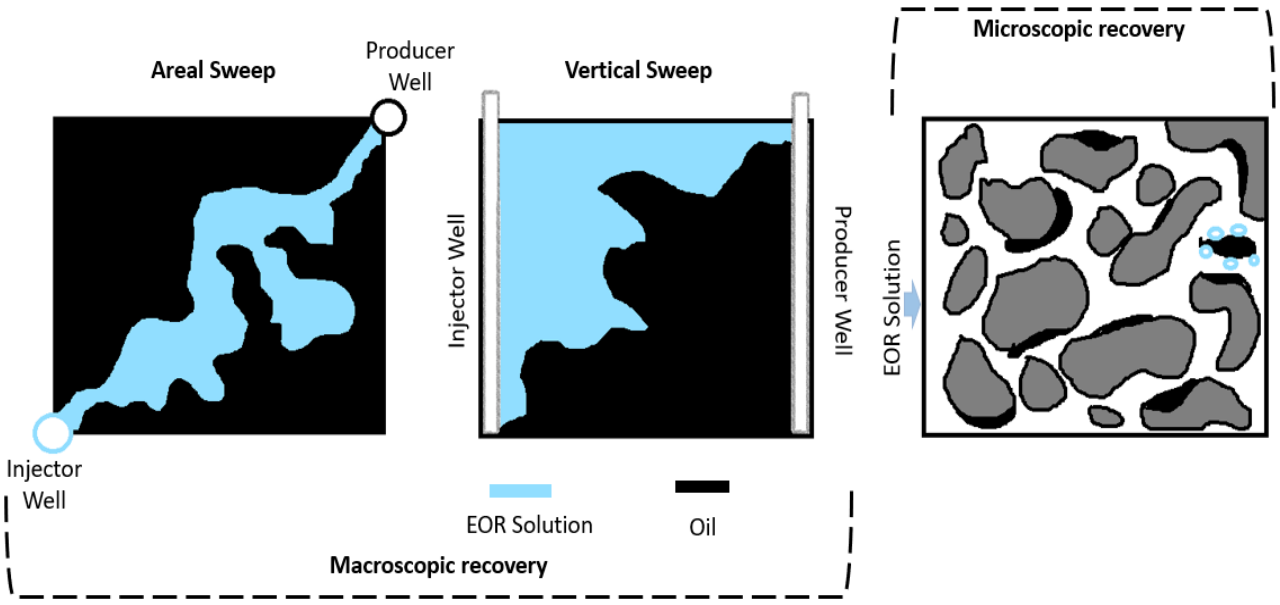

Figure 1.1 Mechanism for the oil Recovery[7]

The most effective way to improve the Capillary Number is by reducing the surface tension forces. This can be done either by adding the suitable surfactant to the displacement fluid or by application of heat. In the majority of cases, the enhancement of the Capillary Number by 3rd order magnitude may result in a 50% reduction in the residual oil saturation[4]. Whereas the Capillary Number approaches the "infinite" value in the case of miscible displacement (by using a surfactant with ultra-low IFT). Under these conditions with a favorable M, the residual oil saturation in the swept zone can be reduced to zero. The other factor, M is defined as the mobility of the displacing fluid over the mobility of displaced fluid as shown in Eq. 1.5.

$$M = \frac{\lambda_{ing}}{\lambda_{ed}} = \frac{k_{ing}}{\mu_{ing}} \times \frac{\mu_{ed}}{k_{ed}} \qquad 1.5$$

Where k is the effective permeability (m^2), and μ is the viscosity of concern fluid (Pa·s)

The M higher than one is considered unfavorable. In such cases, the displacing fluid flows more readily than the oil. So it can bypass some of the residual oil and cause the viscous fingering or channeling of the displacing fluid and reduce the displacement efficiency, as shown in Figure 1.1. The oil recovery can be improved when the value of M approached 1 and is denoted a "favorable" conditions.

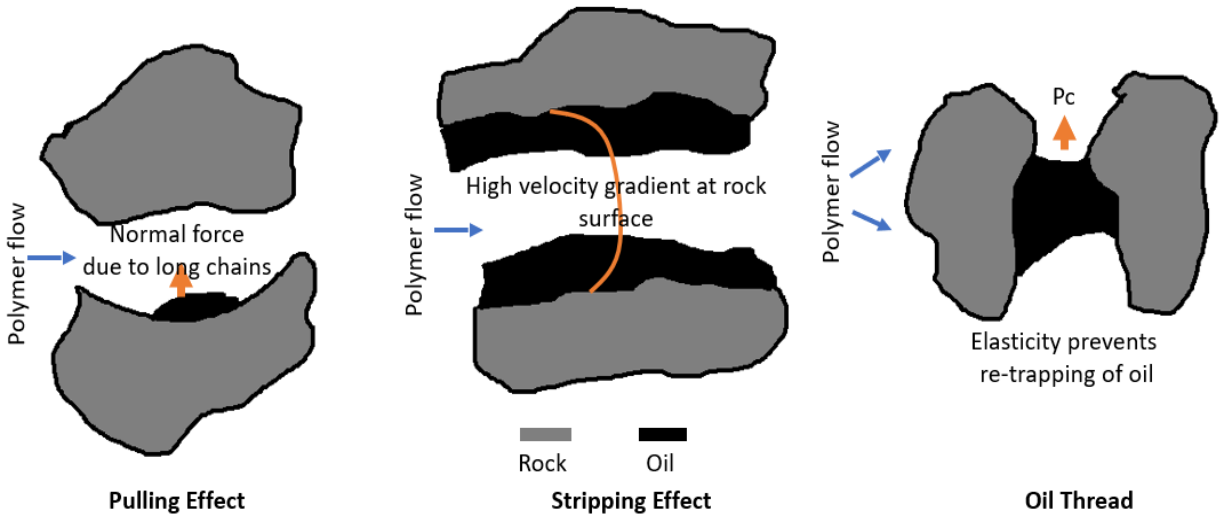

Figure 1.2 Microscopic oil recovery by polymer flooding

For most heterogeneous formations, only 50% of the reserved oil is recovered even after extensive waterflooding. A reason behind it is the higher unfavorable M between oil and water. In this case, the injected water hits directly to the producer by establishing a preferential flow path that bypasses the oil-bearing zones. This may result in low sweep efficiency, and so the oil recovery. To reduce the channeling of water, the polymer is usually added to the injected water that enhances the viscosity of the displacing fluid, called polymer flooding. Polymer flooding helps to improve the poor M encountered in the case of water flooding and reduces the permeability. Due to the swelling and viscoelastic characteristics of polymers the macroscopic recovery improvement is mainly governed by mobility control, disproportionate permeability reduction, and flow resistance induced by elasticity. These characteristics are also attributed to the microscopic recovery improvement explained by a combined oil tread, pulling, stripping, and shear thickening effects as shown in Figure 1.2[8].

1.3 Polymer EOR

Polymer flooding offers several advantages, such as enhancing the mobility of the injected fluid, improving the vertical and areal sweep efficiencies, less water consumption than water flooding, and being a cost-effective alternative to other EOR techniques[9]. Although a barrel of polymer solution is more expensive than regular water, the additional cost is outweighed by the increased oil production. This allows for effective management of costs on a per barrel basis in the long run. The incremental barrels produced in the later stages of the asset's life present a chance to manage the cost structure and prolong the asset's lifespan, as depicted in the general diagram below (Figure 1.3). By providing oil in smaller increments, the cost of polymer injection and facility operation can be offset, resulting in a more sustainable cost per barrel.

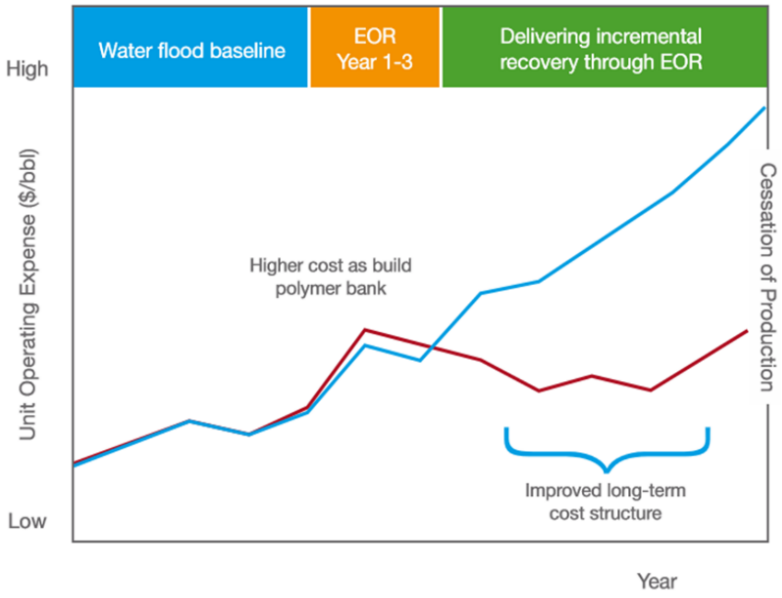

Figure 1.3 An illustration of a lasting advantage associated with polymer EOR adopted from Oil Authority Report [10]

The chemical EOR market had a value of over US$4.00 billion in 2022 and is expected to experience a compound annual growth rate (CAGR) of 7.8% from 2022 to 2032, according to

the forecast. Out of the total global EOR market, the polymer EOR market was valued at around US$3.33 billion in 2020 and was expected to continue to grow in the coming years due to increasing demand for oil and advancements in polymer technology. The market forecast for polymer EOR was positive, with a projected compound annual growth rate (CAGR) of around 6.5% from 2021 to 2027[10]. Table 1.1 shows a list of major successful polymer EOR projects [11]–[15]. Majority of them have used 1000-3000 ppm of HPAM (Hydrolyzed Polyacrylamide) dissolved in high TDS (Total Dissolved Solids) produced water or brine to be used as an injecting fluid for polymer EOR.

Table 1.1 Successful field application of polymer EOR

Field Name	**Country**	**Operator**	**Current Production (bopd)**	**Expected Production (bopd)**	**Polymer Used**
Mangala	India	Cairn India	175,000	240,000 by 2023	HPAM
Tengiz	Kazakhstan	Chevron	Not disclosed	Up to 120,000 by 2022	Xanthan gum
Rumaila	Iraq	BP	1.5 million	100,000 by 2022	HPAM
Halfaya	Iraq	CNPC	200,000	270,000 by 2023	HPAM
Daqing	China	PetroChina	800,000	1 million by 2025	HPAM
Ghawar	Saudi Arabia	Saudi Aramco	5 million	4.5 million by 2023	ASP
Prudhoe Bay	United States	BP Alaska	300,000	400,000 by 2024	HPAM
Lula	Brazil	Petrobras	1.2 million	1.5 million by 2023	Xanthan gum
Kashagan	Kazakhstan	North Caspian Operating Company	370,000	500,000 by 2024	ASP
Zafiro	Equatorial Guinea	ExxonMobil	100,000	150,000 by 2023	Xanthan gum
Cantarell	Mexico	Pemex	800,000	600,000 by 2024	ASP

Johan Sverdrup	Norway	Equinor	400,000	700,000 by 2025	HPAM
Karachaganak	Kazakhstan	Karachaganak Petroleum Operating	250,000	300,000 by 2023	Xanthan gum

One of the major challenges faced during implementation of the polymer EOR projects was polymer degradation and viscosity loss due to high temperature and reservoir conditions, which can reduce the effectiveness of the EOR process. Therefore, developing an understanding of the viscosity loss, degradation, and resultant effect on porous media flow of polymers at the lab scale enable to understand the risks associated with polymer EOR. In addition, gaining a comprehension of the impact mechanism and creating standardized methods for polymer screening helps to mitigating these risks.

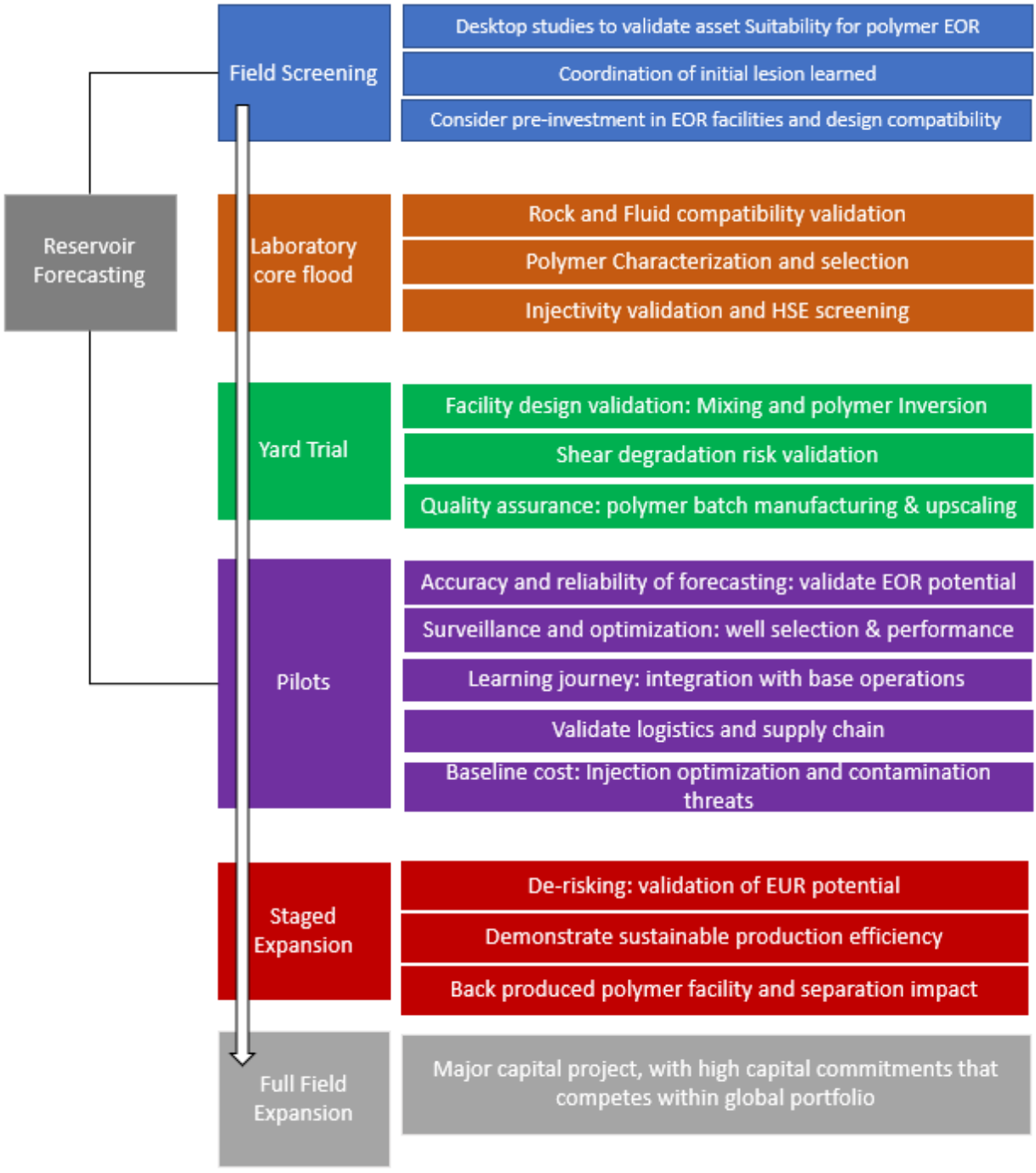

Figure 1.4 Outline roadmap for polymer EOR[10]

Figure 1.4 shows a typically followed roadmap for polymer EOR implementation. The early evaluation of a field's suitability for polymer EOR is crucial as it can impact many techno-economic decisions and pave the way for the future implementation of an EOR scheme. The goal

of a pre-determined laboratory study is to identify and create a suitable polymer solution tailored to the unique characteristics of the field in question. When conducting chemical screening, several factors must be considered, including the stability of the chemical throughout the supply chain from the manufacturer to the reservoir, its effectiveness within the reservoir, the complexity of the facility, its operational reliability, the dependability of the supply chain, and its commercial feasibility. Although implementation of polymer EOR technologies are more expensive per barrel than regular water, the additional cost is outweighed by the increase in oil production. This means that, in the long term, the costs can be effectively managed on a per barrel basis. Late-stage incremental barrels provide an opportunity to manage the long-term cost structure and prolong the lifespan of assets. This is illustrated in the following schematic:

For the EOR industry to establish itself as sustainable and profitable, it is essential to ensure that EOR projects are economically viable and competitive. The viability and competitiveness of these projects are crucial for attracting industry investments and fostering development[16]–[18]. However, achieving economic and competitive EOR projects involves considering multiple factors that contribute to their overall value.

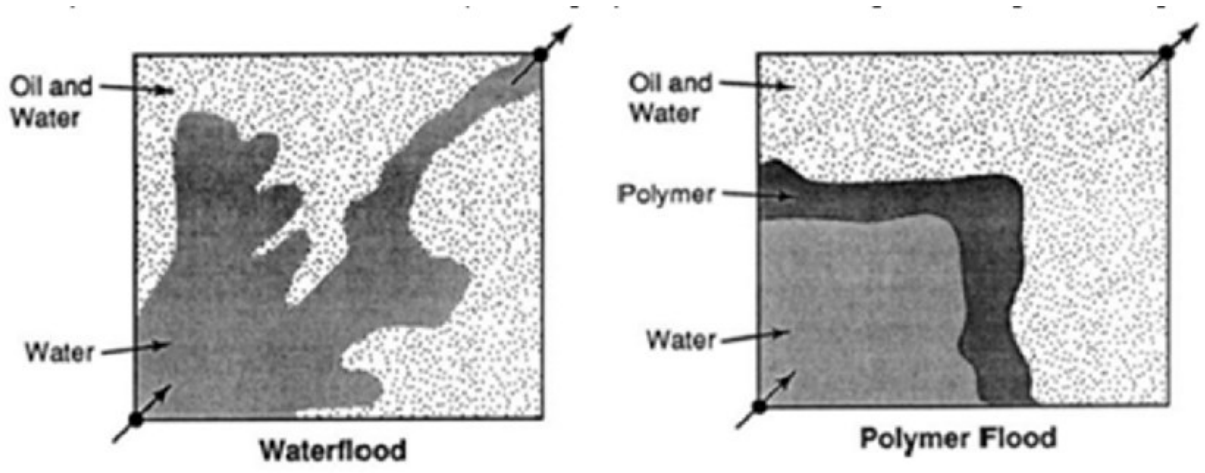

Figure 1.5 Polymer EOR Mechanism[15]

In conventional water flood systems, oil is pushed towards production wells by injecting water through injector wells. However, in many reservoirs, the water flood tends to follow a narrow path between the injector wells and the producers. This leads to the formation of 'coning' or 'fingering' patterns, where significant volumes of oil-saturated rock are bypassed by the water flood, resulting in unrecovered oil, as shown in the Figure 1.5.

Other two factors used to identify the success of polymer EOR are, sweep efficiency, and displacement efficiency. The effectiveness of an enhanced oil recovery process can be measured by sweep efficiency, which is determined by the volume of the reservoir that is contacted by the injected fluid. However, sweep efficiency is a complex parameter that depends on various factors such as the injection pattern chosen, the presence of off-pattern wells, fractures in the reservoir, the position of gas-oil and oil/water contacts, reservoir thickness, areal and vertical heterogeneity, M, and the density difference between the displacing and displaced fluids.

E_D, also known as microscopic sweep efficiency or local sweep efficiency, is a measure of the effectiveness of a polymer solution in displacing oil. It is calculated by dividing the volume of oil displaced by the volume of oil contacted by the displacing fluid (polymer solution) as shown in the Equation 1.3.

The flow of polymer solution through porous media is affected by three main retention mechanisms: polymer adsorption, mechanical entrapment, and hydrodynamic retention[19], [20]. Polymer adsorption occurs when the polymer molecules interact with the solid surface, causing them to attach to the rock's surface. Physical adsorption, mainly dominated by van der Waals bonding and hydrogen bonding, is more prevalent than chemical adsorption. Polymer adsorption is directly proportional to the surface area and can occur in the absence of a porous medium. Mechanical entrapment, on the other hand, occurs when large polymer molecules are trapped in

small pore throats, reducing permeability and retention. This can cause significant issues in polymer flooding, including reduced concentration of the effective polymer solution, viscosity changes, and inefficient sweep. Hydrodynamic retention is the least understood mechanism and is not a significant contributor to polymer retention in porous media.

Referring to Figure 1.6, the phenomenon can be described as follows: polymer molecules are trapped, possibly temporarily, in stagnant flow regions due to hydrodynamic drag forces. Within these localized regions, there is a chance of higher polymer concentration compared to the injected fluid. When the flow stops and the drag force diminishes, these trapped polymer molecules can rejoin the main flow channel. Upon the resumption of flow, they are then produced along with the fluid.

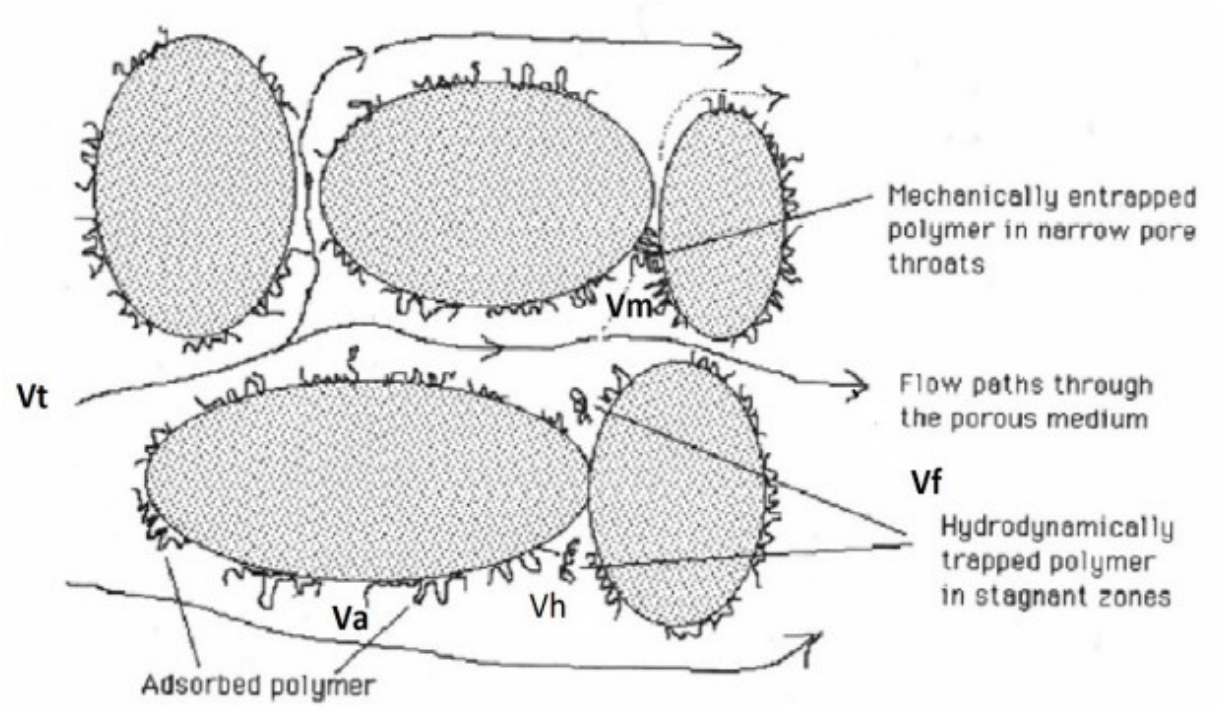

Figure 1.6 Schematic of polymer retention mechanism [21]

1.4 EOR polymers

1.4.1 Introduction to hydrolyzed polyacrylamide

The two most utilized types of polymers for this purpose are synthetic polymers, typically represented by partially hydrolyzed polyacrylamide (HPAM), and biopolymers. Currently, synthetic polymers are the most widely deployed technology solution in the industry. Adequately designed polymer flooding can improve the EOR even under challenging reservoir conditions. The technological, operational, and cost benefits of polymer EOR can be tuned based on the suitable selection of polymer to enhance the viscosity of water that favors mobility control and reduce the relative permeability simultaneously. HPAM and its hydrophobicity-modified derivatives, Associating Polymers (AP) with higher molecular weight have been used at the commercial stage considering the economic factors. The higher molecular weight of these polymers is eventually responsible for enhancing the viscoelasticity of displaced slugs to achieve a favorable M. Therefore rheological characterization has been used to predict the flow behavior of polymer in the porous media.

Regarding polymer flooding, a variety of water-soluble HPAM are being applied successfully in the oilfields. HPAMs are commercially available with different molecular weights (M_w) and degrees of hydrolysis. For the majority classes, the degree of hydrolysis varies from 25-30% with a maximum Mw of up to 30 MDa. These polymers exhibit higher mechanical (shear) and chemical stability (salt and pH tolerance), with the lower bio-degradability and bulk cost compared to the modified natural polymers like carboxymethylcellulose, xanthan gum, and guar gum. Electric double-layer and thick hydration layer formation up on HPAM dissolution of HPAM in deionized water cause swelling of HPAM molecules result in a higher viscosity of the solution. However, under harsh reservoir conditions, conventional HPAMs exhibit degradation

of polymer that may cause loss of polymer injectivity. The degradation of HPAM macromolecules may cause viscosity reduction or precipitation. Chemical, mechanical, and thermal degradation refers to the change in the polymer molecule's structure or loss in M_w responsible for the change in the physicochemical properties of the solution.

During polymer flooding, the higher shear forces on the polymer chains are experienced either near to wellbore region or during pumping operation. The magnitude of the shear acting on the polymer chains is such high that breaks the polymer chains called mechanical degradation. This may reduce the viscoelasticity of polymer solution due to the degraded polymer solution with lower M_w[22]. A hypothesis was made that the polymer chains get starched under the application of high shear forces and most likely break from the C-C bond located at the middle of polymer chains[23], [24]. Later on, it was found that the extent of starching of polymer chains was too low even at the high shear that justifies the chain breaking and so the mechanical degradation. Therefore, the mechanism of mechanical degradation of the polymer solution was explained by an entanglement theory[24]. At high shear rates, the degree of entanglement is increased between polymer chains which induce tensional stresses to the polymer molecules in the center of entanglement. Therefore, the higher entanglements between polymer chains resulting from the application of the high shear forces might be responsible for the polymer solution viscosity losses.

HPAMs are also known as thermally sensible polymers[25], [26]. The acrylamide groups of HPAMs start to hydrolyze above the temperature of 60 °C. The hydrolysis of HPAMs resulting in the generation of sodium acrylate may initiate the polymer precipitation that causes loss of relaxation time and so the viscosity of the solution. The rate of Fenton reaction, responsible for generating carboxyl radical can be accelerated at high temperatures[27]. These free radicals

rupture the acrylic groups resulting in the reduction of M_w. Also, these radicals can abstract the hydrogen from the polymer backbone. Nevertheless, this process requires oxygen and is therefore strongly limited in the reservoir. Therefore another mechanism for the thermal degradation was explained in the terms of ammonia loss[26]. At elevated temperatures, the HPAMs molecules lose ammonia resulting in the formation of imide which is subsequently decomposed. By that, the polymer loses M_w and finally, viscosity and relaxation time.

The hydrolysis of polymer molecules due to variation in pH conditions and reservoir salinity is called chemical degradation. Chemical degradation is the most dominating among all-polymer degradation happens during polymer flooding operations. The sensitivity of pH mainly applies to the larger polymer molecules as the smaller molecules are sensitive to both, low and high pH values. Amide groups are hydrolyzed instantly due to the change in the alkaline or acidic reservoir conditions. The higher HPAM degradation was observed under the acidic condition than the alkaline condition[28]. Under any conditions, if the HPAMs hydrolyzed exceed 33% or higher, the chemical instability comes into consideration[29]. This happens in the presence of cations or salts. The presence of cations or salt can cause charge shielding that weakens the intermolecular forces between polymer molecules. This may cause the loss in M_w or the polymer precipitation and so the loss in the viscosity of polymer solution. Dalsania et al. [25] explained how the conformational changes with pH, and the polymer concentration in the aqueous media. However, they did not study the underlying mechanism.

1.4.2 Associative polymers for EOR

To overcome the operability limits of polyacrylamides, the polymer molecules can be modified to enhance their hydrophobicity. This new class of polymer is called AP. Polymer hydrophobicity refers to the tendency of a polymer to repel or be resistant to water. It is a

measure of how well a polymer interacts with water molecules. Hydrophobicity is determined by the chemical structure of the polymer, specifically the types of functional groups present and the overall polarity of the polymer chain. In hydrophobic polymers, the polymer chains are predominantly composed of hydrophobic (water-repelling) groups. These groups are typically nonpolar or have low polarity, meaning they have a low affinity for water. As a result, hydrophobic polymers tend to form aggregates or repel water molecules, leading to a lack of solubility or wetting ability.

These polymers are expected to improve the efficiency of polymer flooding due to higher hydrophobicity responsible for better viscoelastic stability than HPAMs against higher degradation conditions discussed above. The tunable concentration and temperature-dependent molecular interactions for the AP allow a user-oriented control of its physical properties. The effect of hydrophobic associations or hydrophobicity on the rheological properties hypothesized on the molecular interactions is well understood[30]–[34]. In the dilute regime, intra-molecular hydrophobic associations between attractive groups of the same polymer chains dominate the rheological properties as shown in Figure 1.7[35]. Approaching the critical aggregation concentration (CAC), this self-association may cause the aggregation of several polymer chains into a micelle (complex) of different morphologies. In the semi-dilute regime or above the CAC, a transient network between the polymer chains can be formed by the intermolecular association on the top of pre-existing Van Der Waals forces. These networks may induce the formation aggregate and so rheological behavior[31], [34], [35].

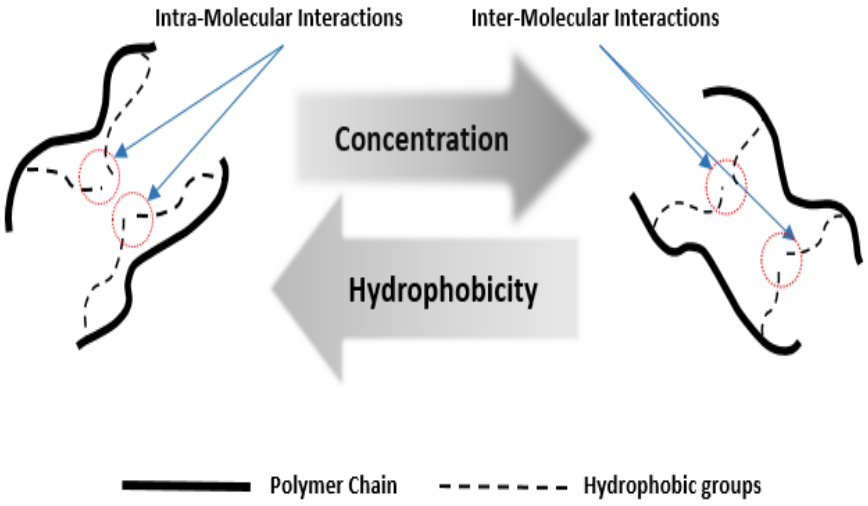

Figure 1.7 Hydrophobic molecular interactions between polymer chains

The reversible bridging among polymer chains reduces its affinity to the aqueous medium and shows an indication of balance between phase separation and intermolecular hydrophobic interactions. Further, in the concentrated regime; strengthening molecular interactions may cause phase separation in the system. On the other side, the intramolecular interactions dominate as the hydrophobicity increases. So, at the higher hydrophobicity, the effective polymer coiling may change the polymer conformations. However, How these molecular interactions affect the polymer conformations are not understood well. APs exhibit excellent shear and thermal stability under harsh reservoir conditions[35]. Here, a detailed study is needed on the effect of the cation charge shielding effect on the hydrophobic interactions.

The above-mentioned polymers (HPAMs and AP) are characterized by ultra-high M_w to achieve high viscoelasticity[36]. Therefore, the M_w is the most important property that has a major influence on the efficiency of polymer flooding and the economics of EOR projects[37]. An experimental study by using HPAM modified with 2-Acrylamido-2-Methylpropane Sulfonate (AMPS) and n-Vinyl Pyrrolidone (NVP) for use in polymer flooding in high-temperature and

high-salinity carbonate reservoirs in the Middle East, showed that the viscosifying power of the associative polymers was dependent on both salinity and hardness, with higher viscosity in desalinated Arabian Gulf Seawater compared to more saline brines [38]. Other studies have also shown that high salinity can also reduce the viscosity due to increased intramolecular association[34], [38]–[45]. Thermal and shear stability showed improved performance compared to conventional HPAM. However, an experimental study shows that the polymers based on sodium-2-acrylamido-2-methylpropane sulfonate (NaAMPS) with high levels of acrylamide may not be suitable for polymer flooding at higher temperatures [46]. An experimental investigation found that the viscosity of AP in saline water is higher than that of conventional high Mw polyacrylamide (PAM) due to the presence of hydrophobic groups and strong intermolecular forces. The rheological characterization showed that the viscosity of associative polymers is largely influenced by the polymer concentration and shear rate, while the conventional HPAM viscosity is not under the brine salinity environment. The high viscosity of AP is due to the formation of a large three-dimensional network structure, which results from the strong association of polymer molecules [45].

1.4.3 Effect of Mw of polymer on the solution viscosity

The Mw of a polymer has a significant impact on its rheological properties. Intrinsic viscosity is considered a more fundamental measure of Mw compared to viscosity alone, as it is independent of concentration[34]. Polymers often have a wide distribution of Mw and can also be branched. The Mark-Houwink relationship provides a viscosity averaged Mw, which is closer to the weight averaged Mw than the number averaged Mw. The value of the exponent in the Mark-Houwink relationship determines if the viscosity averaged Mw is equal to the weight averaged Mw [47]. Additionally, the Mark-Houwink-Sakurada equation is another empirical equation that relates the Mw of a polymer to its intrinsic viscosity. This relationship has been observed for several

polymers including cationic polyelectrolytes and in different solvents. The equation has been supported by a number of studies[48]–[52].

The relationship between the Mw and the viscosity of N-octylacrylamide/acrylamide copolymers has been studied by A. Alquraishi and F. Alsewailem, and T. Dow [38], [41]. C. A. Finch [16] reveals that higher intrinsic viscosity (and therefore, Mw) leads to higher solution viscosity, similar to the trend observed for non-associating polymers. However, more studies are needed to fully understand the dependence of solution viscosity on Mw, MWD, and solution rheology. P. Gupta et al. [49] have shown differing conclusions on the exponential dependency on M_W. E. Zhang et al. [50] suggest that it increases with Mw. There is a lack of clear understanding on the relationship between Mw, MWD and the hydrodynamic radius of associative polymers with polymer rheology and flow through porous media behavior.

Technically the polymers dissolved in the solvents do not exhibit a single monodisperse Mw. Therefore the MWD gives better insights into the molecular characteristics of polymer chains in the solvent. Also, these characteristics along with the Radius of Gyration distribution (R_g) can be used to explain the flow behavior of polymer solutions in the porous media[28]. Patel et al. [22], [23] explained how the conformational changes, MWDs, and R_g s for HPAMs change with pH, and concentration. They have concluded that the polymer conformation changes under these environments are responsible for changes in the viscoelasticity of the concerned HPAM solutions. Whereas for the associative polymers, similar studies are not available in the letature on how the induced hydrophobicity affects the polymer conformations under different environments that result in better solution properties compared to HPAMs.

When the polymer solution is injected into the reservoir, shear rates of 1 (deep in the reservoir) to 100 s^{-1}(near-wellbore region) are achieved. These shear rates are too low to justify the flow

instabilities. In these cases, the bulk shear rheological measurements help to study the flow behavior of polymer solutions in the porous media. Also the problem of polymer selection arises when they exhibit similar shear rheology[27]. At the higher Weissenberg number, the polymer conformations causing the time-dependent elastic instabilities haven't been explored well. Olmsted and Rowley [51] studied the relationship between Mw on the rheology of AP. The authors concluded that the Mw of the polymers is a critical factor in determining their rheological properties and that the conformation of the chains plays a major role in controlling the viscosity in shear and extensional flows. The effect of polymer conformation on rheological properties of polyethylene glycol-based associative polymers were investigated and the authors found that the conformation of the chains is a crucial factor in determining the rheological properties of associative polymers and affects the resistance factor and viscosity in shear and extensional flows. The effect of polymer conformation on the rheological properties of polyethylene glycol-based associative polymers was studied by V. Castelletto et al. [53]. The role of conformation on hydrodynamics and structure in the rheology of associative polymers was also investigated and concluded that the conformation of the chains, hydrodynamics and structure play crucial roles in determining the rheological properties of associative polymers and influence the viscosity in shear and extensional flows [54]. Hiraoka and

Yamakawa [52] highlight the importance of Mw and chain conformation in the rheology of associative polymers. They claim that the conformation of the chains plays a major role in controlling the viscosity in shear and extensional flows and that the Mw is a crucial factor in determining the rheological properties of assocative polymers. Further research on the polymer conformational determination is needed to fully understand the complex behavior of associative polymers and how their molecular structure and behavior can be controlled to optimize their rheological properties. Additionally, it is important to consider the impact of other factors, such

as temperature, solvent composition, and concentration, on the rheology of associative polymers. These variables may interact with Mw and chain conformation to further influence the rheological properties of these materials.

1.4.4 Limitations of solution viscosity on explaining flow behavior in the porous media

Despite extensive research in the field, our understanding of the flow of polymers in solution remains limited. Numerous proposals have been put forward, highlighting the absence of consensus among researchers regarding the mechanisms underlying polymer flow behavior. Additional micro-force or normal stresses were cited by several other researchers as the primary explanation for the remaining oil saturation reduction during viscoelastic polymer flooding[31]. Micro-force is a component of normal stress, which is proportional to extensional viscosity so the extensional viscosity and the relaxation time are the solution characteristics used for the polymer screening[32]. Polymer elasticity would be an important screening criterion especially when the shear rheology enables the explanation of the flow behavior of HPAM and its derivatives exhibit similar bulk shear characteristics[33][34][35]. All these mechanisms emphasize the influence of normal stresses. However, under reservoir conditions, the yielding stress is not always the normal stress even though the polymer is injected at a very low rate[36]. Hence the normal stress-dependent bulk polymer characteristic can not represent the behavior of polymer solutions through a porous media. The non-Newtonian flow of these viscoelastic polymer solutions through porous media under non-uniform conditions (varying porosity, permeability, and yield stress) could be explained by the formation of molecular networks responsible for the fluid flowability, resistance, and retention[37]. These induced networks may not cause considerable change in the viscoelastic properties. Hence the possibility to predict the polymer injectivity from the independent measurements of the fluid's rheological properties and

the porous media's geometrical properties may provide better insights for the flow behavior of polymer solutions in the porous media..

1.5 Mw, MWD, radius distribution and conformational characterization

1.5.1 Gel permeation chromatography

In the Gel Permeation Chromatography (GPC), the polymer sample undergoes dissolution in a solvent. Upon dissolution, the polymer molecules undergo coiling, forming a conformation resembling a tangled ball of string. Polymers with higher Mw tend to form larger coil structures. These coiled polymer molecules are then introduced into the mobile phase and flow into the GPC column[28].

As the dissolved polymer molecules travel through the column, they interact with the beads present. Several scenarios can occur during this process. If the polymer coils are significantly larger than the largest pores in the beads, they are unable to enter the pores and are carried straight through by the mobile phase. In the case where the polymer coils are slightly smaller than the largest pores, they can enter the larger pores but not the smaller ones, occupying only a portion of the available stationary phase. When the polymer coils are smaller than the smallest pores in the beads, they have the ability to enter any of the pores and thus potentially occupy all of the available stationary phases.

Once the molecules enter the column, a repetitive partitioning process takes place, facilitated by diffusion. This process involves the molecules entering and exiting any pores they encounter as they travel down the column. Consequently, small polymer coils capable of entering multiple pores within the beads require a longer time to pass through the column, resulting in slower elution. On the other hand, large polymer coils that cannot enter the pores exhibit a faster exit from the column. Polymer coils of intermediate size elute somewhere between these two

scenarios. Thus, the requirement of pre-filtration limits characterizing the polymer solutions with ultra-high Mw, and containing gels.

1.5.2 AF4-FFF characterization technique

FFF (Field-Flow Fractionation) has experienced significant advancements over time and has emerged as an invaluable analytical separation technique for the characterization of macromolecules. It has become a standard method for quantifying the size and molar mass of various substances, including ultralarge biopolymers, protein aggregates, and synthetic polymers. In cases where conventional GPC falls short due to the inability of large proteins and ultrahigh molar mass polymers (>MDa) to penetrate the pores in the packing material, FFF offers a robust alternative for their separation. FFF operates by combining field-driven and diffusive transport mechanisms, enabling the separation of substances that would otherwise be inaccessible through traditional methods.

As shown in the Figure 1.8, the asymmetric flow field flow fractionation is a separation principle that uses the fact that in a long chain channel a laminar flow has a parabolic flow profile and that particles/polymer, driven by a force perpendicular to this flow, will arrange themselves in different mean layer thickness, so that they are transported with different velocities through the channel.

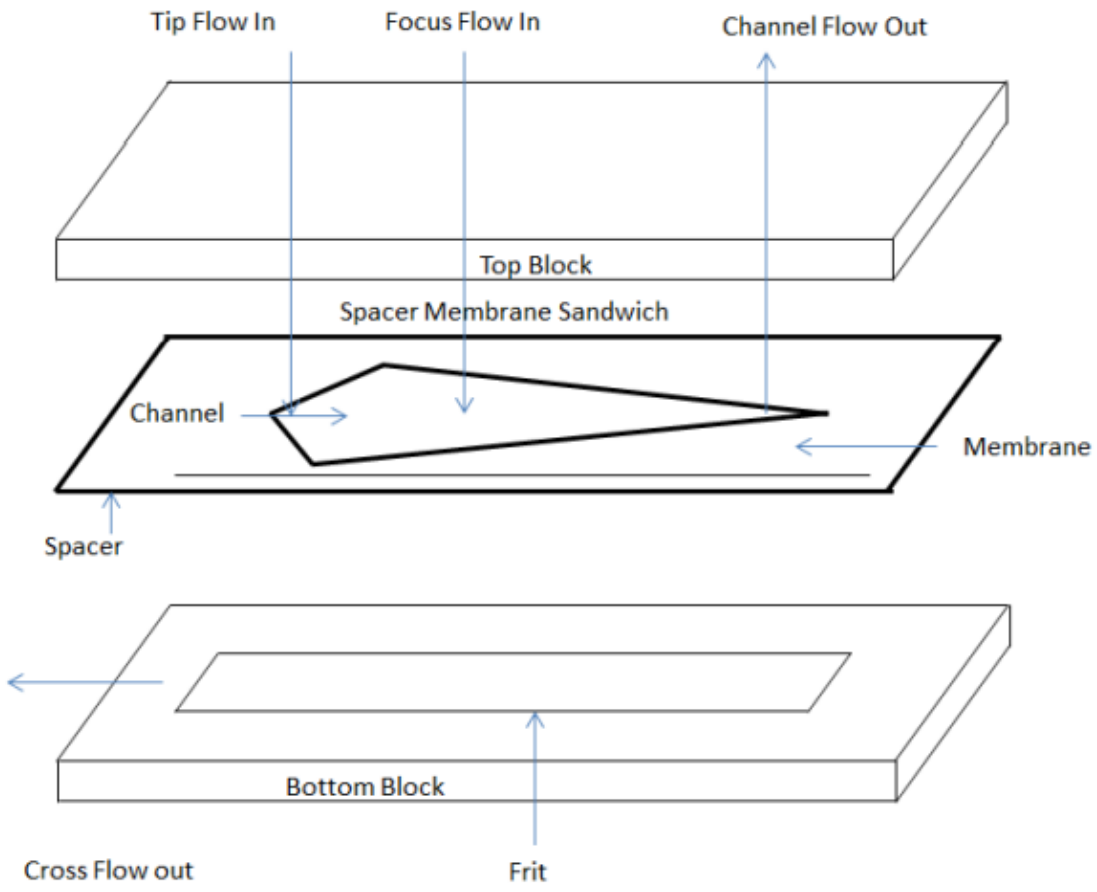

Figure 1.8 Schematics of AF4-FFF principle

The bottom of the channel consists of a porous frit and a semipermeable membrane. Particles in the channel are moved by a flow perpendicular to the membrane to the membrane towards side. On the other hand, all particles can diffuse back into the channel. The smaller the particles are, the higher the diffusion caused by the Brownian motion of the particles. The interaction of the driving field and the diffusion causes the particles to have a different average distance from the accumulation wall, the membrane. The outstream can be connected to the light scattering detectors (multi-angle light scattering (MALS) and refractive index (RI)) for determination of Mw and radius distributions. The light scattering function under MALS is shown in Figure 1.9.

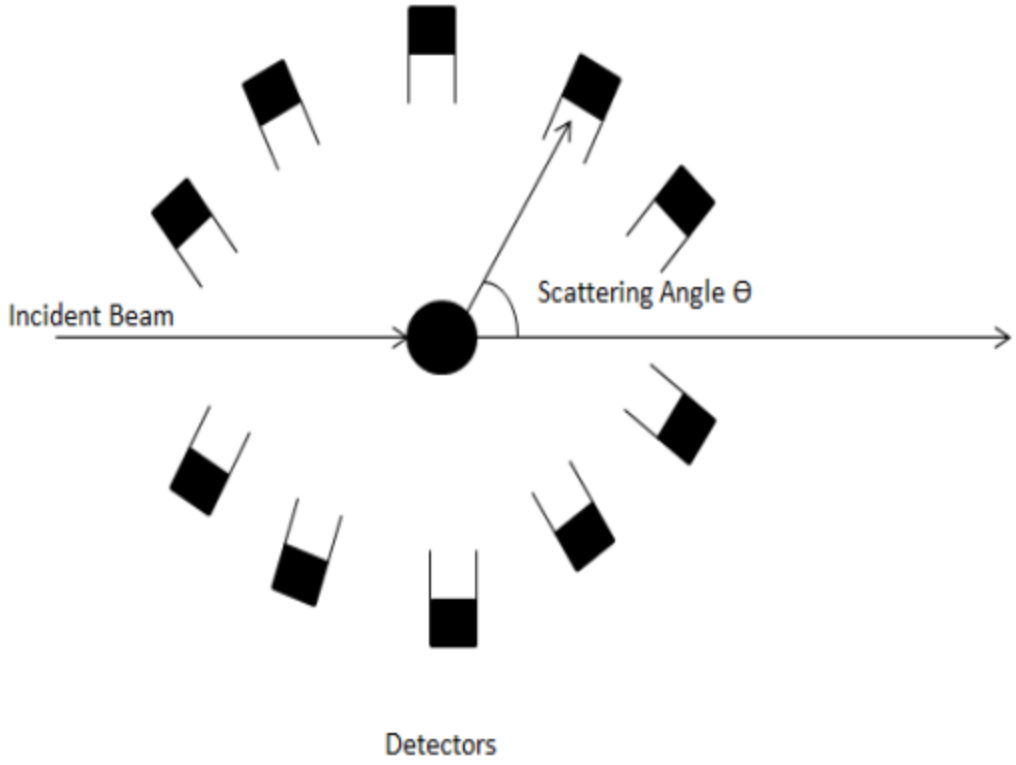

Figure 1.9 Light Scattering under MALS detector

The data collected is utilized to establish an autocorrelation function, which allows for the direct derivation of the diffusion coefficient. By applying the Stokes-Einstein equation, it becomes possible to calculate both the hydrodynamic radius and the size distribution. The fundamental principle of Multi-Angle Light Scattering (MALS) is similar to that of Static Light Scattering (SLS) at a single angle. A beam of polarized light is directed onto the sample molecule, and the resulting scattered light is captured by a photo detector. However, in MALS, the scattered light is detected at multiple different angles simultaneously. The intensity of the scattered light at each angle correlates with both the molar mass and the concentration of the molecules being studied. For smaller macromolecules that do not exhibit angular dependence in the scattered light, detecting at a single angle is adequate. However, as the sample molecules increase in size, more

light scatters in the forward direction at smaller detection angles. In such cases, it becomes crucial to capture the scattered light at multiple angles simultaneously. the expression for Multi-Angle Light Scattering can be represented by the following equation:

$$\frac{R(\Theta)}{K_c} = M\mathrm{P}(\theta) - 2A_2M^2P(\theta)^2c \mp \cdots \quad 1.6$$

With K

$$K = \frac{(2\pi n\frac{dn}{dc})^2}{{\lambda_0}^4 N_A} \quad 1.7$$

Where, $R(\Theta)$ = Excess intensity of scattered light at a given angle, C= sample concentration, M= molar mass, A_2= second viral coefficient, K= optical constant, n= solvent refractive index, $\frac{dn}{dc}$ = refractive index increment, N_A= Avogadro number, $\lambda_0 = \text{Wavelength of laser light}, P(\theta) =$ Function of angular dependent light scattering intensity

By combining the aforementioned scattering equation with the Taylor expansion for the form factor P(θ), we arrive at the following equation for light scattering:

$$\frac{R(\Theta)}{K_c} = M\left[1 - \left(\frac{2}{3!}\right) < r_g >^2 \left[\frac{4\pi n}{\lambda}\sin\left(\frac{\theta}{2}\right)\right]^2 + \cdots\right] \quad 1.8$$

Utilizing this formula, it becomes possible to plot R(θ)/(K*c) as a function of $\sin^2(\theta/2)$. Through this plot, the gyration radius Rg and the molar mass M can be calculated. The slope of the function at angle 0° represents Rg, while the intercept of the curve with the y-axis provides the value for M. The determined conformational properties for the polymer solutions were used to explain the polymer injectivity in the porous media.

Figure 1.10 displays the experimental setup for AF4-MALS-RI analysis. The setup comprises essential components such as an AF4 module, focus and tip pump, MALS detector, and RI detector. The AF4 module used was the AF2000 MF supplied by Postnova Analytics in Landsberg, Germany. This module serves the purpose of controlling and measuring all the necessary operating variables required for system operation and elution data analysis. Pumps, valves, and flow rates are precisely controlled, and the NovaFFF Data Acquisition and Control Software is used to acquire elution data.

Figure 1.10 AF4-FFF system set-up

The focus and tip pump employed was the PN 1130 by Postnova Analytics, which is a dual piston solvent delivery pump designed for this purpose. The MALS system utilized was the PN3621 by Postnova Analytics, which operates with a 532 nm laser beam and incorporates 21

different scattering angles for detecting scattering intensities. These angles range from 7o to 164o, allowing for comprehensive measurements. The MALS system has a measurement range for molar mass from 10^3 Dalton to 10^9 Dalton. Finally, the refractive index detector used was the PN 3150, also supplied by Postnova Analytics. Overall, this experimental setup ensures accurate and reliable AF4-MALS-RI analysis by incorporating advanced components and precise control mechanisms.

The spacer membrane sandwich configuration creates a trapezoidal channel geometry. The dimensions of the channel are as follows: the tip-to-tip length is 27.9 cm, the breadth at the inlet is 2 cm, and the breadth at the outlet is 0.6 cm. The total area of the channel is calculated to be 34 cm^2. To define the channel, a spacer with a nominal thickness of 300 μm is utilized. For the separation channel, a regenerated cellulose membrane with an average molar mass cut-off of 10 kDa (Z-MEM-AQU-631, RC amphiphilic, supplied by Postnova Analytics) is employed.

The experimental methodology employed for the conducted experiments is outlined in Figure 1.11. The samples were introduced into the channel through manual injection. The experiments commenced with sample injection and focusing, utilizing a main pump flow rate of 0.20 mL/min and a focus pump flow rate of 0.80 mL/min. A low inlet flow rate was chosen to prevent shear degradation. The cross-flow rate remained constant at 0.50 mL/min during the injection and focusing phase. The focusing process typically lasted for 3 minutes, with the focusing position set at 8.9 cm.

Following the injection/focusing phase, a transition time of 1 minute was allowed for the switch to elution mode. Elution commenced at an initial cross-flow rate of 0.50 ml/min for a duration of 2 minutes, after which it gradually decreased to 0.1 ml/min over a period of 35 minutes, following a power function with an exponent of 0.3. A final cross-flow rate of 0.1 ml/min was

maintained for 15 minutes. After each experiment, rinsing was performed using a tip pump flow rate of 1 ml/min, and the purge valve remained open for 5 minutes.

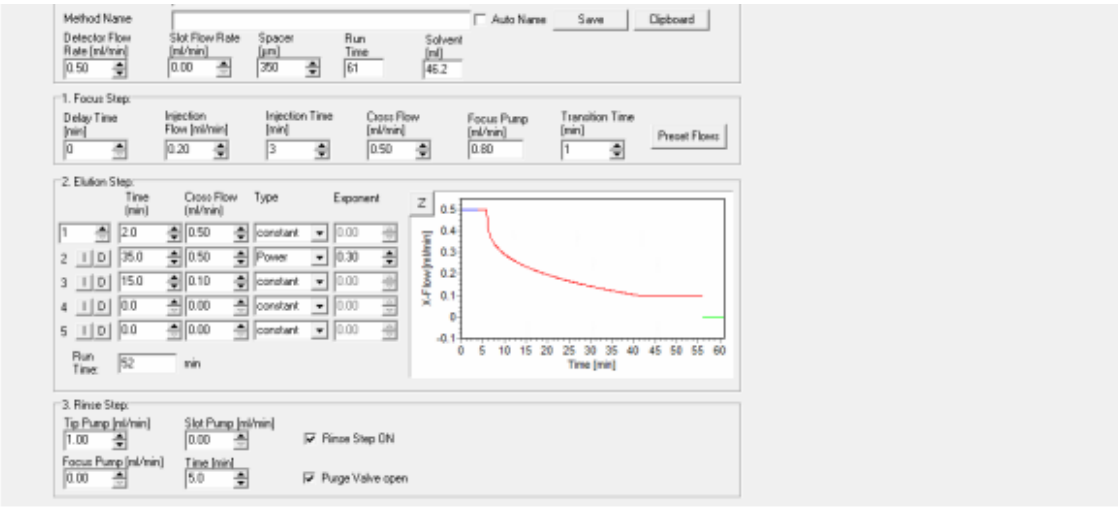

Figure 1.11 AF4-FFF experimental steps to characterize polymer samples

In each separation experiment, approximately 50 µL of the sample was injected into the membrane. All experiments were conducted under room temperature conditions. After the separation process within the channel, the eluent from the channel flows into in-line detectors, including the MALS detector and RI detector. The coupling of these detectors to the outlet of the separation channel allows for direct determination of the molar mass and radius of the eluted fraction, eliminating the need for any standards. The entire system is connected to a unified software platform (Nova FFF software, supplied by Postnova Analytics, Landsberg, Germany) for controlling data acquisition and performing system evaluation of all connected detectors. A polymer recovery was measured to optimize the above-mentioned parameters and a method of polymer elution was finalized when a polymer revery over 95% was observed.

1.6 Determining the polymer solution viscosity

1.6.1 Shear viscosity

The AR2000 instrument from TA Instruments was employed to analyze the shear behavior of polymer samples at room temperature. The instrument offers a minimum torque resolution of 0.1 μN·m and a displacement resolution of 0.04 μrad. The polymer samples were assumed to have a density of 1000 kg/m3, and the probe volume used was 1 mL.

$$[\eta] = kM^{\alpha} \tag{1.9}$$

Where, $[\eta]$ is intrinsic viscosity of polymer solution, M is the average molar mass of polymer solution, and k & α are the empirical constants obtained from the experimental data

The Mark-Houwink-Sakurada relationship Equation 1.9 is commonly employed to establish a connection between the intrinsic viscosity of a polymer in solution and its average molar masses. This relationship is utilized in a widely adopted polymer characterization technique, which is relatively straightforward and empirical in nature. By determining the intrinsic viscosity, typically achieved through the extrapolation of viscosity-concentration data, an estimation of the polymer's average molar masses can be obtained. While modern rotational viscometry instruments are capable of performing such measurements, a simpler approach involving an Ostwald or Ubbelohde viscometer is typically employed.

This method is constrained to the examination of polymers where the Mark-Houwink-Sakurada (MHS) constants are already known. Additionally, the MHS constants are applicable only to the solvent or closely related solvents for which they have been determined. It is important to note that brine composition changes with varying reservoir conditions, making it challenging to

analyze the behavior of a polymer since the MHS constants may not be available for that specific brine. This method also presents limitations when dealing with novel polymers or copolymers designed for specific purposes. Additionally, when the polymer solutions exhibit the similar rheological profiles, it is very difficult to use the characteristic molar mass for the flow behavior predictions.

Furthermore, this characterization method is quite rudimentary in nature. It provides only a single value for the molar mass and does not offer information regarding the mass distribution of the polymer or the radius of gyration. Consequently, the intrinsic viscosity has limited utility when dealing with novel ultrahigh Mw polymers and copolymers that are being specifically developed.

1.6.2 Extensional viscosity

The Capillary Breakup Extensional Rheometer (CaBER) is conceptually based on the designs of Bazilevsky et al. The instrument uses a laser micrometer to monitor the diameter of a thinning filament. Quantitative information that can be obtained from these data are time-to-breakup, and, from the slope of the curve, the "stringiness" of the fluid.

In the CaBER, the polymer sample is constrained axially between two smooth coaxial disks of the same radius such a way that the liquid polymer solution sample bridges in the cylindrical configuration between two plates. The plates separate rapidly over a short distance to generate an instantaneous strain. Once the unstable necked configuration has been established, the midpoint diameter is monitored as a function of time.

The principal experimental results can be obtained from CaBER are the evolution of the midpoint diameter if the polymer samples with the time. This evolution is driven by the capillary pressure and the resistance by the extensional stress in the polymer sample. The

measurements can thus be represented in terms if an apparent extensional viscosity. The respective model fits to the raw data are explained in the subsequent chapters.

1.7 Problem Statement

Polymer displacement in the porous media is always subjected to the shear and extensional forces. However, the yielding stress on the polymer molecule in the porous media is not always normal or the shear stress even though the polymer is injected at a very low rate. Hence the existing viscoelastic models encountering only shear or normal stress fails to explain the behavior of HPAM and APs in the porous media. This arises the scope of study to enable polymer screening criteria that are independent of the stress factor and also can able to explain the underlying mechanism favoring the M.

Technically the polymers dissolved in the solvents always exhibit a polydisperse Mw. Therefore, MWD rather than the average Mw along with the other conformational parameters can provide better insights into the molecular characteristics of polymer molecules. Determination of MWD for the ultra-high Mw polymer molecules using the existing techniques like Gel Permeation Chromatography (GPC) or Size Exclusion Chromatography (HEC) has been a major challenge. limitations of this technique may lead to results that are not only incorrect, but even completely misleading. Here AF4-FFF technique provides important insights to characterize the ultra-high Mw polymers. Also, AF4-FFF technique is very useful determining Mw and radius distributions for the polymer solutions along with the conformational characteristics. These characteristics further functionalize depending on the nature of the polymer along with the solvent type. That is why it is important to study the effect of concentrations and hydrophobicity of polymers dissolved in the different solvent types, deionized water, and brine on the resulting conformational characteristics. Furthermore, how the polymer aggregates (above the critical

aggregation concentration) affect the properties of the formed complex network can be explored. The effect of these complex networks on the rheological behavior of solutions also needs to be explored well.

Where rheology fails to explain the typical flow behavior of associative and non-associative polymers triggered by intermolecular hydrophobic association, the conformational properties (the molecular characteristics) can provide better insights. This led to a scope of study to correlate these conformational properties with the triggered pressure profiles by polymer solutions flowing through the porous media. The resulting pressure profiles can be used further for estimating the resistance and residual resistance factors. So, the ultimatum could lead us to estimate the polymer retention based on the conformational characteristics.

To verify the above-mentioned hypothesis, a comprehensive analysis can be performed on how measured polymer conformations explicitly explain the available core-flood data in the literature and overcome the limitations of using rheology. Also, determining the conformational properties for the produced water samples can provide a better understanding of the role of varying polymer molecule chains on the polymer retention in the porous media.

Employing the conformational characteristics to enhance polymer flow behavior holds the potential to address current hypotheses and overcome limitations associated with rheology explaining polymer flooding. This research aims to deepen understanding of molecular network formations and explain the injectivity behavior of polymer solutions in the porous media.

1.8 Objectives of our research

To address the aforementioned challenges, this thesis is organized into four distinct tasks. The subsequent section provides an overview of the research objectives and the corresponding problem statements that will be addressed:

1. The produced water samples along with injecting fluid were subjected to determination of Mw and radius distributions for fluid flow fractionation method validation for the field applications.
2. Characterization of Co- and Post- Hydrolyzed PAM conformations, Mw, and radius distribution under a saline environment that affect the rheological behavior.

    A. To investigate the role of monovalent salt (NaCl) and divalent salt ($CaCl_2$) on polymer interactions. The effects of these interactions changing the conformational characteristics of polymer chains in the different brine can be studied.

    B. These conformational properties along with Mw and radius distributions can be correlated with the rheological profiles exhibited by the polymer solutions.

3. Influence of hydrophobic association in the aqueous and saline media on the rheology and polymer conformation of associative polymers.

    A. Investigating the role of hydrophobicity and the polymer concentration on the Mw and radius distributions in the aqueous media.

    B. How these distributions affect the rheological properties of polymer solutions?

    C. A method estimating the critical aggregation concentration for the polymer in specific solvent.

4. A study of the flow behavior of polymers with different hydrophobicity in the porous media.

A. Investigating how hydrophobic interactions overcome the charge shielding effect by salt cations.

B. Effect of the charge shielding effect on the Mw and radius distributions of polymer solutions.

C. Effect of hydrophobicity dependent polymer conformations on the polymer injectivity in the Bentheimer Sandstone (consolidated) and sand pack (un-consolidated)

Chapter 2: Characterization of Co and Post Hydrolyzed PAM molecular weight and radius distribution under saline environment

2.1 Abstract

The structural changes in the hydrolyzed polyacrylamide (PAM) under different saline conditions show significant effects on the rheological properties. At the higher shear rates, these conformational changes cannot be discerned in the shear rheological field but the extensional rheology can probe the polymer's microstructure can provide a better description. In this paper, two types of polymers: co-hydrolyzed polyacrylamide (PAM) and post –hydrolyzed PAM were tested under different saline conditions. The polymer conformation results were interpreted to ascertain the underlying mechanisms of polymer and cation interactions and their effect on the extensional properties. The results showed that the interactions of polymer chains with divalent cations lead to the formation of the cross-linked chelating structures corresponded to the narrow Molecular Weight Distribution (MWD) with a lower radius of Gyration (R_g). However, the uniform carboxylate ion density across the co-hydrolyzed PAM restricted shrinkage of the polymer chains after interactions with cations showed the high strain hardening due to polymer chain entanglement at high Hencky strain. Whereas, monovalent cation interactions with the carboxylate groups resulted in the monodentate structures that sustained the broader molecular weight distribution that explains the observed higher strain hardening and extensional relaxation time.

2.2 Introduction

Partially hydrolyzed polyacrylamide (HPAM) and its derivatives have a variety of applications mainly as a viscosity modifier, flocculent, soil conditioning agent, Enhanced Oil Recovery (EOR) fluid, wastewater treatments, and agriculture applications respectively[34], [61]–[66].

Under various environments, an increase in the degree of hydrophilicity may increase the mobility of polymer molecules result in viscosity reduction [67]. The efficiency of HPAM can be evaluated based on changes in its physicochemical properties under different process conditions. Interactions of hydroxyl groups in HPAM with various cations may cause chemical degradation of polymer that results in chain scission. The rate of Fenton reaction, responsible for generating carboxyl radical can be accelerated at high temperature and high salinity environment[68]–[70]. The chemical transformations are shown in Figure 2.1. Electric double-layer and thick hydration layer formation up on HPAM dissolution of HPAM in deionized water cause swelling of HPAM molecules result in a higher viscosity of the solution. Interactions of these swelled molecules with different cations reduce electrostatic repulsion (or Coulomb repulsion) between COO^{-} and cause hydration layer thinning. As a result, the size of HPAM molecules may change depending on the potential of interaction as a function of the valency of cations. Figure 2.1 shows the interaction of Na^{+} and Ca^{2+} with $–COO^{-}$. Shielding electrolyte effect caused by cations results in shrinkage of the molecule from the extended coil to collapsed coil structure responsible for the viscosity reduction of solution[70], [71]. At high temperatures, the degree of hydrolysis can be accelerated by the iridization of amide groups and hence polymer loses its stability. Also, higher salt content can catalyze hydrolysis more rapidly[72]. Also, degradation of HPAM is more pronounced in the presence of divalent cations than monovalent[73].

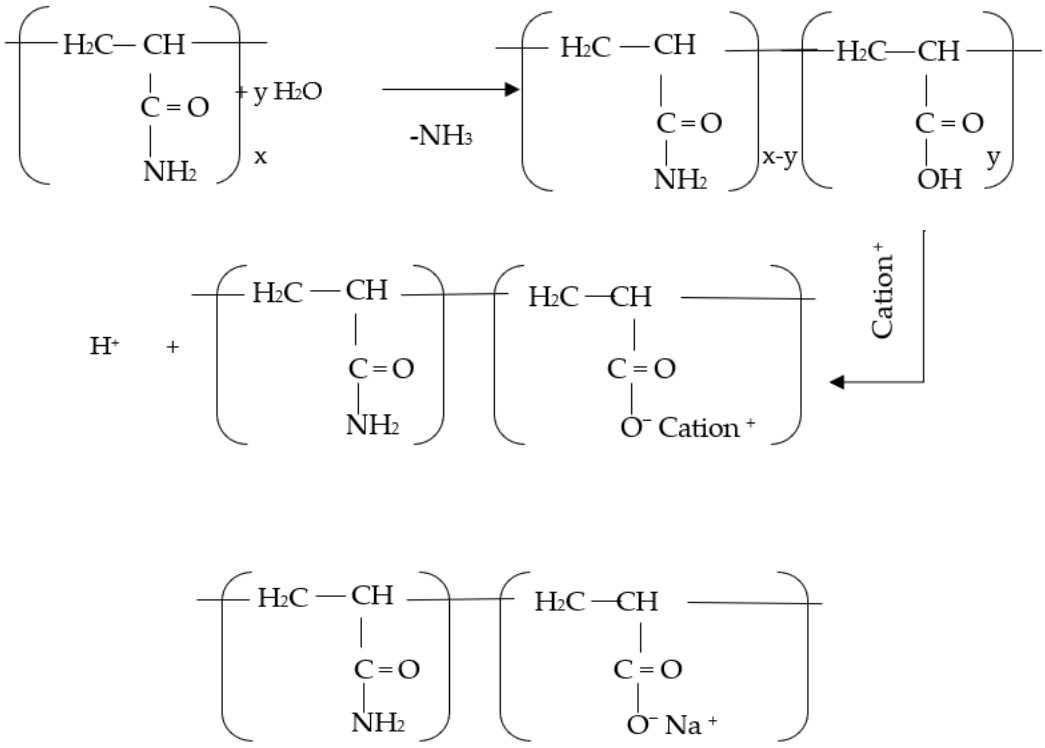

Figure 2.1.1 Interaction of Na^+ with $–COO^-$

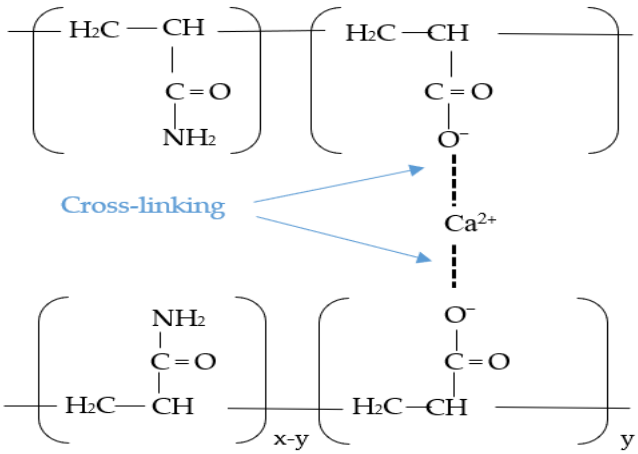

Figure 2.1.2 Interaction Ca^{2+} with $–COO^-$

Figure 2.1 Interaction of HPAM molecule with cation

On the other side, mechanical degradation occurs when the polymer is subjected to a high flow rate, or turbulent flow through narrow pores at high shear and elongational rates as shown in Figure 2.2. HPAM molecules persist in the coil structure because drag force from the fluid flow is not able to overcome entropic force at the low flow rate condition and so constant intrinsic viscosity can be considered equal to zero shear viscosity (ZSV). At high drag due to high flow rate, these coil structures extricate and aligned completely. Due to high orientation (amorphous structure), they will start to starch under high hydrodynamic forces from fluid flow. The chain structure of a polymer may break where the flow regime changes from extensional to shear. These chains face maximum elongational stress at pore-throat[74]–[76], and most likely rupture near the midpoint[77]–[79]. This phenomenon cause change in viscoelastic properties of HPAM solution may be governed by the change in Molecular Weight Distribution (MWD), not by average molecular weight. The pure shear flow of polymer through valves, pumps, and chokes can cause minimum mechanical degradation may result in minimum chain scission [80]–[82].

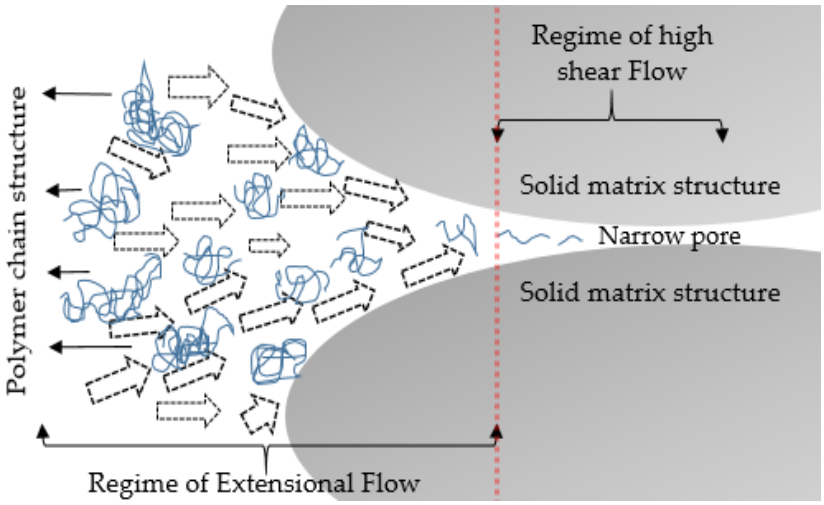

Figure 2.2 Mechanical Degradation of polymer subjected to high shear and elongational rates

Degradation summaries structural changes of HPAM regardless of the type of degradation. These structural changes can be justified by determining the change in MWD, the radius of gyration (R_g), and extensional properties of HPAM solutions. This paper addresses a brief study to understand structural changes in polymer chains while interacting with cations of different valencies. Conventional Gel Permeation Chromatography (GPC) restricts MWD measurements for ultra-high molecular weight polymers (such as HPAM) due to clogging of the column, agglomeration, and shear degradation. Also, pre-filtering of the polymer sample may remove molecules with higher molecular weight, results in inaccurate measurements. Their problems can be resolved by using asymmetrical-flow field flow fractionation (AF4) system. Inline attachments of static Multi-Angle and Dynamic Light Scattering detector (MALS) and Refractive Index (RI) detector can enable accurate measurements for concentration, absolute molar mass (Mw), and sizes of molecules (Rg). Additionally, these results can confirm structural changes observed during Fourier-Transform Infrared Spectroscopy (FTIR)spectrums. A study to understand the effect of brine containing various salts with varying concentrations on polyacrylamide (PAM) was performed by Uranta et al[83]. However, a combined study to understand the effect of ion specificity on the structural changes of co-hydrolyzed and post – hydrolyzed PAM solutions using AF4-MALS-RI and FTIR have not been studied.

Viscoelastic behavior of pure polymer solutions and blends were studied to establish property correlations with a change in MWD[84]–[86]. In general, many studies were performed to understand the change in shear behavior with molecular interactions[87]–[89]. However, it is important to understand extensional behavior than shear properties of polymers in the case of polymer flow through the porous media, polymer extrusion, and film boiling where polymer solutions with the same shear properties may exhibit different elongational properties[89]–[93]. Besides, two polymer solutions having the same shear properties except extensional viscosities

could result in varying end product properties i.e. cellulose textile fibers with different tenacity and elongation. Therefore, it is important to correlate elastic properties as a function of the MWD of polymer with structural changes. Effect of changes in hydrodynamic radii (Rg) and MWD for HPAM solutions prepared with different salinity was measured using AF4-MALS-RI system, and the corresponding effect on bulk extensional properties was examined by Capillary Breakup Extensional Rheometer (CaBER).

Shear degradation studies have been performed to investigate structure deformation of HPAM or HPAM modified polymers in the presence of different salinities[93], [94]. These studies show that shear degradation cannot be understood well at a higher shear rate as the difference in shear viscosities of HPAM solutions contains different salt types were negligible. The polymer solutions possessing higher shear viscosity will not necessarily possess higher extensional viscosity[95]. That means the mechanism that resists stretching of the polymer chains is very week under the application of shear forces. Therefore, extensional rheology is used in this study to identify the differences in the structural conformation at different salinities. Also, the coil-stretching transition is very well established under the finite extensibility limits cannot be detected by shear flow. Hence, it is important to enlarge the window for extensional measurements to be understood with structural changes in the polymer chains. CaBER capable of generating Hencky strain of up to 10 was used in this work to characterize the extensional viscosity of various solutions.

2.3 Materials and Methods

2.3.1 Chemicals

Polymer-brine molecular interactions were examined by using two types of polymers; Co-Hydrolyzed Polyacrylamide and Post Hydrolyzed Polyacrylamide at different concentrations of

monovalent and divalent inorganic salts; sodium chloride (NaCl) and calcium chloride ($CaCl_2$), respectively. Anionic and water-soluble polymers, co-hydrolyzed PAM, and post –hydrolyzed PAM with specification shown in Table 2.1, were supplied by SNF in the dry powder form Fisher scientific supplied lab-grade NaCl and $CaCl_2$ (with percentage purity ≥ 99.0 %).

Table 2.1. Specification of Polymers from SNF

Polymer-PAM	**Post-hydrolyzed (SNF HPAM 3630)**	**Co-hydrolyzed (SNF HPAM 3630S)**
Hydrolysis in mole %	25-30	25-30
Approximate Molecular Weight (million Dalton)	20	20

2.3.2 Polymer Solution Preparation

Polymer solutions having the total salinity of 1000 ppm and 5000 ppm; were prepared to represent the semi-dilute regime to ensure the absolute value of the degree of entanglements. Firstly, the saline solution was prepared by mixing the desired quantity of specific salt(s) into the deionized (DI) water at room temperature (~20° C). A predefined quantity of polymer; to make up polymer concentration of 2000 ppm, was then gradually added into the saline solution and mixed by continuous stirring until the disappearance of vortex formation. All test solutions were then sealed to minimize oxygen take-up or evaporation of water and left under the low stirring speed of 260 rpm for 24 hours at ambient temperature to avoid mechanical degradation of the long chain of HPAM molecules.

2.3.3 Measurements

All the measurements, AF4, FTIR, and uniaxial extensional rheology were performed at room temperature. Also, the chances of solvent loss during the measurements are negligible because of the very short experimental run time. In AF4, similar to chromatography, the separation takes place by a liquid crossflow across a membrane consist of a trapezoidal spacer as shown in Figure 2.3. This narrow trapezoidal geometry is sandwiched between a top non-porous and a porous plate at the bottom consist of porous frit which acts as an accumulation wall. In general, the accumulation wall usually permeable to eluent and retains particles. Particles/molecules with different sizes and weights face a drag force resulting from the cross-flow and concentration difference against diffusion can be formed. According to Fick's law these results in steady-state distribution with the highest concentration at the wall and decrease exponentially while approaching a higher distance to the accumulation wall. As a result, a parabolic flow profile can be formed by combining various concentration profiles due to the variation in diffusivity associated with different particles. A focus reversed flow is applied to avoid spreading of particles on the channel or to concentrate the molecules in the slender zone. Due to the dependency of elution rate on diffusion coefficient, faster elution corresponds to molecules with small size may exhibit a higher distance from the accumulation wall as shown in Figure 2.3 as a normal elution stage. Exceed molecule size (> 1μm) show a change in retention behavior to Brownian mode where larger particles elute first as shown in steric elution mode in Figure 2.3.

An AF4 system (Postnova Analytics, Landsberg, Germany) was coupled with MALS-PN3621 (Postnova Analytics, Landsberg, Germany) and RI-PN3150 (Postnova Analytics, Landsberg, Germany) detectors. A trapezoidal spacer with a nominal thickness of 350 μm was used to form an AF4 channel with a total area of 34 cm^2. A regenerated cellulose membrane (Z-MEM-AQU-631, RC amphiphilic, Postnova Analytics) having a molecular weight cut off of 10kDa was used

as an accumulation wall. The total sample loop was 50 μL for each separation experiment. To maintain the detector flow rate of 0.5 ml/min, the cross-flow was kept constant at 0.5 ml/min, and the focus flow rate was adjusted automatically to 0.8 ml/min. Sample focusing was continued for 3 minutes to allow sample accumulation and longitudinal diffusion. Flow transition to elution mode was allowed after a transition time of 1 min. Initial sample elution was allowed by keeping a constant crossflow rate of 0.5 ml/min for 2 minutes; then for subsequent 35 minutes, it decreased to 0.1 ml/min by a power decay function with an exponent of 0.3. A constant crossflow rate at 0.1 ml/min was turned on for 15 minutes. The cross-flow was stopped at the end of each run to avoid cross-contamination and measure sample recovery. A combined study on separation principle combined with detectors enables determination of MWD and radius of the eluted fraction by using NovaFFF software (Postnova Analytics, Landsberg, Germany). For the known concentration of polymer solutions, a valve for increment in refractive index was considered as 0.19 for all solutions to determine molecular weight from MALS data. The radius of gyration was determined by using a random coil model based on the average mass distribution within the particle. Also, dropping off the fractograms for the lower scattering angles reduced spurious noise.

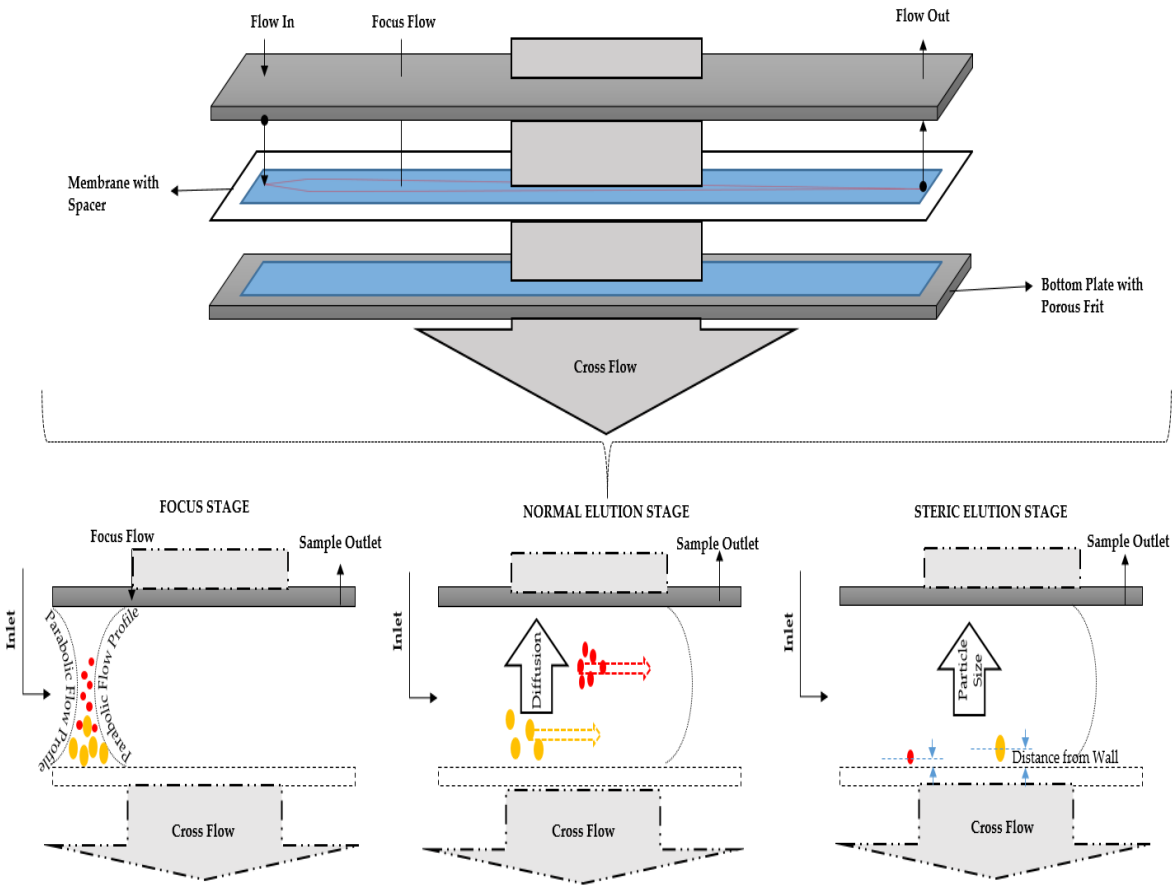

Figure 2.3. Schematic of AF4 principle

Although all solutions prepared with a different combination of salinity were tested in AF4, only eight solutions that showed marked differences in the conformation behavior were selected for comparative studies with FTIR and CaBER focused on ions specificity. FTIR measurements were conducted using an MB3000 (ABB) infrared spectrometer. Transmission responses for all samples were recorded in the spectral range of 400 cm^{-1} to 4000 cm^{-1} with 4 cm^{-1} resolution, 120 scans, and the dictator gain (DTGS) of 9.06.

The polymer solutions were tested with CaBER (ThermoFisher HAAKE 1). Samples were filled between two plates (2mm apart) and then subjected to the Hencky Strain of 1.2 applied by lifting the upper plate to 6.5 mm within 50 milliseconds. All measurements were done at ambient

temperature. The filament is formed whose drainage is governed by the balance between the driving capillary force and resisting viscous and elastic forces. The filament diameter was monitored by the laser micrometer as a function of time for all eight solutions.

2.4 Results and Discussion

2.4.1 AF4 measurements to determine structural changes in HPAM molecules

The results show a significant effect of the valency of cation on the MWD and radius of gyration depending on the type of polymer. Also, the Polydispersity Indexes show that the solutions were mono-dispersed. Table 2.2 summarize average molar masses; number average molecular weight (M_n), weight average molecular weight (M_w), Z-average molecular mass (M_z) and Radius of gyrations; number average (R_n), weight average (R_w), Z-average (R_z)for post-hydrolyzed PAM under various salinity environment.

Table 2.2 Average molar mass and radius of gyration for 2000 ppm post-hydrolyzed PAM under different salinity environment

Solutions	M_n MDa	M_w MDa	M_z MDa	R_n (nm)	R_w (nm)	R_z (nm)	PDI	Slope of Conformational Plot
post-hydrolyzed PAM+ 1000 ppm NaCl	15.56	19.81	24.49	326.4	368.7	407.3	1.27	0.573
post-hydrolyzed PAM+ 1000 ppm $CaCl_2$	11.10	11.99	13.04	212.9	222.4	233.1	1.08	0.509
post-hydrolyzed PAM+ 500	13.58	14.74	11.10	259.8	272.3	285.1	1.09	0.528

ppm NaCl + 500 ppm $CaCl_2$								
post-hydrolyzed PAM+ 5000 ppm NaCl	9.98	13.58	17.12	267.8	317.2	359.4	1.36	0.516
post-hydrolyzed PAM+ 5000 ppm $CaCl_2$	8.55	8.71	8.87	140.9	142.1	143.3	1.02	0.467
post-hydrolyzed PAM+ 2500 ppm NaCl + 2500 ppm $CaCl_2$	9.34	9.58	9.78	160.1	162.4	164.1	1.03	0.478

A thick hydration film and an electrostatic double-layer consist stern and diffusive layer may have formed when HPAM is dissolved in deionized water. As a result, HPAM molecules swell and increase in the hydrodynamic volume. The presence of cations may extinguish electrostatic repulsions may compress hydration film around COO^- groups result in shrinkage of polymer molecules. Regardless of the type of salt, the average molar mass and radius of polymer molecules were found to be decreased with an increase in salinity. However, it is important to compare polymer solutions prepared with the same salinity but different salt types to study the impact of ion specificity on polymer conformations. At the same salinity (1000 ppm), shifting from monovalent to divalent cation salts, the average molar mass (M_n)and radius of gyration (R_g) decreased from 15.56 M g/mol and 326.4 nm to11.10 M g/mol and 212.9 nm, respectively. Intra and/or inter crosslinking of polymer chains under influence of Ca^{2+} may cause additional coiling of polymer chains and reduce M_n and R_g. Conversely, at high salinity (5000 ppm), the effect of salt type on the M_n increased but R_g decreased further from 267.8 nm to 140.9 nm. This

significant diminution in R_g may not be just due to the shielding of electrostatic repulsion but also because the density charge around macromolecule structure increased as shown in Figure 2.4. At higher salt concentration (5000 ppm), after saturation of COO^- groups with cations, numbers of total ions in the case of $CaCl_2$ may cause additional shrinkage of polymer molecule without affecting the molecular weight.

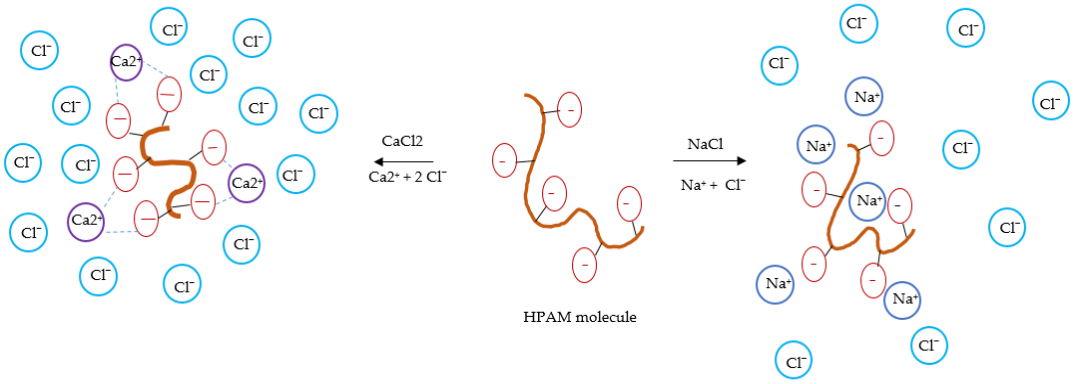

Figure 2.4 Charges distribution around HPAM molecules under different salinity conditions

The variation in molar mass and radius of gyration for post-hydrolyzed PAM as a function of cation type and concentration are shown in Figures 2.5 to 2.8. At the same brine salinity, distribution curves of the radius with bimodal peak values show a cross-linking behavior in the presence of divalent cations (without Na^+ ions) as shown in Figure 2.8. Besides, these distributions are broader for the solutions prepared with 1000 and 5000 ppm NaCl compared to the solutions prepared with 1000 and 5000 ppm $CaCl_2$ respectively. An increase in the Ca^{2+} concentration from 500 to 5000 ppm makes cumulative radius distributions steeper with the higher value of differential fraction as shown in Figure 2.7. These may be since the steric effects

are more dominant over the electrostatic repulsions in the presence of divalent ions and could cause agglomeration of polymer molecules.

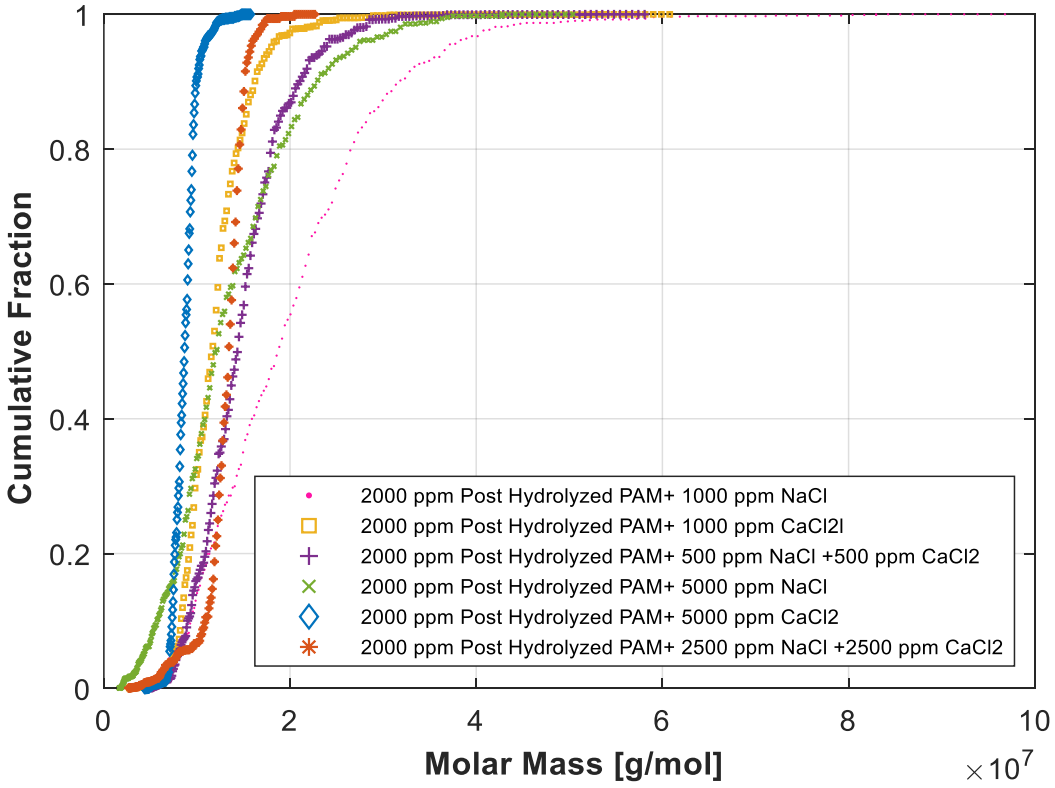

Figure 2.5 The cumulative molar mass of post-hydrolyzed PAM

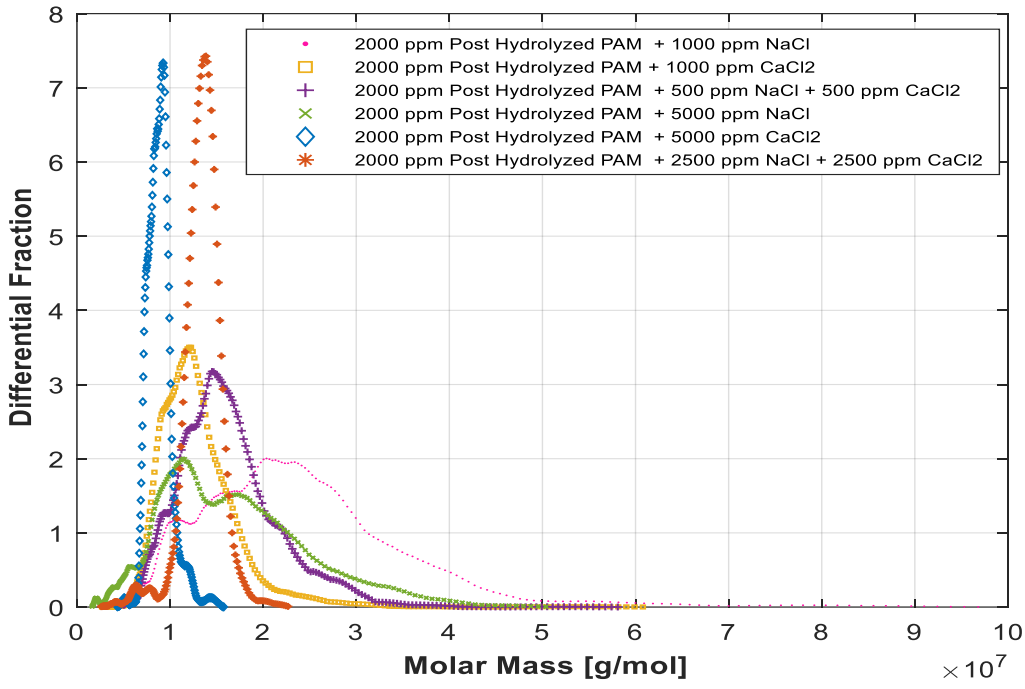

Figure 2.6 The differential molar mass of post-hydrolyzed PAM

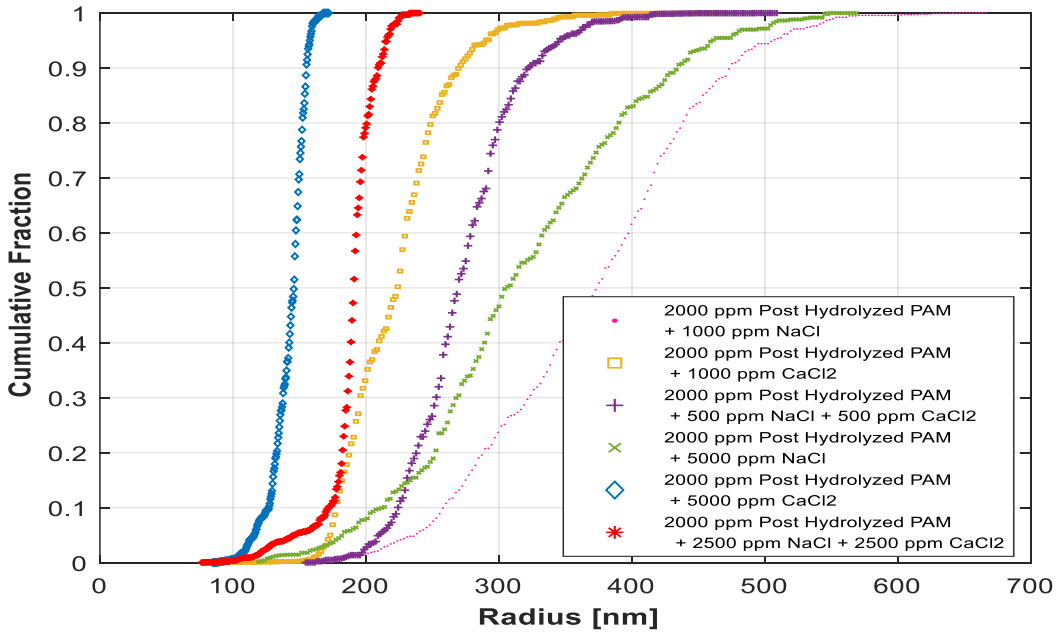

Figure 2.7. The cumulative radius of post-hydrolyzed PAM

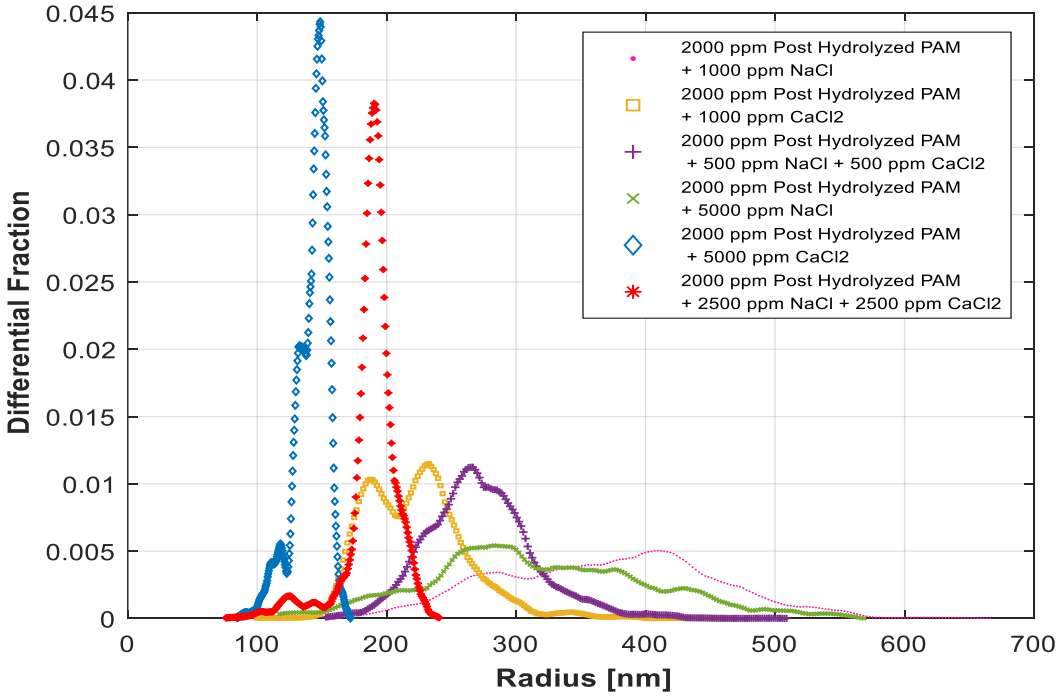

Figure 2.8 The differential radius of post-hydrolyzed PAM

Table 2.3 summarize average properties changes of co-hydrolyzed PAM under different salinity conditions. For all salt concentrations, the type of salt does not show a significant effect on average molar mass while a considerable drop in radius was observed. At the salinity of 1000 ppm, this phenomenon is slightly different from what was observed in the case of post-hydrolyzed PAM. The difference in the distribution of active groups on HPAM may vary according to the manufacturing scheme and so the scheme of interaction of cations may differ according to polymer type as shown in figure 2.9. The charge density of cations on the polymer backbone may affect the magnitude of intra- and inter-molecular DLVO (Derjaguin–Landau–Verwey–Overbeek) forces. Co-hydrolyzed PAM exhibits a constant cation density on each polymer backbone due to the uniformly available active sites across the chain length. The

constant charge density may cause a similar extent of shrinkage and hindrance of polymer molecules and so similar values for molar masses were observed at the salinity tested in this study regardless of the type of cation. Higher values for the M_n and R_g for solutions of co-hydrolyzed PAM in 1000 ppm $CaCl_2$ and 5000 ppm $CaCl_2$ compared to those for the post-hydrolyzed PAM show high divalent salt tolerance of co-hydrolyzed polymer.

Table 2.3 Average molar mass and radius of gyration for 2000 ppm co-hydrolyzed PAM under different salinity environment

Solution	M_n MDa	M_w MDa	M_z MDa	R_n (nm)	R_w (nm)	R_z (nm)	PDI	Slope of Conformational Plot
co-hydrolyzed PAM+ 1000 ppm NaCl	14.96	18.54	20.2	322.6	361.6	395.2	1.24	0.638
co-hydrolyzed PAM+ 1000 ppm $CaCl_2$	15.28	18.42	21.49	223.5	248.2	270	1.21	0.574
co-hydrolyzed PAM+ 500 ppm NaCl + 500 ppm$CaCl_2$	14.32	18.82	23.9	248.1	286.1	324.3	1.31	0.573
co-hydrolyzed PAM+ 5000 ppm NaCl	10.85	11.43	12.01	200.7	207.3	213.9	1.05	0.536
co-hydrolyzed PAM+ 5000 ppm $CaCl_2$	10.47	10.75	10.97	175.4	178.4	180.3	1.03	0.515
co-hydrolyzed PAM+ 2500 ppm NaCl + 2500 ppm $CaCl_2$	10.50	11.03	11.65	196.3	200.1	190.8	1.05	0.530

Figures 2.10 to 2.13 show the distribution of molar mass and gyration radius for co-hydrolyzed PAM at different salinity scenarios. Cumulative fraction curves were steeper for a total salt concentration of 5000 ppm than 1000 ppm. On the other side, differential mass distribution was broader in the case of Na^+ions. High salt tolerance was observed for co-hydrolyzed PAM and uniform interactions may narrow the distribution of R_g compared to post-hydrolyzed PAM especially in the case of Na^+cations. R_g values decreased with increasing the concentration of $CaCl_2$. For co-hydrolyzed PAM in 1000 ppm brine salinity, the number average value of R_g was 322.6 nm in the presence of NaCl which was reduced to 248.1 nm in $CaCl_2$ brine. The effect of $CaCl_2$ was less severe at 5000 ppm versus NaCl as the difference of R_g was ~25 nm.

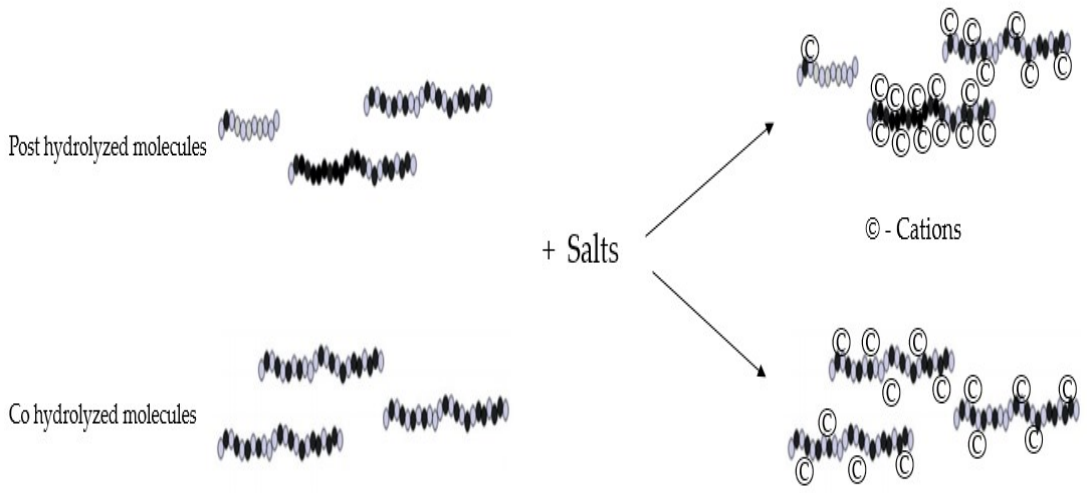

Figure 2.9 cation attachments with a different type of polymer molecules

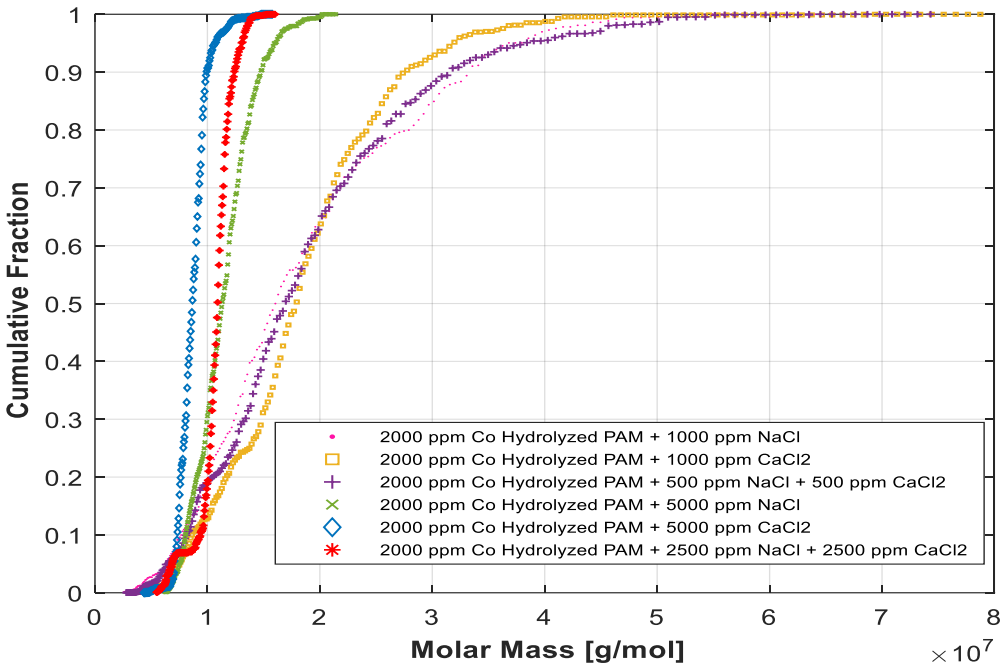

Figure 2.10 The cumulative molar mass of co-hydrolyzed PAM

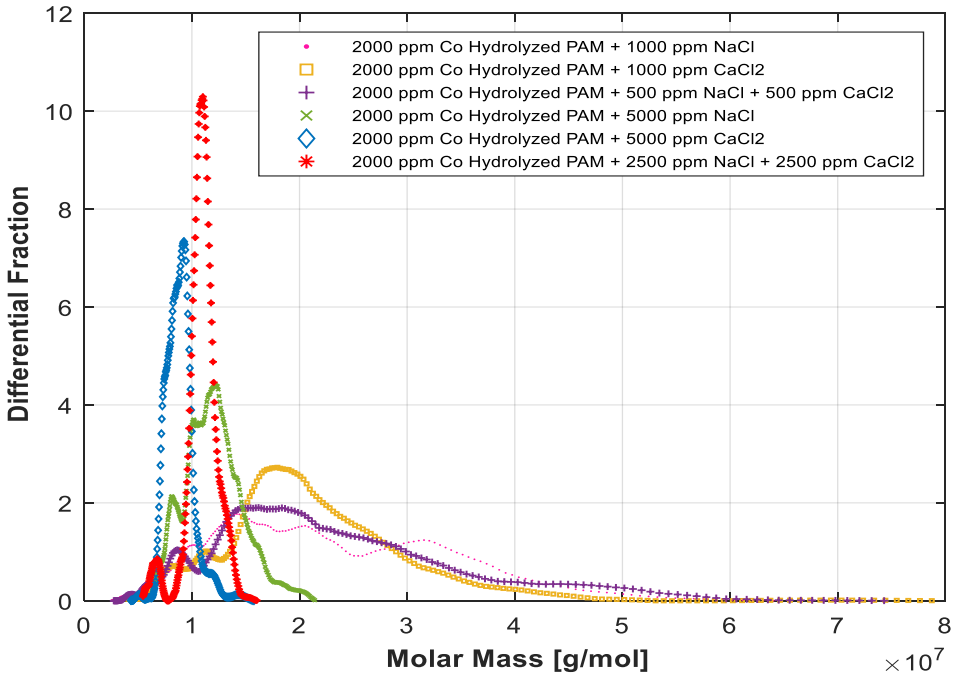

Figure 2.11 Differential molar mass of Co-hydrolyzed PAM

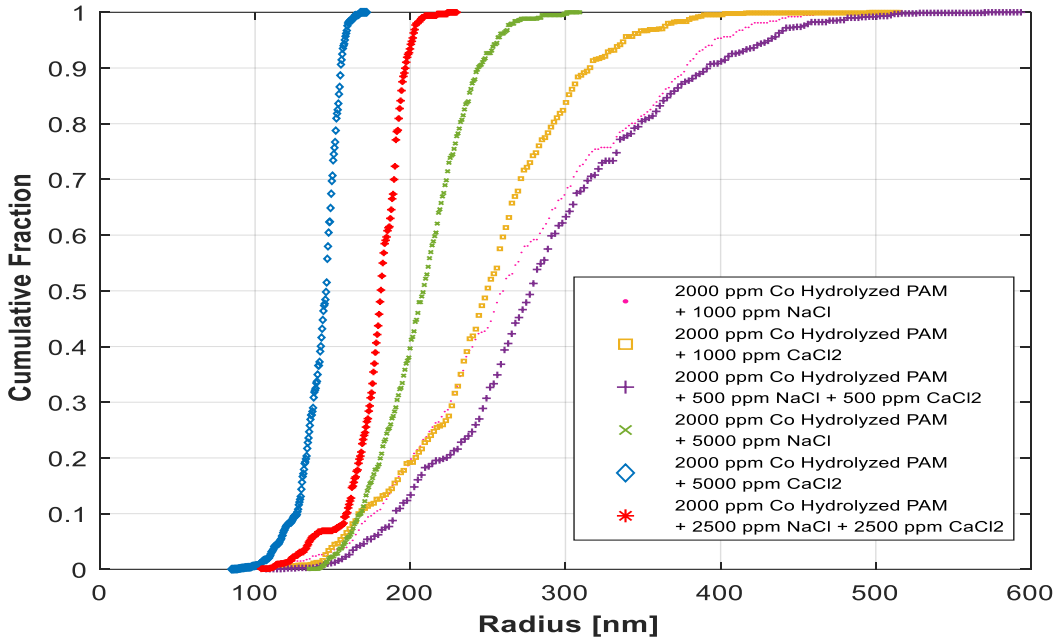

Figure 2.12 The cumulative radius of co-hydrolyzed PAM

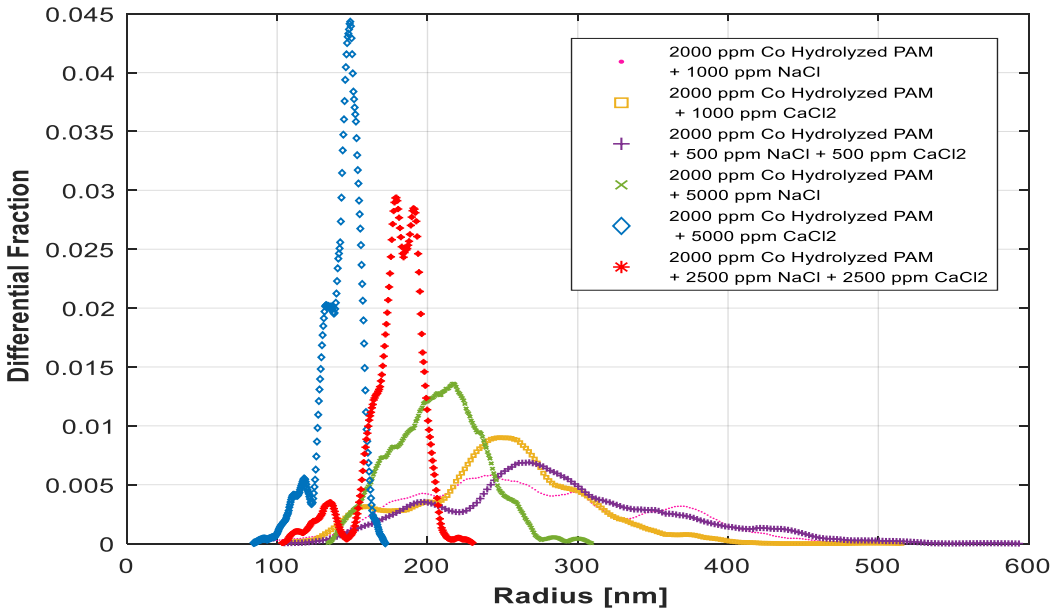

Figure 2.13 Differential radius co-hydrolyzed PAM

Size approximation of polymer chains present in different salinity environments is shown in Figures 2.14 and 2.15. All data points were fitted linearly and the slope of each series is mentioned with the corresponding solution. Depending on polymer type, the value of the slope of each series (Log M vs Time) increases with $CaCl_2$ concentration indicate effective shrinkage of polymer chain compared to the same NaCl concentration. Interestingly, these shrinkages were very effective at 1000 ppm and became more identical at 5000 ppm irrespective of salt type. These may be due to triumphing maximum intramolecular force regardless of ion type and so an increase in the charge density may lead to the precipitation of the polymer. On the other side, slope values in conformation plots shown in Figures 2.16 and 2.17; changes from ~0.5-0.6 indicate random coil structure of polymer chains. The decrease in the slope at 5000 ppm confirms compact or branched-chain structures. Ca^{2+} ions show a significant effect on polymer conformation as the value of the slope is lower in the case of $CaCl_2$ compared to NaCl at the same salt concentration. This may indicate bridging bidentate attachment of Ca^{2+} with two polymeric chains.

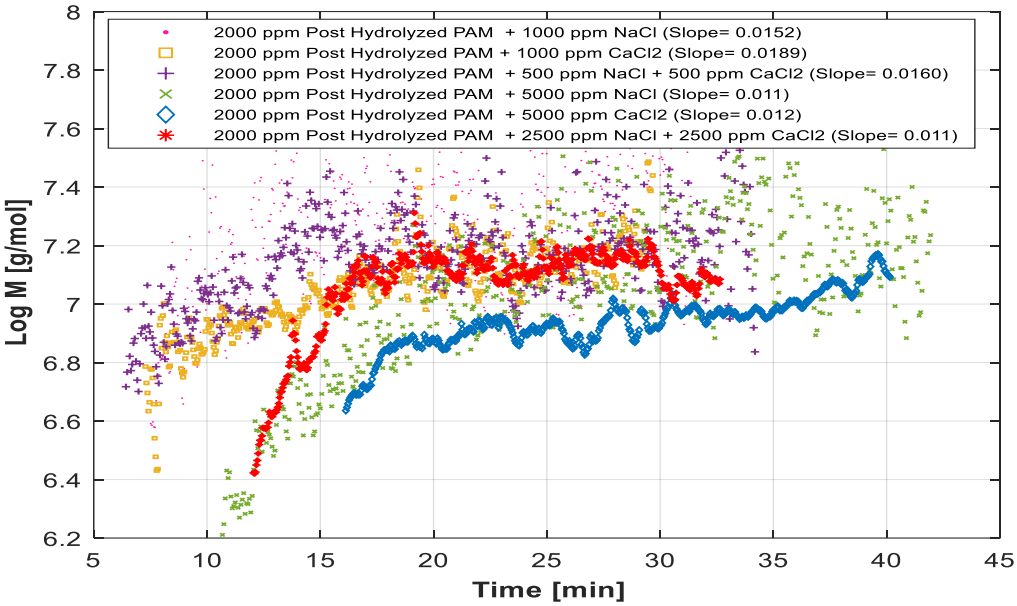

Figure 2.14 The molecular weight of post-hydrolyzed PAM

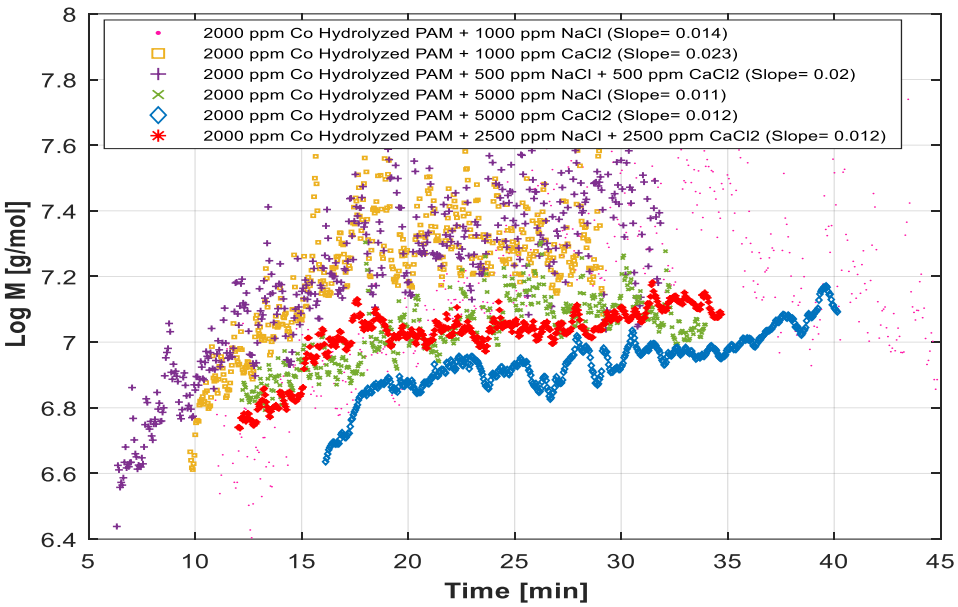

Figure 2.15 The molecular weight of co-hydrolyzed PAM

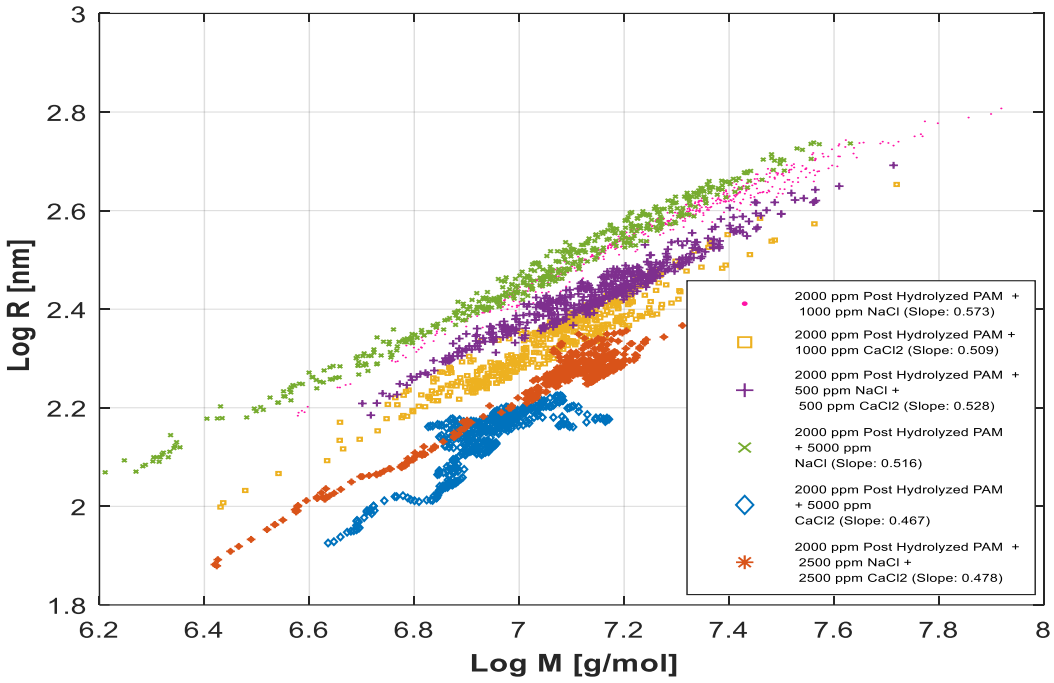

Figure 2.16 Conformation plot for post-hydrolyzed PAM

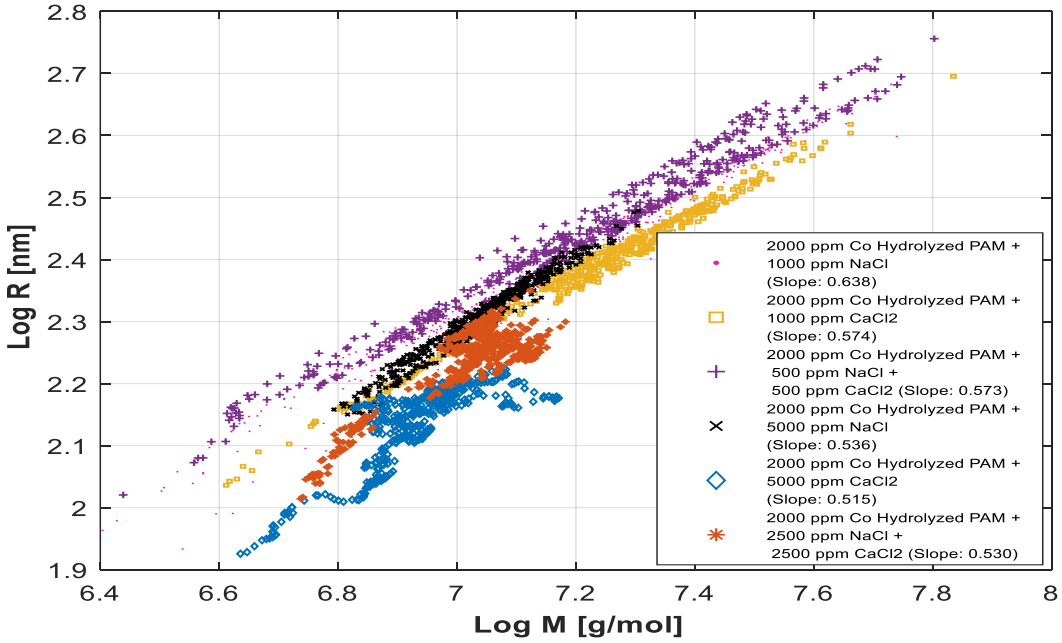

Figure 2.17 Conformation plot for co-hydrolyzed PAM

2.4.2 FTIR measurements to understand molecular interactions

The degree of hydrolysis of amide groups to carboxylate groups result in stretching of secondary amide can be quantified by FTIR analysis [82], [96], [97]. Understanding the interactions of individual salt with co- or post- hydrolyzed PAM provide insight into structural changes that could be useful for the selection of polymer type and concentration under different salinity environments. Interaction between COO^{-} with different metal ions can result in four different modes of attachments: 'monodentate', 'chelating', 'bridging bidentate', and 'pseudo bridging' [97], [98] as shown in Figure 2.18.

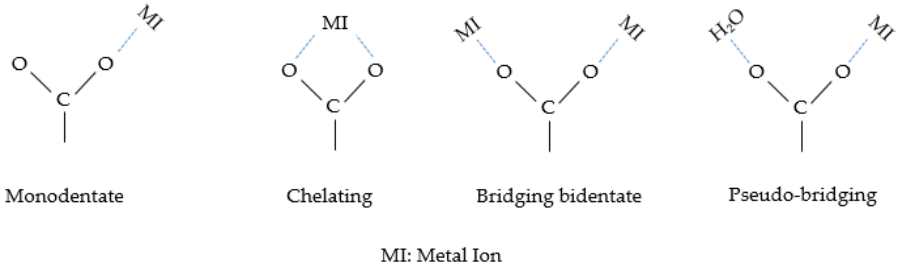

Figure 2.18 Coordination structures of COO^{-} with metal ion

Figure 2.19 shows the FTIR characterization of HPAM in DI water and brine. For all solutions, two major peaks were found at around 3250 $cm^{-1}$and 1630 cm^{-1} correspond to deformation mechanisms associated with N-H starching vibration and C=O starching vibration subsequently. Specifically, a band at 1630 cm^{-1} corresponds to asymmetric starching of the COO^{-} group. A very low intensity of peaks around the frequency 1697 cm^{-1} in the presence of $CaCl_2$ indicate Ca^{2+} ions in chelating mode[97], [99]. These attachments result in the screening of double layer that may cause effective shrinkage of polymer molecules and reduce average molecular weights compared to Na^{+} ions. Also for the asymmetric starching of COO^{-}group, $(\Delta\nu_{a\text{-}s})_{Na^{+}} > (\Delta\nu_{a\text{-}s})_{Ca2+}$ may confirm the unidentate mode of the interaction between Na^{+}ions and carboxylate groups.

The strong transmissions around 1200 cm^{-1} and 1400 cm^{-1} in the fingerprint region were assigned to CH_2 scissoring and angular distortion of CH_2. Interestingly, these peaks were only appeared in the case of divalent interactions with co hydrolyzed PAM whereas, for post hydrolyzed PAM, these intensities have appeared irrespective of salt type. Hence, effective shrinkage was observed in the case of post hydrolyzed PAM at similar salt conditions as shown in Tables 2.2 and 2.3.

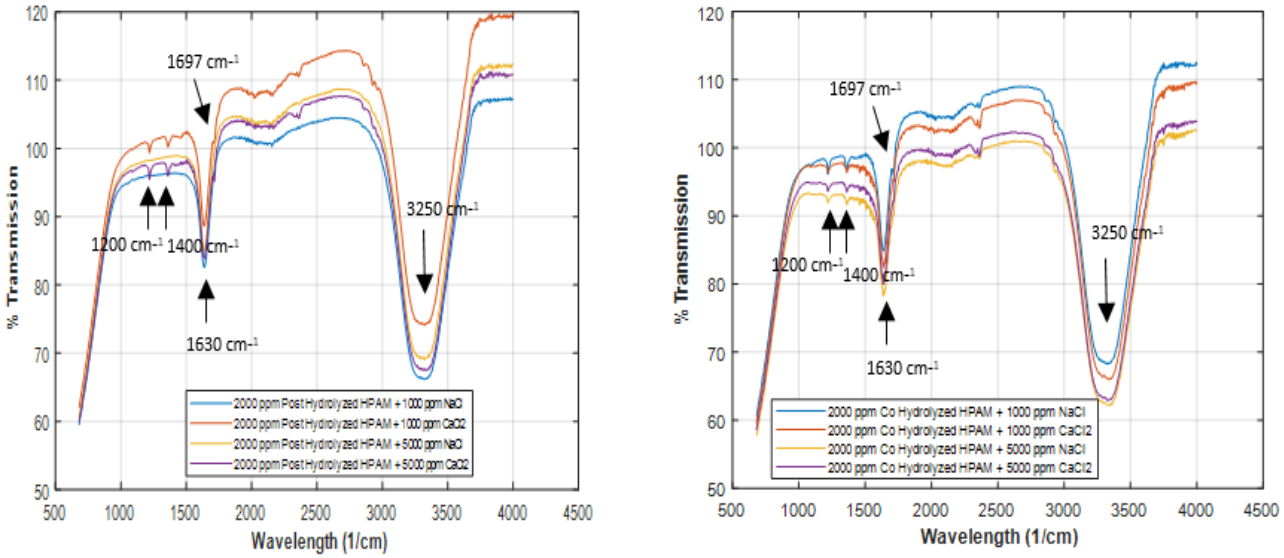

Figure 2.19 FTIR spectra of polymers under different brine concentrations

2.4.3 Effect of structural changes on extensional viscosity measurements for HPAM saline solutions

Figure 2.20 and Figure 2.21 show filament diameter as a function of time and extensional viscosity as a function of Hencky strain for all the right solutions. The relaxation time was determined using Upper Convected Maxwell (UCM) model by performing the linear fit to the filament diameter vs time data on a semi-log plot for all the solutions[74]. Solving the slope factors, the average values of relaxation time were calculated as shown in Table 2.4 by considering the surface tension of water as 72 mN/m.

Table 2.4 Relaxation time for 2000 ppm polymer solutions with varying salinity conditions

Solutions	Total Salinity (ppm)	Relaxation Time (s)
Post-Hydrolyzed PAM + 1000 ppm NaCl	1000 (NaCl)	0.3229
Post-Hydrolyzed PAM + 1000 ppm $CaCl_2$	1000 ($CaCl_2$)	0.1220
Post-Hydrolyzed PAM + 5000 ppm NaCl	5000 (NaCl)	0.1616
Post-Hydrolyzed PAM + 5000 ppm $CaCl_2$	5000 ($CaCl_2$)	0.0595
Co-Hydrolyzed PAM + 1000 ppm NaCl	1000 (NaCl)	0.4833
Co-Hydrolyzed PAM + 1000 ppm $CaCl_2$	1000 ($CaCl_2$)	0.1970
Co-Hydrolyzed PAM + 5000 ppm NaCl	5000 (NaCl)	0.3156
Co-Hydrolyzed PAM + 5000 ppm $CaCl_2$	5000($CaCl_2$)	0.08490

The elongational behavior affected by the flexibility of chains can be linked with extended polymer coiling. The shapes of the exponential decay show difference in the extended coiling structure of polymer chains in the different saline environments. Results show effective coiling of the polymer chains in the presence of calcium ions for the case of post-hydrolyzed PAM.

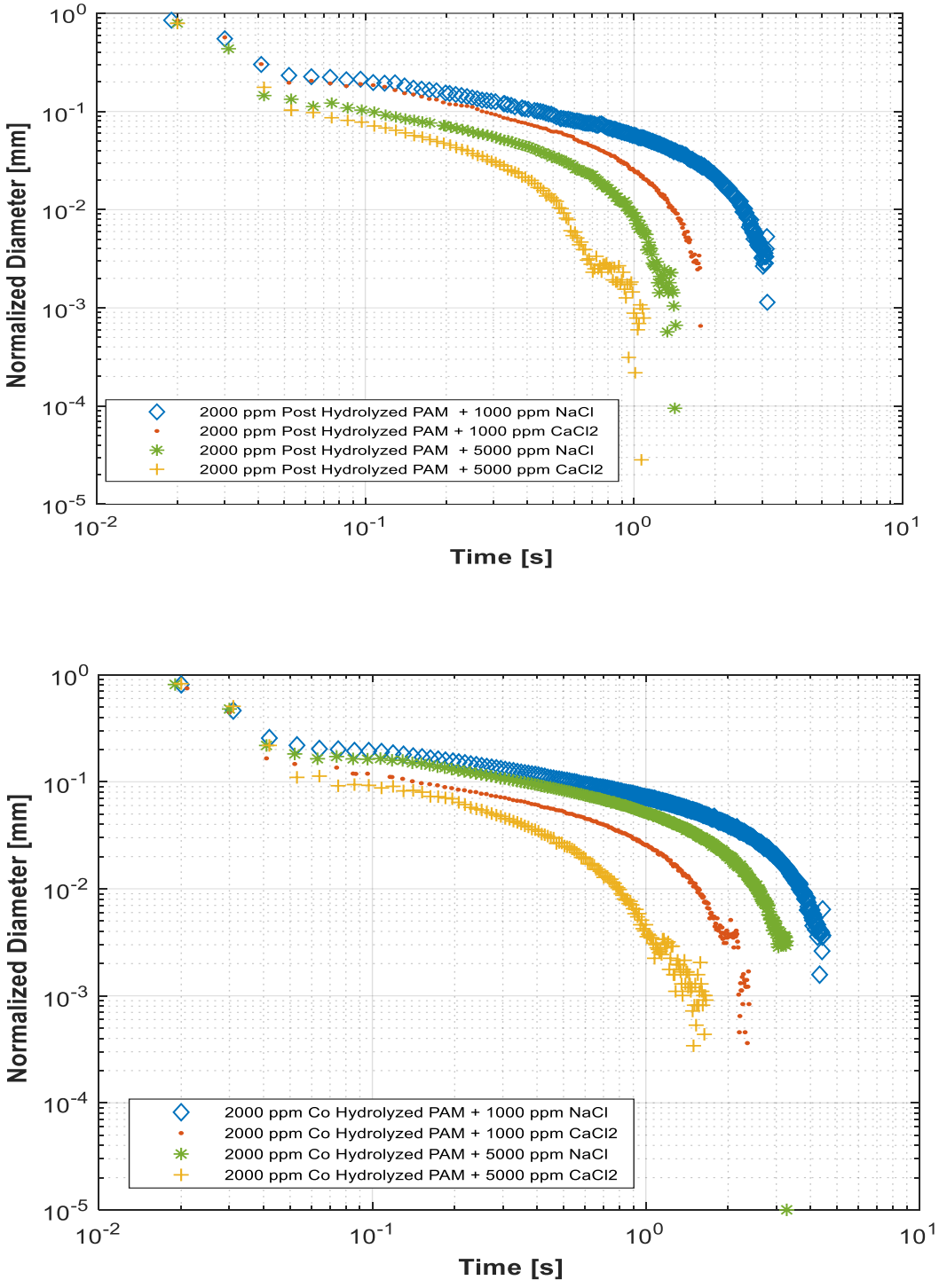

Figure 2.20 Normalized filament diameter vs time

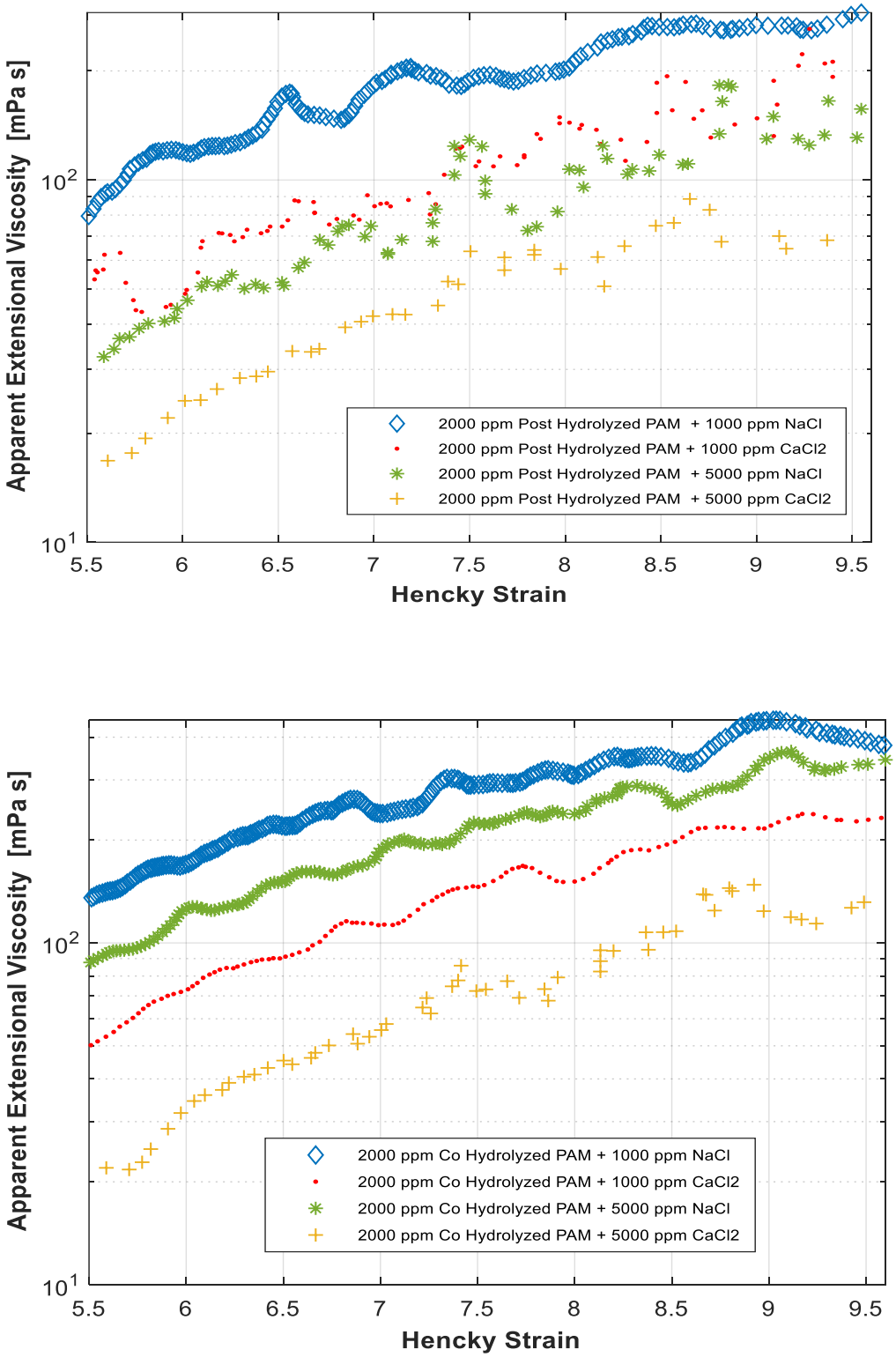

Figure 2.21 Straining hardening of polymers under saline environments

As shown in Table 2.4, relaxation time and apparent viscosity decrease with an increase in the salinity irrespective of polymer type. Comparing post-hydrolyzed and co-hydrolyzed PAM, the relaxation time for co-hydrolyzed polymer was higher for the salinity tested here. Relaxation time for the co-hydrolyzed PAM decreased from 0.3229 s to 0.1220 s when the brine solution was changed from 1000 ppm NaCl to 1000 ppm $CaCl_2$ whereas the Rg reduced from 322.6 nm to 223.5 nm. Similarly, at 5000 ppm brine salinity, in the presence of $CaCl_2$ Relaxation time decreased from 0.1616 s to 0.0595 s and R_g from 200.7 nm to 175.4 nm. It is important to note that at both salinity tested here, the change of ions had no significant effect on average molecular weight. However, the MWD of co-hydrolyzed PAM was broader in NaCl brine. In general, broader MWD (Figures 2.6 and 2.11) for the solutions corresponded to higher relaxation time (Table 2.4) and longer breakup time (Figure 2.20) and vice versa for the solutions with the narrow MWD. Therefore, the dominant effect of divalent ions is the increase in the flexibility of polymer due to the shrinkage of chains. Similar observations were made for post-hydrolyzed PAM.

The degree of strain hardening seems dependent on the MWD (a function of salt concentration and ion specificity), and R_g. The broader MWDs (Figure 2.6 and 2.11) and high R_g (Table 2.2 and 2.3) for the Post-Hydrolyzed PAM + 1000 ppm NaCl and Post-Hydrolyzed PAM + 5000 ppm NaCl compared to Co-Hydrolyzed PAM + 1000 ppm NaCl and Co-Hydrolyzed PAM + 5000 ppm NaCl subsequently, corresponds to the lower strain hardening. Whereas, in the presence of the divalent ions, broader MWDs and higher R_g for the co-hydrolyzed PAM + brine solutions correspond to the slightly higher strain hardening as shown in Figure 2.21. These may be due to the uniform charge density of COO^- groups across the polymer chain increases the entanglement between co-hydrolyzed PAM chains after cross-linking. So, the higher strain hardening for the co-Hydrolyzed PAM + 5000 ppm $CaCl_2$ than post -Hydrolyzed PAM + 5000

ppm $CaCl_2$ was observed because the entanglement network can be effectively strengthened during extension at the higher Hencky strain.

2.5 Conclusion

The effect of interactions between polyelectrolytes in the aqueous solution with added salt has been studied by combining polymer conformations with the extensional properties. It was observed that the valency of cation plays an important role along with concentration. The uniform anion (carboxylate groups) density across the polymer chain is a key factor for the polymer-salt interactions. Effective charge screening effect in the presence of divalent ions results in narrow MWD curves with low R_g for both types of PAMs. However, higher Rg values for the co-hydrolyzed PAM in the presence of $CaCl_2$ brine indicate high divalent salt tolerance. Whereas, divalent ions reduced extensional viscosities of PAM solutions efficiently than monovalent ions. The co-hydrolyzed PAM with $CaCl_2$ brine having higher relaxation and breakup times shown higher strain hardening at high Hencky strain. Strain hardening was significant at the high Hencky strain for the co-hydrolyzed PAM with 5000 ppm $CaCl_2$. These could be explained by the decrease in polymer amorphousity due to entanglement between polymer chains. Strain hardening of both polymers, even after interactions with salts; expand its application in the variety of fields such especially for EOR. This study will be expanded to combine density functional theory with the Hofmeister series to study how anion density causes structural changes in the polymer chains.

Chapter 3: Influence of Hydrophobic Association in the aqueous media on the Rheology and Polymer Conformation of Associative Polymers

3.1 Abstract

The concentration and hydrophobicity-dependent hydrophobic associations are responsible for distinct rheological behavior for associative polymers (AP) to prove its application in various industrial operations. In this study, commercially available water-soluble, associative polymers (AP) C319, P329, and D118 with similar weight-average molar masses (Mw) with varying hydrophobicity were characterized by the Field-flow fractionation (FFF) method to determine molecular weight distribution (MWD) and size distribution (Rn), steady shear flow, and the uniaxial elongation in capillary breakup experiments. The domination of intramolecular and intermolecular hydrophobic associations was found to be responsible for the polymer shrinkage (with hydrophobicity) and aggregation (with concentration), respectively. The tumbling of polymer macromolecules under the shear field resulted in a similar shear behavior for all polymers. However, higher shear viscosities due to the formation of polymer aggregates in the semi-dilute regime justify the domination of intermolecular hydrophobic associations. These associations also contributed to broader MWD for polymer solutions having higher relaxation time and extensional viscosity compared to the corresponding solutions in the dilute regime. For C319, the formation of flexible aggregates at 2000 ppm resulted in higher strain hardening compared to 1000 ppm. Whereas, at 1000 ppm the higher entanglements between polymer chains due to the lowest hydrophobicity for C319 resulted in the higher strain hardening. At high hydrophobicity, the coiled structure became rigid due to reduced solvent holding inside the compacted structure formed due to the domination of intramolecular hydrophobic associations.

Therefore the relaxation time and extensional viscosity decrease with an increase in the hydrophobicity in both regimes.

3.2 Introduction

The tunable concentration and temperature-dependent molecular interactions for the associative polymers (AP) allow a user-oriented control of its physical properties. This characteristic alone makes its role valuable as a viscosity modifier in the field of polymer extrusion, textile coating and finishing, inkjet printing, drag reduction, and enhanced oil recovery (EOR); and as a flocculant for wastewater treatments[35], [100], [101]. In paints, higher zero shear viscosity of the polymer solutions is preferred to prevent the settling whereas the lower viscosity at the high shear rates enhances its brush-ability. Also, the right level exponent of decay for viscosity over the shear rates is required to fade the brush marks and hold the coating over the surface. Further away, the pendant hydrophobic network structure serves as a sieving medium for DNA sequencing[35]. Recently, APs of polyacrylamide were tested for their potential applications in the oilfields as an EOR agent due to favorable M and reduced fingering effect that result in efficient flooding, and as a high viscosity friction reducer during hydraulic fracturing. The better polymer flood efficiency mainly depends on the stable displacement due to the remarkably higher viscosity of the injected polymer solution and thereby mobility control. Therefore, the rheological characterization of the polymer solution gives good insights to determine the estimated oil recovery. However, the concentration-dependent polymer architecture and conformation resulting from the molecular attractions play an important role in rheological behavior [102]–[105].

In the dilute regime, intra-molecular hydrophobic associations between attractive groups of the same polymer chains dominate the rheological properties as shown in Figure 3.1[34], [35], [106],

[107]. The associations between end groups lead to the formation of weak reversible physical bonds like hydrogen bonds that result in the partial shrinking or collapse of the polymer chains. So, the resulting lower hydration radius with no intermolecular bonding may result in lower solution viscosity[33], [34], [38], [106]–[111]. Approaching the critical aggregation concentration (CAC), this self-association may cause the aggregation of several polymer chains into a micelle (complex) of different morphologies[35].

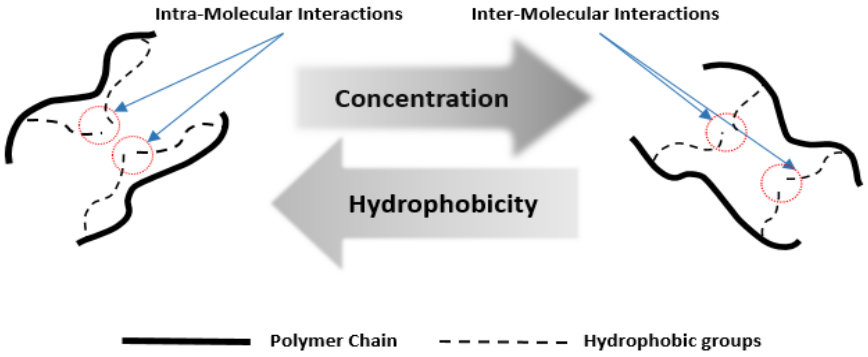

Figure 3.1 Force domination during hydrophobic molecular interactions

In the semi-dilute regime or above the CAC, a transient network between the polymer chains can be formed by the intermolecular association on top of pre-existing Van Der Waals forces. These networks may induce the aggregate formation and so rheological behavior[31], [32], [35], [104]. However, these flexible aggregates contribute to the higher extensional resistance due to the stabilization of starched coiled polymer chains under the strong extensional flow[30]. Also, the reversible bridging among polymer chains reduces its affinity to the aqueous medium and shows an indication of balance between phase separation and intermolecular hydrophobic interactions[30], [32], [35]. Further, in the concentrated regime; strengthening molecular interactions may cause phase separation in the system. On the other side, the intramolecular interactions dominate as the hydrophobicity increases. So, at the higher hydrophobicity, the

effective polymer coiling may change the polymer conformations. This behavior is identical for both, dilute and semidilute regimes.

The flow of polymer solution through the porous media which is made up of converging and diverging flow paths is subjected to deformations due to both, shear and extensional forces[58], [92], [93], [112]–[117]. Higher magnitude (10^1-10^2 times the thermal energy *kT, k*: Boltzmann constant, and *T*: absolute temperature) of these forces are unable to break the molecular attractions resulting in the shear thinning behavior in the porous media. This could result in a higher pressure drop and flow instability. Generally, APs are characterized by ultra-high molecular weight (Mw) to achieve high viscoelasticity. Technically the polymers dissolved in the solvents do not exhibit a single monodisperse molecular weight. Therefore the Molecular Weight Distribution (MWD) gives better insights into the molecular characteristics of polymer chains in the solvent. In addition, the higher ends of MWD and Rg predict the gel formation behavior that may cause poor injectivity or reservoir blockage. At the higher Weissenberg number, the MWD and polymer conformations causing the time-dependent elastic instabilities have been not explored well [105] However, the consequences of the overlooked effect of extensional forces [118] on the EOR were justified where the effect of shear forces was negligible [56]. In general, the importance of determining the conformational changes affecting the extensional behavior only gets attention in industrial processes like polymer extrusion and film boiling where the shear behavior can not reveal the property correlations [27]. The APs of different hydrophobicity but similar shear rheology with different conformations may result in disparate extensional behavior. Hence, understanding the hydrophobicity-dependent conformational or structural changes provide a better understanding of its flow through porous media. Where the conventional characterization techniques like GPC (Gel permeation chromatography) or SEC (Size-exclusion chromatography) have operability limits for high Mw

polymers, Coupling the AF4 with Multi-Angle Light Scattering (MALS) and Differential Refractive Index (dRI) measurements can provide useful information on the structural behavior of polymer in the aqueous media. So in this study, all-polymer solutions were characterized using AF4-MALS-dRI to determine the molecular weight and size distributions to gain structural information. Since all polymers have been synthesized (by manufacturer) with identical monomers, acrylamide; a single light scattering technique can properly characterize the polymers to gain the structural information because of the same scattering power of the monomer. The subsequent effects of these structural changes on the rheology were characterized by shear and extensional rheometer, CaBER.

3.3 Materials and Methods

3.3.1 Reagents

The associative polymers with different hydrophobicity were obtained from SNF Floerger. The trade names for the samples used here are C319, P329, and D118. These polymers are modified polyacrylamides with a controlled number of hydrophobes on the backbone of polymer chains. The higher number of hydrophobes results in higher hydrophobicity as defined in Table 1. According to the manufacturer, all samples have similar estimated M_w and an ionicity. All other specifications for the polymer samples are listed in Table 3.1. Fisher Scientific supplied lab-grade NaCl (with percentage purity ≥ 99.0 %)

Table 3.1: Specifications of polymers from SNF Floerger

Polymer Name	Polymer Type	Weight-average Molecular Weight (Mw) by the supplier (MDa)	Hydrolysis (% mol)	Hydrophobicity	Anionicity (%) or Hydrolysis in mole %
Superpusher C319	Hydrophobically Associating Polymer (AP)	16-20	25-30	Very Low	30
Superpusher P329	Hydrophobically Associating Polymer (AP)	15-17	25-30	Low	30
Superpusher D118	Hydrophobically Associating Polymer (AP)	16-20	30	Medium	30

3.3.2 Sample Preparation

Polymer solutions with the desired concentrations of 1000 ppm and 2000 ppm in DI water were prepared at room temperature (~20° C) to represent the dilute and semi-dilute regimes respectively. A predefined quantity of polymer was gradually added to the DI water and mixed by continuous stirring at 350 rpm until the vanishing of vortex formation. This allows the dry

polymer powder to disperse uniformly in the DI water. All test solutions were then sealed to minimize the solvent loss through evaporation and left under the low stirring speed of 150 rpm for 24 hours at ambient temperature to avoid mechanical degradation of the long chain of polymer molecules.

3.3.3 Rheology Experiments

Shear Rheology

AR2000 (TA Instruments), with a minimum torque resolution of 0.1 μN·m and displacement resolution of 0.04 μrad was used to characterize the shear behavior of polymer samples at room temperature. The density of 1 $\frac{g}{cm^3}$ was assumed for all polymer samples and the probe volume is 1 mL. A constant sample volume of 0.6 mL and the cone and plate geometry with a 2° steel cone and 40 mm diameter were used to perform the shear experiments.

Extensional Rheology

The uniaxial elongation experiments were performed at room temperature by using CaBER (ThermoFisher HAAKE 1) having the maximum operating Hencky strain of 10. The polymer samples (~ 0.2 -0.3 mL) were placed between two parallel plates (2 mm apart) and then starched uniaxially by applying the Hencky strain of 1.2 (move the upper plate to 6.5 mm within 50 milliseconds).

The viscoelastic solutions and melts follow a rapid initial viscous-dominated phase [119]–[122] followed by a time scale in which the dynamics of filament drainage are governed by a balance of elasticity and surface tension, rather than fluid viscosity. In this regime, the upper-convected Maxwell model was fitted to the experimental data to determine the extensional relaxation time. The surface tension (σ) of 73 $\frac{mN}{m}$ was measured for all polymer samples.

$$D_{mid}\,(t) = D_0(\frac{GD_0}{\sigma})^{\frac{1}{3}}\, e^{\frac{-t}{3\lambda_c}} \tag{3.1}$$

D_{mid}: Mid-point diameter of the filament (mm), D_0: Initial diameter of the loaded sample (mm), λ_c: Characteristic relaxation time (s), G: Elastic modulus (Pa), $[\tau_{zz} - \tau_{rr}]_{total}$: Non-Newtonian elastic stress, $\dot{\varepsilon}(t)$: Hencky strain

The evolution of the midpoint diameter of the polymer samples driven by the capillary pressure with the extensional resistance stress can be represented in the terms of the apparent extensional viscosity (defined as given in Equation 3.2) is maximum around the strain rate of 0.66 [121]–[123].

$$\underline{\eta}_{app}(\varepsilon) \cong \frac{[\tau_{zz}-\tau_{rr}]_{total}}{\dot{\varepsilon}(t)} \tag{3.2}$$

3.3.4 AF4-FFF Experiments

The details of the working principle of FFF were explained in the previous publication[27], [28], [56], [119]–[123]. According to the separation principle, the smaller particles are eluted first followed by the larger particles as shown in Figure 3.2. So, the molecular interactions that result in polymer aggregations or associations may be detected in the plots for the differential MWD and Radius distribution as a secondary peak or the changing intensities of peaks.

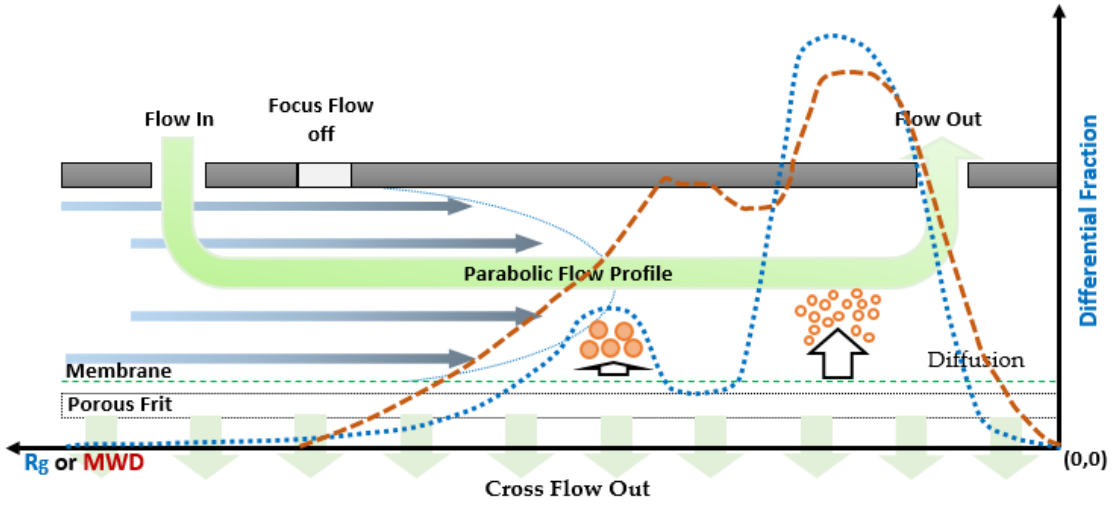

Figure 3.2. Flow scheme of the channel (side view) while eluting

An AF4 system (Postnova Analytics, Landsberg, Germany) was equipped with MALS-PN3621 (Postnova Analytics, Landsberg, Germany) and DRI-PN3150 (Postnova Analytics, Landsberg, Germany) detector was used to characterize the MWD and Root mean square (RMS) radius (R_n) or R_g of polymer samples. The MALS detector contains a 10-50 mW laser as the light source operating at $\lambda_0 = 532$ nm with twenty-one scattering angles, 7°, 12°, 20°, 28°, 36°, 44°, 52°, 60°, 68°, 76°, 84°, 90°, 100°, 108°, 116°, 124°, 132°, 140°, 148°, 156°, and 164°. The effluent, 100 ppm NaCl; based on the previous studies [10] to characterize the Partially Hydrolyzed Poly-Acrylamide (HPAM) was used for FFF analysis of associative polymers. The selected very lower concentration of effluent also minimizes the chemical degradation of injected polymer samples during the experiments. A regenerated cellulose membrane (Z-MEM-AQU-631, RC amphiphilic, Postnova Analytics) having a molecular weight cut-off of 10kDa was used as a separation channel. The volume of the sample injected was 50 µL for each FFF experiment. The sample accumulation and longitudinal diffusion on the membrane were allowed by adjusting the focus flow rate to 0.8 $\frac{mL}{min}$ for 3 minutes and then the flow transition to elution mode was allowed after

1 minute. The sample elution was allowed by keeping the crossflow rate to 0.5 $\frac{mL}{min}$ for 2 minutes and then allowed to decrease exponentially (with an exponent of 0.3) to 0.1 $\frac{mL}{min}$ over the total duration of 35 minutes. At last, the cross-flow rate was kept constant to 0.1 $\frac{mL}{min}$ for 15 minutes and then stopped to avoid cross-contamination. The $\frac{\partial n}{\partial c} \approx 0.17$ was measured for all polymer samples to determine the number average(M_n) molar mass, the weighted average (M_w) molar mass, and the R_n using the random coil model[28].

3.4 Results and Discussion

3.4.1 Rheological characterization

The AP solutions of 1000 ppm and 2000 ppm were evaluated for the shear behavior as shown in Figure 3.3 [57]. All polymer solutions showed the shear thinning behavior in the range of shear rate of 0.1 s^{-1} to 100 s^{-1}. The viscosity peaks near 0.1 s^{-1} represent the point at which this elastic structure breaks down (yields) and the polymer sample starts to flow. Before these viscosity peaks, the polymer solutions are undergoing elastic deformation where the polymer chains are simply stretching. The polymer chains disentangled to align along the direction of shear and cause shear thinning at the higher shear rates. In the semi-dilute regime, higher shear viscosities due to polymer aggregation for the solutions with the polymer concentration of 2000 ppm indicates the domination of intermolecular interactions over the intramolecular interactions [124]–[126]. The hydrophobic molecular interactions coil the polymer chains that get tumbled under the direction of the shear stress. So, the resulting stress acting on the polymer chains gets canceled[28], [57], [119]–[127]. Hence, the shear-thinning profiles are almost similar at identical concentrations irrespective of the difference in the estimated average molar masses. Therefore, the rotational measurements may not distinguish the behavior of AP solutions in the weak shear

field [127], [128]. However, the coiled polymer chains can be stretched under the uniaxial elongational force. This starched state helps to study the hydrophobic molecular interactions that are intense under the extensional field [129]–[133].

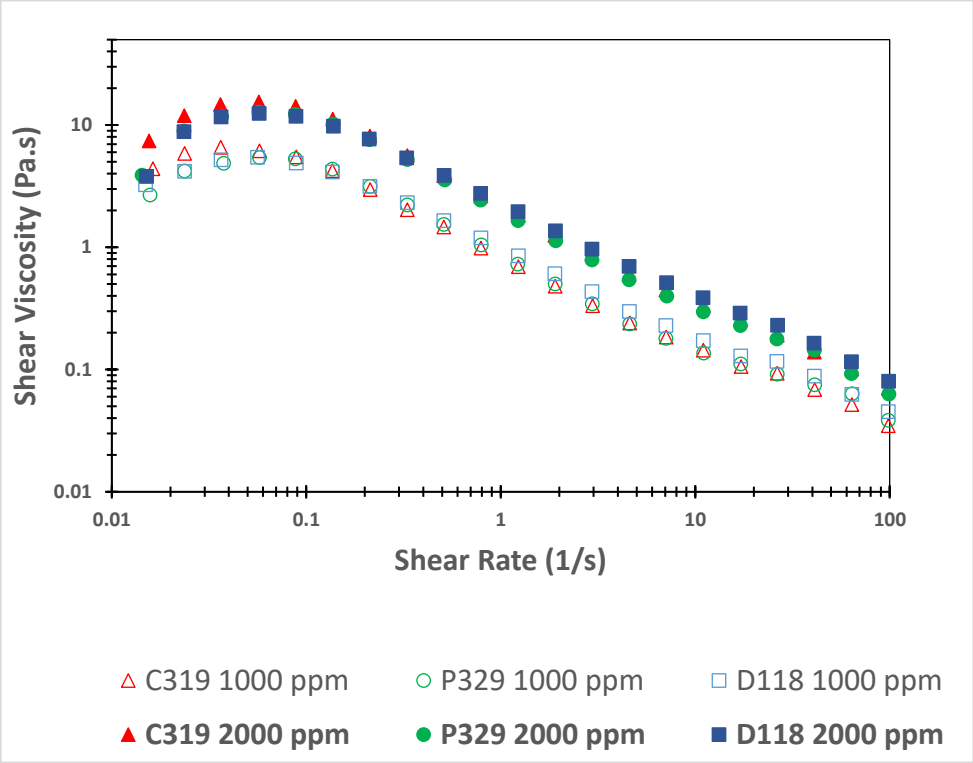

Figure 3.3: Influence of polymer concentration and hydrophobicity on the shear rheology

The results for experimental break-up time, relaxation time, and the maximum apparent viscosity for all polymer solutions are reported in Table 3.2. These data are aligned with the literature[125]. The results summarize that the experimental break-up time, relaxation time, and the maximum apparent viscosity increase with the polymer concentration whereas the values of these parameters decrease with hydrophobicity. The longest experimental break-up times of 5.33 s and 9.17 s were observed for the low hydrophobic associative polymer (C319) solutions with a concentration of 1000 ppm and 2000 ppm, respectively. Also, these solutions show the highest relaxation time of 0.403 s and 0.601 s, and the maximum apparent extensional viscosity of 353

Pa·s and 530 Pa·s at the polymer concentration of 1000 ppm and 2000 ppm, correspondingly. On the other side, the high hydrophobic polymer solutions (D118) show a minimum experimental break-up time of 3.13 s and 4.49 s, relaxation time of 0.270 s and 0.403 s, and the maximum apparent extensional viscosity of 127 Pa·s and 210 Pa·s at the concern polymer concentration.

The experimental temporal evolution of mid-point diameter is depicted in Figure 3.4. The figure shows that the elastocapillary thinning of filament consists of two-phase progress, linear and exponential decay for all solutions. The AP chains uncoil and the viscous stress of the formed cylindrical filament can be neglected over the entire elastocapillary regime. Therefore, the experimentally measured diameter is only a function of the relaxation time and the average relaxation time determination was employed by regressing the experimental data points in the intact regime to Equation 3.1. At the late times, the uncoiled polymer chains remain extended under the higher extension rate and the FENE factor (Equation 3.3 [133]) related to the averaged molecular weight cannot be neglected as the finite extensibility limit is approached. This means the thinning behavior deviates from the exponential regime of elastocapillary thinning and the decay rate becomes linear again corresponding to a viscous liquid with a very high and anisotropic elongational viscosity resulting from the fully extended polymer chains. This is because the viscous resistance to thinning is determined by the viscosity of the total entangled solution rather than by the pure solvent [131]. As a result, the evolution of mid-point diameter shows an exponential decay followed by a linear regime again. This behavior indicates the maximum extension of polymer chains responsible for the high and anisotropic elongational viscosity.

$$f_i = \frac{1}{1-\frac{tr\,A_i}{{L_i}^2}} \tag{3.3}$$

f_i : FENE factor, A_i : internal polymer conformations normalized with equilibrium coil size, ${L_i}^2$: finite extensibility parameter is a function of molar mass and bond angle.

Table 3.2: Experimental break-up time, relaxation time, and maximum apparent extensional viscosity of polymer samples

Polymer	Concentration (ppm)	Experimental Break-up time (s)	Relaxation time (s)	Maximum Apparent Extensional Viscosity (Pa·s)
C319	1000	5.33	0.403	353
	2000	9.17	0.601	539
P329	1000	4.72	0.389	245
	2000	6.49	0.509	330
D118	1000	3.13	0.270	127
	2000	4.49	0.403	210

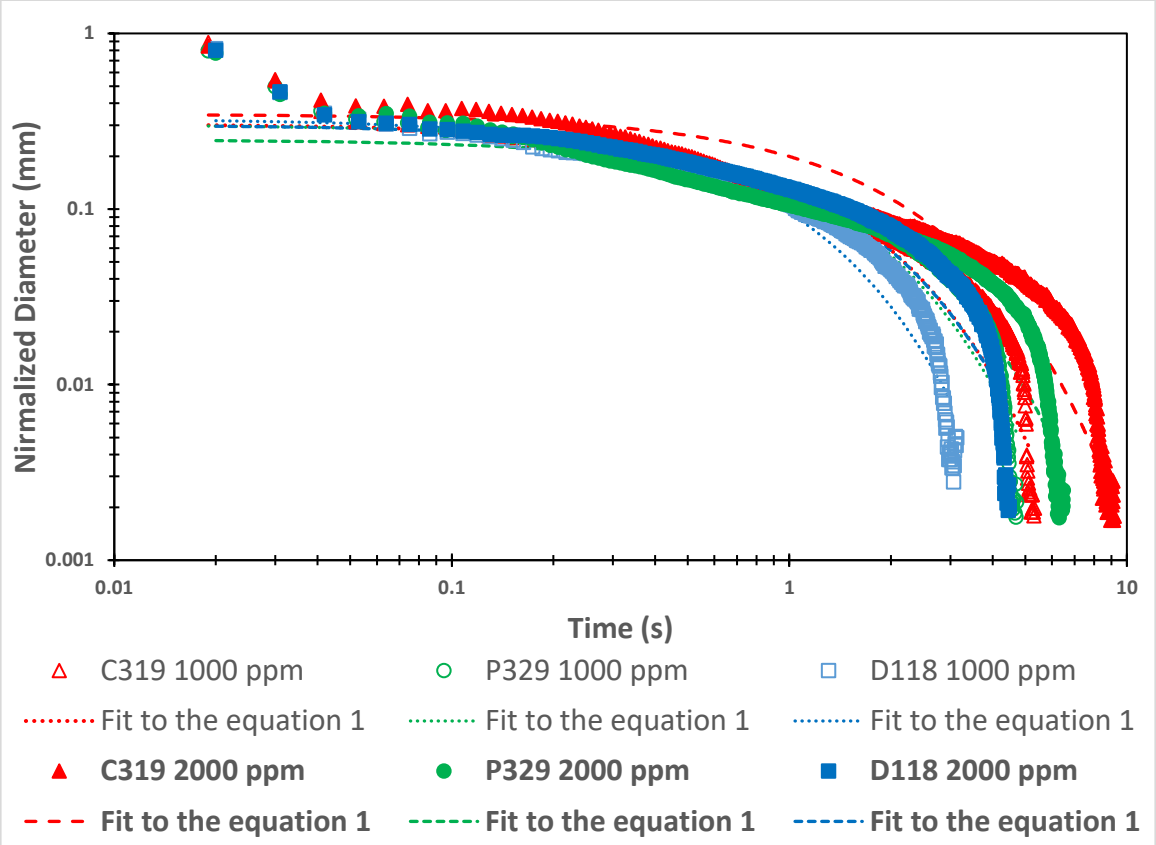

Figure 3.4: Uniaxial elongation and filament breaking for the polymer samples

As shown in Figures 3.1 and 3.4, extended exponential decay for the solutions with the polymer concentration of 2000 ppm represent the extended coiling or contraction of polymer chains (Table 3.3) due to the domination of intermolecular hydrophobic interactions over the intramolecular hydrophobic interactions for the polymer solution with 1000 ppm concentration. As a result, the extensional properties listed in Table 3.2 increase with the concentration regardless of hydrophobicity. At the lower hydrophobicity, the polymer chains may act as a flexible randomly coiled Hookean spring, and it can snap back to its original structure easily. However, at the higher hydrophobicity, these deformations become too large due to electrostatic repulsions (as shown in Figure 3.5) and the rigid sphered polymer coils exhibit non-Hookean behavior that cannot withstand under the high extensional field. The lowest R_n values due to the

domination of intramolecular (as shown in Figure 3.1) for D118 reported in Table 3.3 justify the shrinkage of polymer chains discussed above at both concentrations, 1000ppm and 2000 ppm. So the relaxation time decreases from 0.403 to 0.389 and 0.270 at 1000 ppm, and from 0.601 to 0.509 and 0.403 at 2000 ppm as hydrophobicity increases. From the presented data, the D118 is a less suitable polymer for EOR (Enhanced Oil Recovery) due to the instability of thin filament under the extensional forces compared to P329 and C139, a flexible polymers.

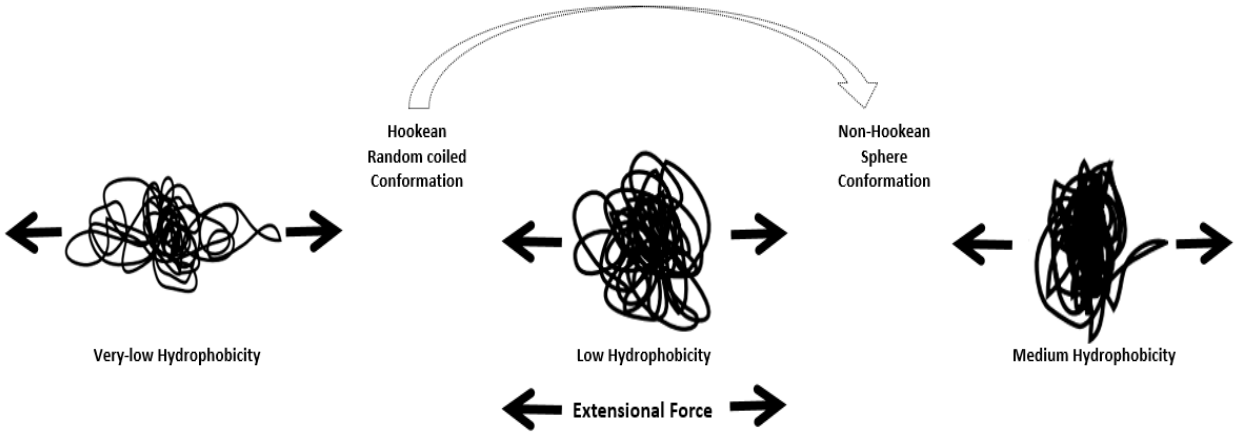

Figure 3.5: Effect of hydrophobicity on the polymer conformations

Figure 3.6 shows the extensional viscosity as a function of strain rate for all polymer solutions. As discussed, at the critical Deborah number that is a product of relaxation time and strain rate, the corresponding relaxation time shown in Table 3.2 was used to calculate the maximum extensional viscosity. The intermolecular transit network at the polymer concentration of 2000 ppm generates high extensional resistance corresponding to a higher extensional viscosity than the solutions with a polymer concentration of 1000 ppm. So the extensional viscosity increased from 359 Pa·s, 245 Pa·s, and 127 Pa·s to 539 Pa·s, 245 Pa·s, and 210 Pa·s for C319, P329, and D118 respectively. Whereas, at the identical polymer concentration of 2000 ppm, the rigid sphere conformations formed due to the strong electrostatic repulsions at the higher

hydrophobicity do not contribute to the higher internal resistance and so the extensional viscosity decreased from 353 Pa·s to 245 Pa·s and 127 Pa·s at 1000 ppm and 539 Pa·s to 330 Pa·s and 210 Pa·s at 2000 ppm for C319, P329, and D118 correspondingly.

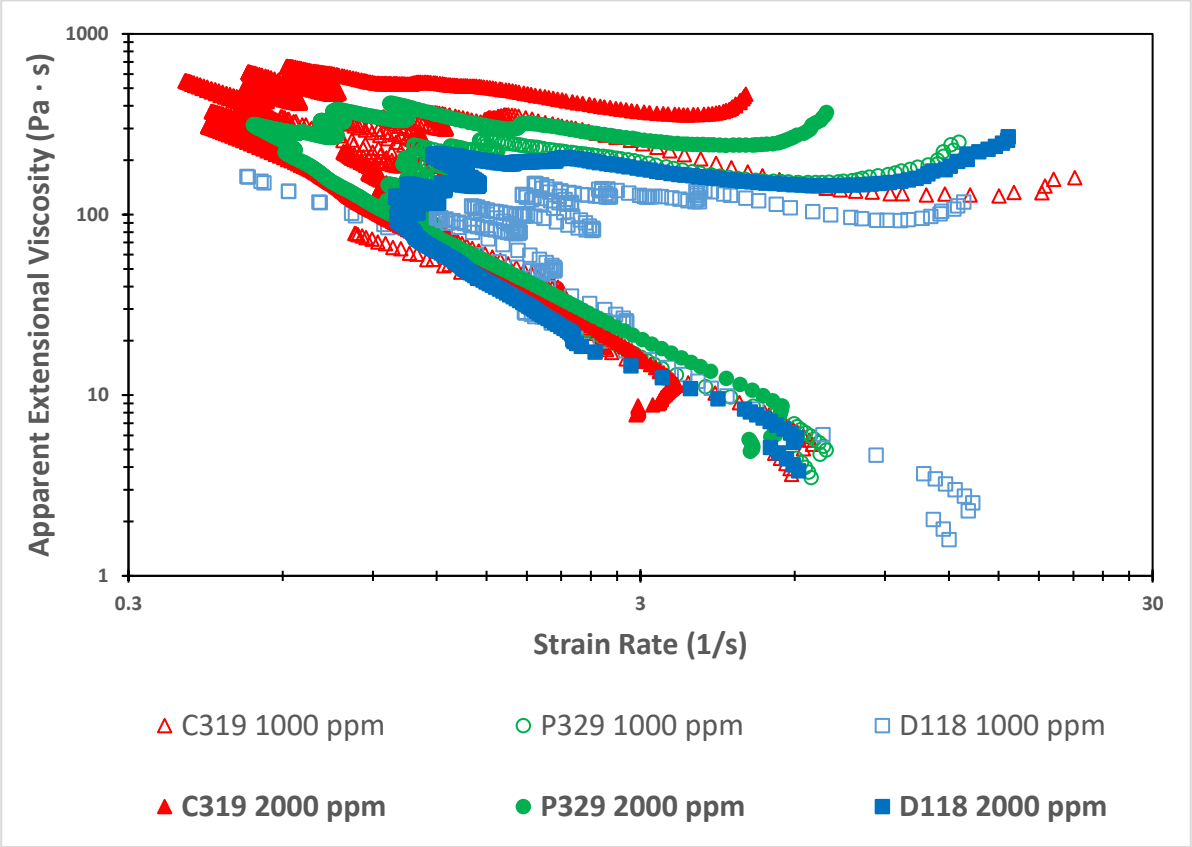

Figure 3.6: Apparent extensional viscosity as a function of strain rate

Also, Figure 3.6 shows the bifurcation of extensional data into two regimes. Initially, the apparent extensional viscosity increases as the strain decrease due to gravitational sagging and doesn't represent any material function. Once the maximum extensional viscosity is attained, the weak nature of viscous resistance is the reason that causes the strain rate to increase due to high deformation [92]. These transitions observed at the lower strain rate indicate the high elasticity for the solutions with the low hydrophobic polymer, C319 at 1000 ppm and 2000 ppm. The strain rate increases until the elastic stresses of unraveling polymer chains develop to resist the

deformation driven by the capillary action [92]. The intermolecular interactions give higher stability due to higher elastic stress[17]. Therefore, higher apparent extensional viscosity was observed at 2000 ppm polymer concentration.

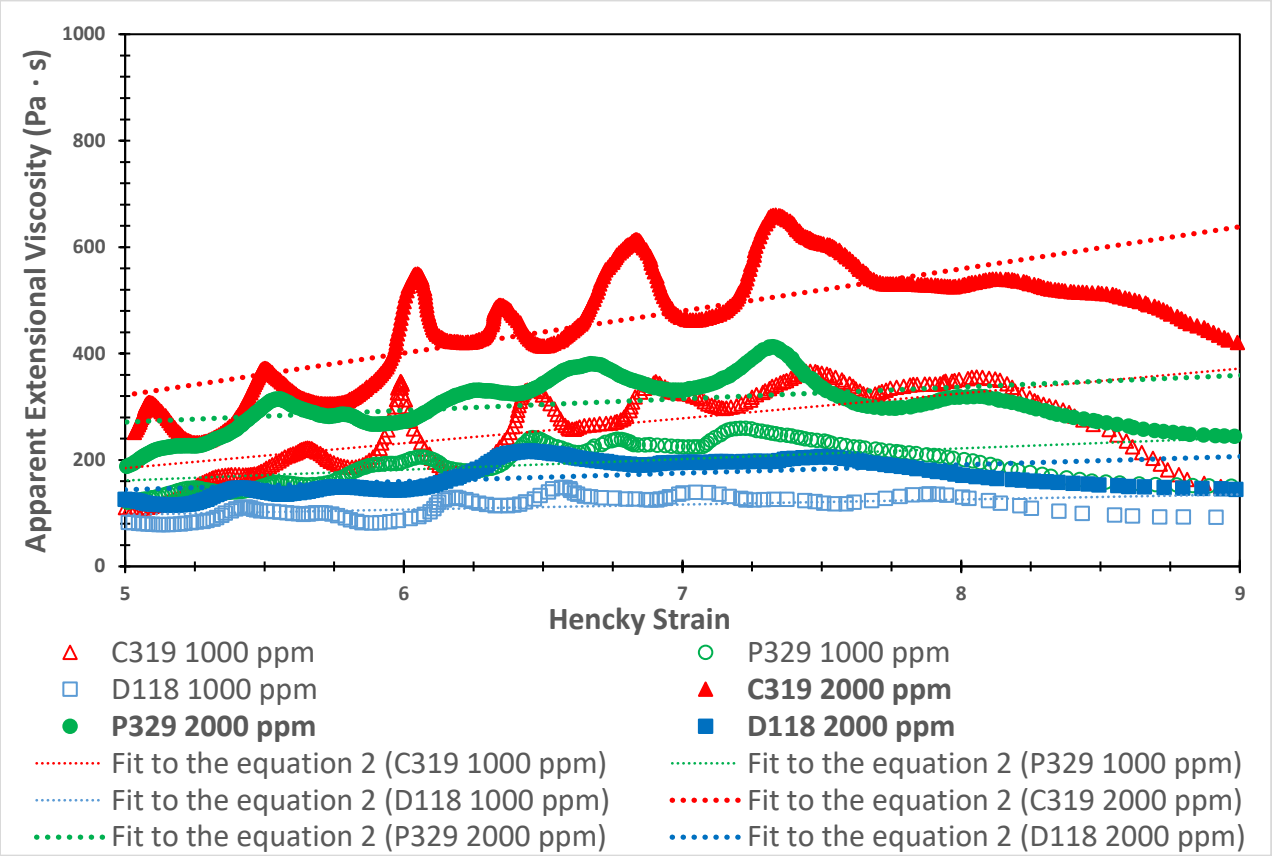

Figure 3.7: Straining hardening for polymer samples

The strain hardening behavior resulting from delayed mechanical disruption is shown for all solutions in Figure 3.7. The experimental data points were fitted by using Equation 3.2. The extended linear thinning of filaments shown in Figure 3.4 directly reveals the strain hardening due to the starched-induced extended polymer coils[32]. At 1000 ppm polymer concentration, C319 and P329 show similar strain hardening but higher than D118 due to reduced entanglement between polymer chains at the higher hydrophobicity. So at the lower hydrophobicity and concentration, the entanglements may be capable of causing stress overshoot but may not be

strong enough to cause hardening. However, the effect of hydrophobicity on the strain hardening is observed for the solutions prepared with the polymer concentration of 2000 ppm. At 2000 ppm, C319 (lowest hydrophobicity AP) shows higher strain hardening due to higher polymer chain entanglements. However, the strain hardening behavior became dominant at the higher Hencky strain because the entangled polymer networks can be effectively strengthened under the higher extensional forces[27]. As a result, positive slopes (for the fitted dashed lines) were observed regardless of concentration and hydrophobicity.

3.4.2 AF4-FFF characterization

Associative polymers and their aggregates were characterized by AF4–MALS–dRI to study the conformation of polymers in the aqueous media. An array of polymer chain lengths corresponding to the MWD can be represented by polydispersity. The polydispersity index (PDI), the ratio of weight and number of average molecular weights, was used to represent the broadness of the MWD. Higher the PDI, the broader the MWD. Table 3.3 shows the averaged molecular weights and averaged RMS radius. The shape of polymer conformations can be described by using the shape factor, V_g in the model shows the relation between Rn and average molar mass[134],

$$R_{n,i} = K_g M_i^{V_g}, \qquad K_g \text{isconstant} \tag{3.4}$$

Table 3.3: Effect of polymer concentration and hydrophobicity on the average molar mass and radius of gyration

Polymer	Concentration (ppm)	M_n (MDa)	M_w (MDa)	M_z (MDa)	R_n (nm)	R_w (nm)	R_z (nm)	PDI	The slope of the Conformation Plot
C319	1000	14.20	22.22	29.62	981.3	987.9	997.9	1.579	0.57
	2000	14.32	27.09	36.53	1039.4	1048.9	1058.1	1.891	0.51
P329	1000	18.61	24.59	32.22	964.1	993.3	1011.4	1.322	0.49
	2000	25.87	39.25	47.28	1000.9	1032	1039.3	1.517	0.40
D118	1000	29.39	36.38	42.67	938.6	951.8	959.4	1.238	0.41
	2000	31.15	43.79	54.2	989.1	995.7	1004.3	1.406	0.20

Table 3.3 shows that the average molecular weight (M_w) increases with polymer concentration and hydrophobicity. M_w increases from 22.22 MDa to 27.09 MDa for C319, 24.59 MDa to 39.25 MDa for P329, and 36.38 MDa to 43.79 MDa for D118 as the polymer concentration in the aqueous media increases from 1000 ppm to 2000 ppm. There was no significant change in the Rn values observed but a very small marginal increase of 58.1 nm, 36.8 nm, and 50.5 nm was observed for C319, P329, and D118 respectively as the polymer concentration increased. In the dilute regime, M_w increases from 22.22 MDa to 36.38 MDa and Rn decreases from 981.3 nm to 938.6 nm as the hydrophobicity increases. Whereas in the semi-dilute regime, M_w increases from

27.09 MDa to 43.79 MDa and Rn decreases from 1039.4 nm to 989.1 nm as the hydrophobicity rises.

Figure 3.8 shows the structural conformational changes in the polymer chains as a function of concentration and hydrophobicity. Fitting Model 3.4 for the Rn vs M_W of the same fraction provides useful information on the polymer shape. The shape factor, V_g (or the slope of the fitted dashed lines) of 1, 0.5, and 0.3 describes the polymer shape as a rod, random coil, and sphere respectively[132]. In the dilute regime, C319 undergoes the minimum chain shrinkage due to weak electrostatic forces and results in the linear rod structure with an Rn of 981.3 nm. Whereas, higher hydrophobicity results in V_g of 0.41 for D118 shows the compacted sphere structure than the P329 with V_g of 0.49 shows a randomly coiled structure. This corresponds to the lower Rn of 938.6 nm for D118 compared to 964.1 nm for P329. At 2000 ppm, the intermolecular hydrophobic association shows polymer aggregation (Figure 3.10(a)) resulting in a higher Rn compared to the polymer with 1000 ppm concentration. However, the lower slopes indicate compact conformations for the polymer solutions at 2000 ppm (Figure 3.8 (b)) compared to the corresponding solution at 1000 ppm. The lowest V_g of 0.2 for D118 at 2000 ppm shows the formation of sphere conformations. Also, the intermolecular hydrophobic associations for solutions at 2000 ppm may cause the long-chain branching that supports the formation of flexible species formations. These formations increase the solvent holding capacity. So higher relaxation times and extensional viscosities were observed for these solutions compared to solutions at 1000 ppm.

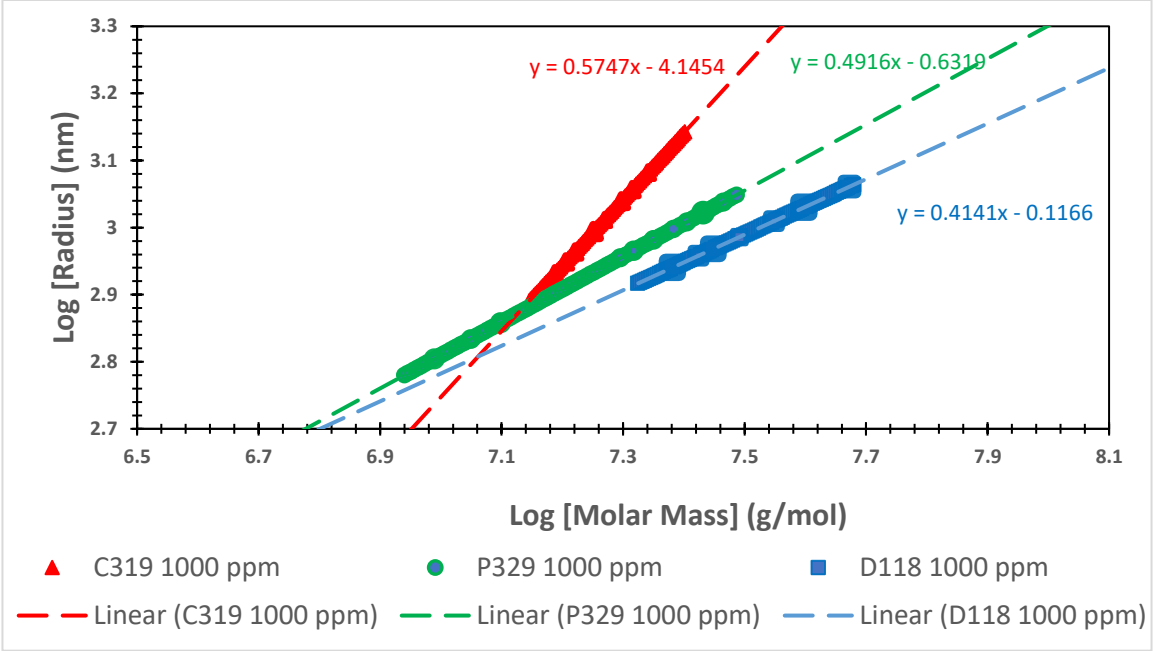

(a) Conformational plot for polymer samples (concentration 1000 ppm)

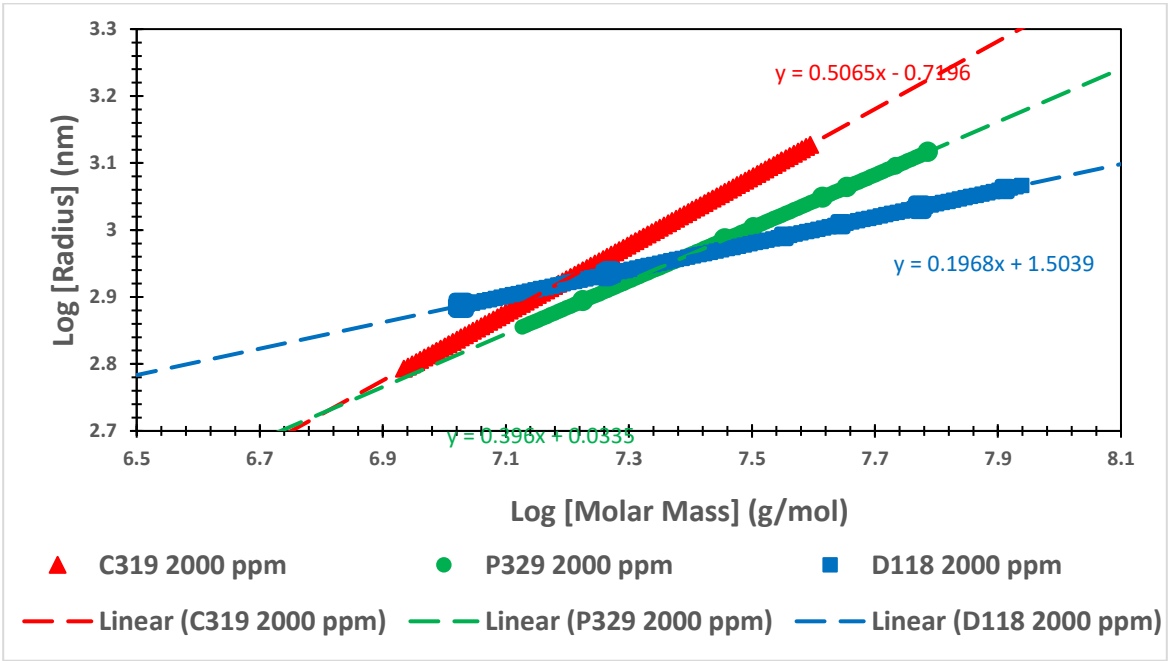

(b) Conformational plot for polymer samples (concentration 2000 ppm)

Figure 3.8: Conformational for the associative polymer samples

Figures 3.9 and 3.10 show the molecular weight and size distribution respectively for all polymer solutions. The broadest MWD (Figure 3.9(a)) for C139 at 2000 ppm concentration shows the highest PDI (Table 3.3) of 1.891. Whereas the narrowest MWD for D118 at 1000 ppm corresponded to the lowest PDI of 1.238. The MWD became broader at the higher concentration of 2000 ppm thus the PDI increased from 1.579 to 1.891, 1.322 to 1.517, and 1.238 to 1.406 for C319, P329, and D118 correspondingly. Consequently, the observed steeper cumulative distributions (Figure 3.9(b)) also show the narrow MWD for the polymer concentration of 1000 ppm than 2000 ppm. On the other side, a higher differential fraction for the second peak (Figure 3.9 (a)) and slightly higher Rn values at 2000 ppm show the domination of intermolecular hydrophobic association at 2000 ppm that causes the polymer aggregation as shown as a secondary peak in Figure 3.10 (a). This indicates the Critical Aggregation Concentration (CAC) for all polymers falls between 1000 ppm and 2000 ppm. The size of aggregates was reported as 1268.5 nm, 1123.0 nm, and 1294.6 nm for C319, P329, and D118 respectively so there was no trend found between the size of the aggregates and the hydrophobicity. However, this polymer aggregation can be one of the reasons for the higher shear viscosities (Figure 3.3) for the polymer solutions at 2000 ppm than 1000 ppm. Besides, disparate behavior was observed where MWD became narrow as the hydrophobicity increased, therefore the PDI decreased from 1.579 to 1.238 at 1000 ppm and 1.891 to 1.406 at 2000 ppm. Simultaneously, a decrease in the Rn indicates effective coiling of polymer chains at higher hydrophobicity due to domination of intramolecular hydrophobic interactions at the identical polymer concentration as shown in Figure 3.1.

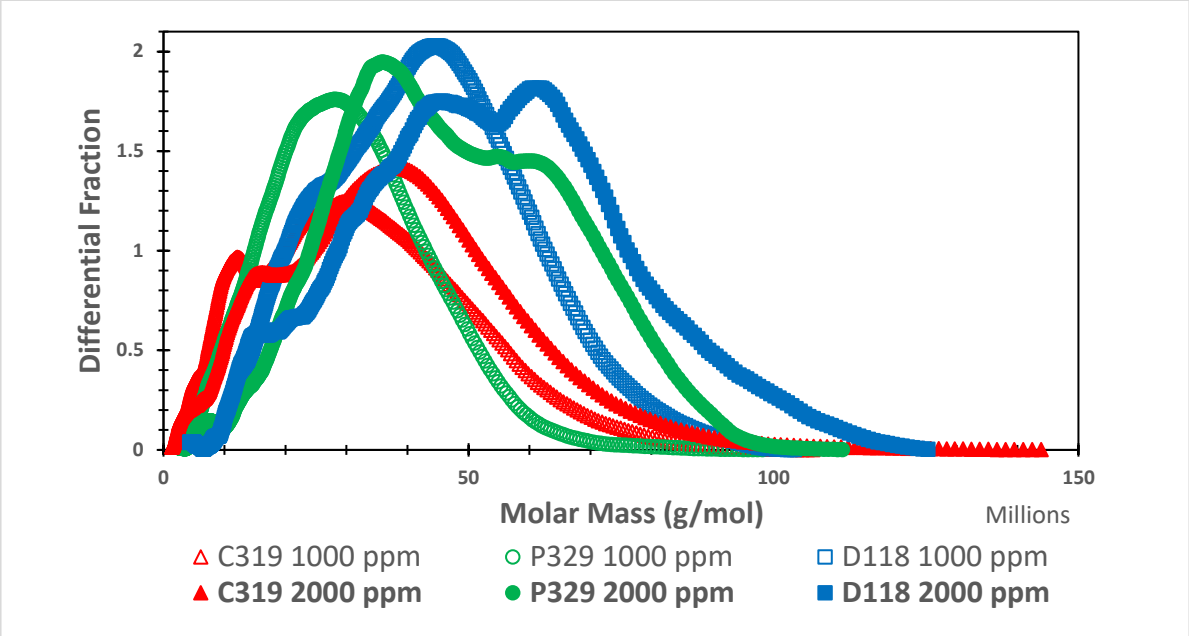

(a) Differential molar mass for polymer samples

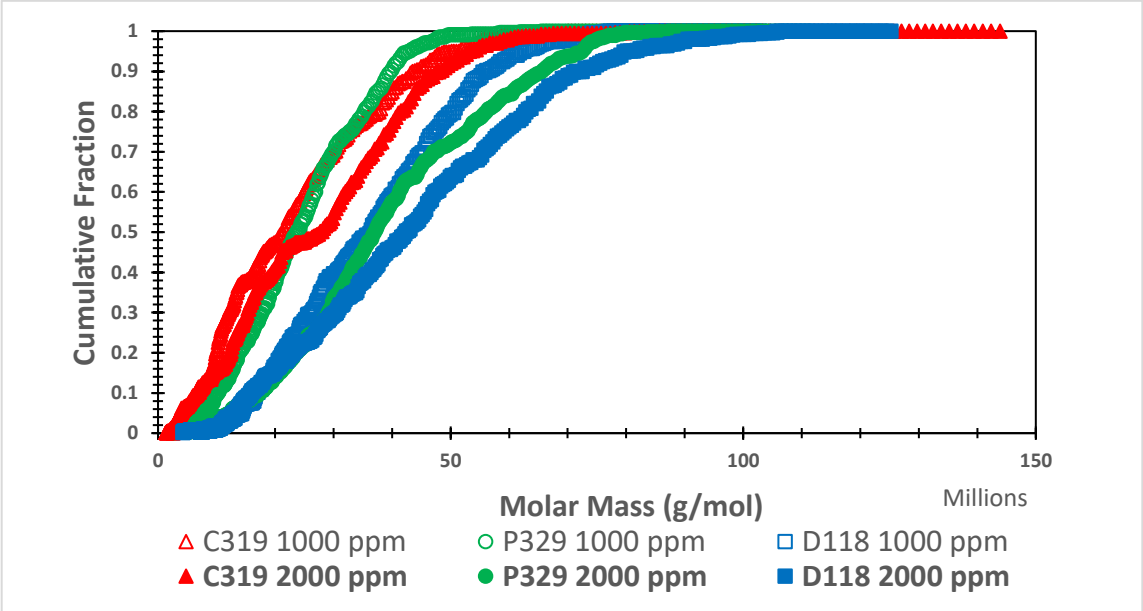

(b) Cumulative molar mass for polymer samples

Figure 3.9: Molar mass distribution for the assocative polymer samples

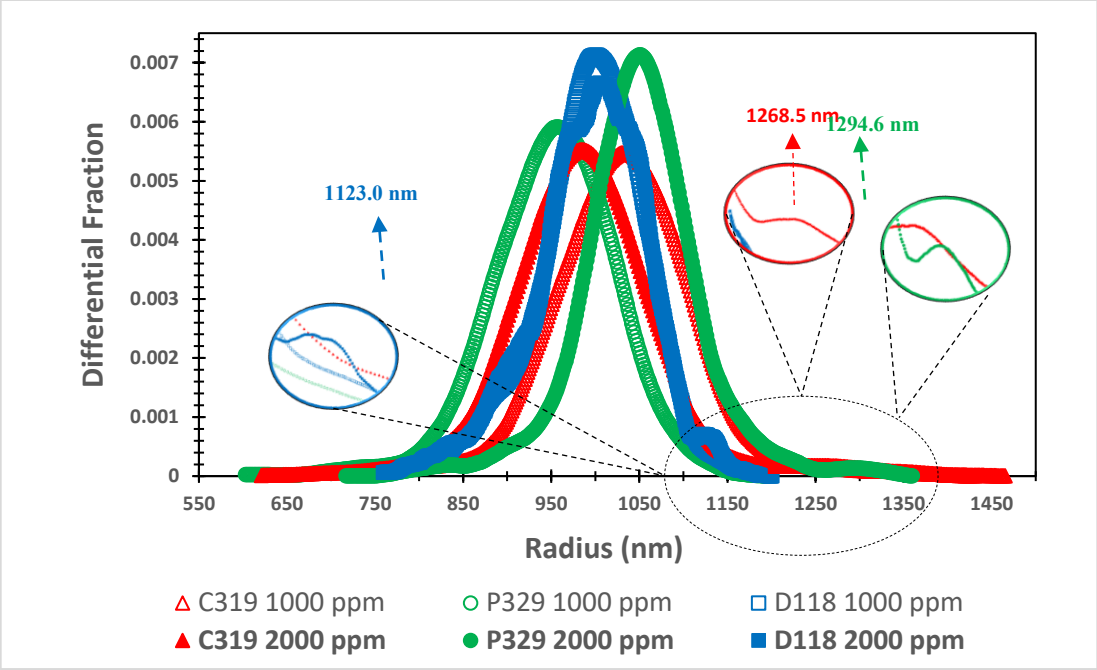

(a) Differential radius for polymer samples

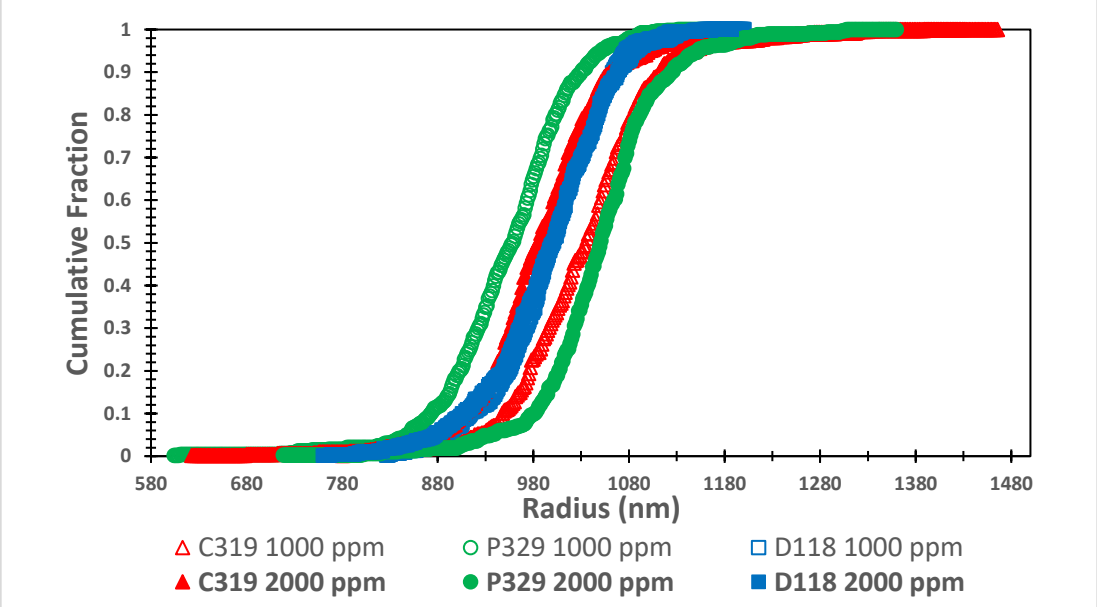

(b) Cumulative radius for polymer samples

Figure 3.10: Radius distribution for the associative polymer samples

In the dilute regime, the broadest MWD for C319 corresponded to the maximum relaxation time of 0.403 s. This may be due to the low hydrophobicity limiting the molecular interactions and the polymer chains hold their initial linear rod-like states. At the higher hydrophobicity, these polymer chains coil up and form a complex rigid sphere structure that won't allow the solvent to penetrate inside. These rigid structures with lower Rn contributed to narrowing the MWD and can't withstand the external extensional resistance. So the relaxation time decreased to 0.389 and 0.270 for P329 and D118 respectively. Whereas, in the semi-dilute regime, the domination of intermolecular hydrophobic interactions supported the formation of flexible aggregates responsible for broader MWD corresponded to the higher relaxation time. These flexible aggregates became rigid again because of reduced solvent holding at the high hydrophobicity so the relaxation time decreases as shown in Table 3.2.

3.5 Conclusions

A major advantage of the AF4-FFF technique is to characterize the molar mass and size distribution for high-molar mass polymers which are challenging to discrete using conventional chromatographic techniques like GPC and SEC. Varying hydrophobicity for the polymer resulted in a similar behavior due to the rolling of macromolecules under the shear field that cancels out the stress effect. However, the identical conformation for each polymer solution contributed to disparate extensional behavior. The polymer aggregations observed only in the semi-dilute regime indicate the CAC for all polymers falls between 1000 ppm and 2000 ppm. Intramolecular hydrophobic associations coil the polymer chains that were dominant in the dilute regime whereas the intermolecular hydrophobic associations were dominant in the semi-dilute regime causing the polymer aggregation. In both regimes, hydrophobicity plays an important role to change the entanglement between polymer chains responsible for the formation of rigid or

flexible complex structures. Whereas the higher entanglements were responsible for strain hardening for C319, the rigidity and compaction of polymer complexes increase with the hydrophobicity may result in a lower relaxation time and extensional viscosity. On the other side, the formation of flexible polymer networks that withstand the higher extensional resistance result in a higher relaxation time and extensional viscosity for the polymer solutions in a semi-dilute regime. Overall, this study provides valuable insights into the selection of associative polymers for various applications not only based on the shear rheology but the polymer conformations affecting the extensional rheology as well.

Chapter 4: Effect of Polymer Conformations on Rheology and the Flow of Polymer through the Porous Media

4.1 Abstract

The concentration and hydrophobicity-dependent molecular associations are responsible for distinct rheological behavior for polymers to prove their application in various industrial operations specifically for enhanced oil recovery. These molecular associations change the polymer conformations, molecular weight, and radius distributions. The presence of salts that changes these conformations results in polymer chains with lower molecular weight. This may cause loss of the visco-elasticity loss of polymer solution due to polymer precipitation and reduce the efficiency of polymer flooding. So, the underlying mechanism of molecular interactions in the presence of cations needs to be understood well. Correlating these conformational changes with its flow behavior in the porous media enables the polymer selection criteria especially when the polymer solutions exhibit similar shear rheology. In this study, commercially available polymers with different hydrophobicity, HPAMs, C319, and D118 were used to characterized by the Field-flow fractionation (FFF) method to determine molecular weight distribution (MWD) and size distribution (Rn). The effect of the change in these properties on the rheological properties was studied to justify the behavior of the polymer solutions in the porous media.

4.2 Introduction

Crude, natural gas, and Coal are the most valuable non-renewable energy sources and essential feedstock for many processes as well. Among them, oil plays the foremost role in the world of increasing energy demand. Once the current crisis gets stabilized, the global oil demand could be boosted by 500 kb/d to reach about 170 kb and 210 kb daily by end of 2021 and 2022

respectively[1]. Additionally, the recent sharp drop in oil prices compelled oil corporations to revise their production strategies and optimize their production cost based on the current oil price scenario. To satisfy the oil demand with the traded oil prices, the implementation of enhanced oil recovery (EOR) techniques has been gaining more and more attention as the formation and exploration of new oil reserves continue [2]. Chemical EOR is the pronounced technique applied to 11% of the EOR projects worldwide. Specifically, more than 77% of methods are polymer flooding (as shown in Figure 4.1) considering the several technical, operational, and cost benefits [135][9]. These benefits can be tuned based on the suitable selection of polymer to enhance the viscosity of water that favors mobility control and reduce the relative permeability simultaneously[4], [5], [29], [136], [137]. The selection criteria for polymer flooding projects include but are not limited to cost, filtration properties, oil viscosity, mobile saturation, reservoir conditions (rock type, temperature, and salinity), and mechanical stability[135].

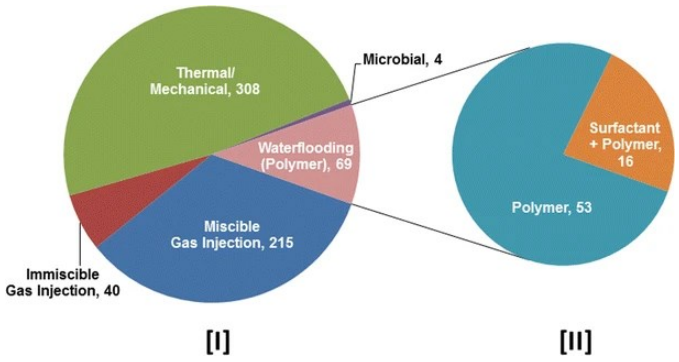

Figure 4.1 A summary of EOR projects performed worldwide including polymer flooding [135]

Partially Hydrolyzed polyacrylamide (HPAM) and its derivatives having a higher molecular weight (M_w) have been used at the commercial stage considering the economic factors[138].

However, HPAM shows high shear sensitivity at elevated temperatures and high salinities. Hence, its other hydrophobically modified or sulfonated derivatives are being used[139]. Even though having reasonable bulk characteristics, especially viscoelasticity, these polymers showed limited success due to polymer degradation (mechanical and chemical), loss of polymer in the porous media, and loss of injectivity[4].

The polymers used often with higher molecular weight, which could provide the displaced slugs more viscosity, to overcome the oil's high viscosity and achieve a favorable M. The impact of viscoelasticity on extra recovery after chemical flooding has been studied to understand any resulting favorable mechanism that affects the oil recovery[16], [16], [18], [140]–[143]. Additional micro-force or normal stresses were cited by several other researchers as the primary explanation for the remaining oil saturation reduction during viscoelastic polymer flooding[55]. Micro-force is a component of normal stress, which is proportional to extensional viscosity so the extensional viscosity and the relaxation time are the solution characteristics used for the polymer screening[56]. Polymer elasticity would be an important screening criterion especially when the shear rheology enables the explanation of the flow behavior of HPAM and its derivatives exhibit similar bulk shear characteristics[57][58][59]. All these mechanisms emphasize the influence of normal stresses. However, under reservoir conditions, the yielding stress is not always the normal stress even though the polymer is injected at a very low rate[60]. Hence the normal stress-dependent bulk polymer characteristic can not represent the behavior of polymer solutions through a porous media. The non-Newtonian flow of these viscoelastic polymer solutions through porous media under non-uniform conditions (varying porosity, permeability, and yield stress) could be explained by the formation of molecular networks responsible for the fluid flowability, resistance, and retention[19]. These induced networks may not cause considerable change in the viscoelastic properties. Hence the possibility to predict the

polymer injectivity from the independent measurements of the fluid's rheological properties and the porous media's geometrical properties arises as a scope of the study.

This structure-function relationship with polymer injectivity is of critical importance to producing commodity objects as well as for new emerging areas of applications for polymers like EOR. Polymer solutions always exhibit polydisperse molecular weight so the molecular weight distribution of a polymer is one of its most fundamental structural characteristics. The processability, mechanical strength, and morphological phase behavior of a polymer are all influenced by its molecular weight distribution. Hence, considering molecular weight distribution as an additional criterion for polymer screening may give better insights into polymer retention in the porous media.

4.3 Materials and Methods

4.3.1 Reagents

HPAM along with its hydrophobically modified derivatives, C319 and D118 were supplied from SNF Floerger. Table 4.1 shows the specifications for these polymers provided by the manufacturer. According to the manufacturer, all samples have similar estimated M_w and ionicity. Fisher Scientific supplied lab-grade NaCl (with percentage purity ≥ 99.0 %)

4.3.2 Sample Preparation

5000 ppm of NaCl was added into de-ionized (DI) water to prepare the base brine. The desired amount of dry-powdered polymer was gradually added into the base brine to prepare the concerned polymer solutions of 1000 and 2000 ppm. All solutions were stirred at 350 rpm until diminishing vortex. This allows uniform dispersion of polymer into the brine. All solutions were sealed to minimize oxidative degradation and stirred at 150 rpm for 24 hours at room temperature (~20° C) to avoid mechanical degradation.

Table 4.1: Specifications of polymers from SNF

Polymer Name	**Polymer Type**	**Weight-average Molecular Weight (Mw) by the supplier (MDa)**	**Hydrolysis (% mol)**	**Hydrophobicity**
HPAM 3630	Non-Associating Polymer	20	25-30	Not Applicable
Superpusher C319	Hydrophobically Associating Polymer (AP)	16-20	25-30	Very Low
Superpusher D118	Hydrophobically Associating Polymer (AP)	16-20	30	Medium

4.3.3 Rheology Experiments

Shear Rheology

AR2000 (TA Instruments) was used to characterize the shear rheology of polymer solutions at room temperature. The density of 1 $\frac{g}{cm^3}$ was assumed for all polymer solutions. A sample volume of 1 mL was placed between the cone and plate geometry with a 2° steel cone and 40 mm diameter to perform the shear experiments.

Extensional Rheology

The uniaxial elongation experiments were performed at room temperature by using CaBER (ThermoFisher HAAKE 1). A fixed volume of polymer solutions (~ 0.2 -0.3 mL) was placed between two parallel plates initially positioned 2 mm apart. This polymer solution then starched uniaxially by applying the Hencky strain of 1.2 (move the upper plate to 6.5 mm within 50 milliseconds). The surface tension (σ) of 65 $\frac{mN}{m}$ was measured for all polymer solutions. Various extensional rheological parameters i.e. filament break-up time, relaxation time, and apparent extensional viscosities are obtained by fitting the appropriate model to the filament diameter to time plot. The upper-convected Maxwell model (Equation 4.1) with an exponential regression was applied to filament diameter to time data to determine the extensional relaxation time.

$$D_{mid}\,(t) = D_0\left(\frac{GD_0}{\sigma}\right)^{\frac{1}{3}} e^{\frac{-t}{3\lambda_c}} \tag{4.1}$$

D_{mid}: Mid-point diameter of the filament (mm), D_0: Initial diameter of the loaded sample (mm), λ_c: Characteristic relaxation time (s), G: Elastic modulus (Pa). σ: surface tension of polymer samples (mN/m).

The evolution of the midpoint diameter of the polymer solutions driven by the capillary pressure with the extensional resistance stress can be represented in the terms of the extensional viscosity (defined as given in Equation 4.2).

$$\underline{\eta}_{app}(\varepsilon) \cong \frac{(2X-1)\sigma}{\frac{d\,D_{mid}}{dt}} \tag{4.2}$$

X: axial correction factor (=0.7127).

$$\varepsilon\,(t) = 2\ln\left(\frac{D_o}{D_{mid}\,(t)}\right) \tag{4.3}$$

$$\dot{\varepsilon} = -\frac{2}{D_{mid}(t)}\left(\frac{dD_{mid}(t)}{dt}\right) \tag{4.4}$$

ε: Hencky strain and ε̇: strain/elongation rate (s^{-1}).

The apparent extensional viscosity vs strain rate and strain hardening plots can be generated by using Equations 4.2 and 4.4. The filament drainage result in the maximum elastic limit and so the apparent extensional viscosity at the critical Deborah number of 0.66[56]. This value is reported as the maximum apparent extensional viscosity.

4.3.4 AF4-FFF Experiments

The details of the working principle of Fluid flow fractionation were explained in the previous publications[27], [59]. According to the separation principle, the smaller particles are eluted before the larger particles as shown in Figure 4.2. This time-scaled elution coupled with AF4 system (Postnova Analytics, Landsberg, Germany), MALS-PN3621 (Postnova Analytics, Landsberg, Germany), and DRI-PN3150 (Postnova Analytics, Landsberg, Germany) detectors results in the molecular weight distribution (MWD) and radius distribution curves.

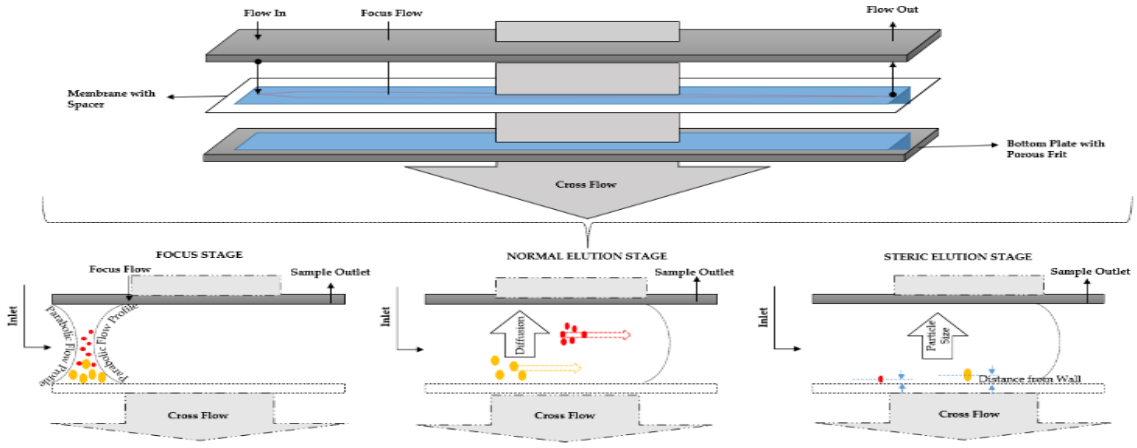

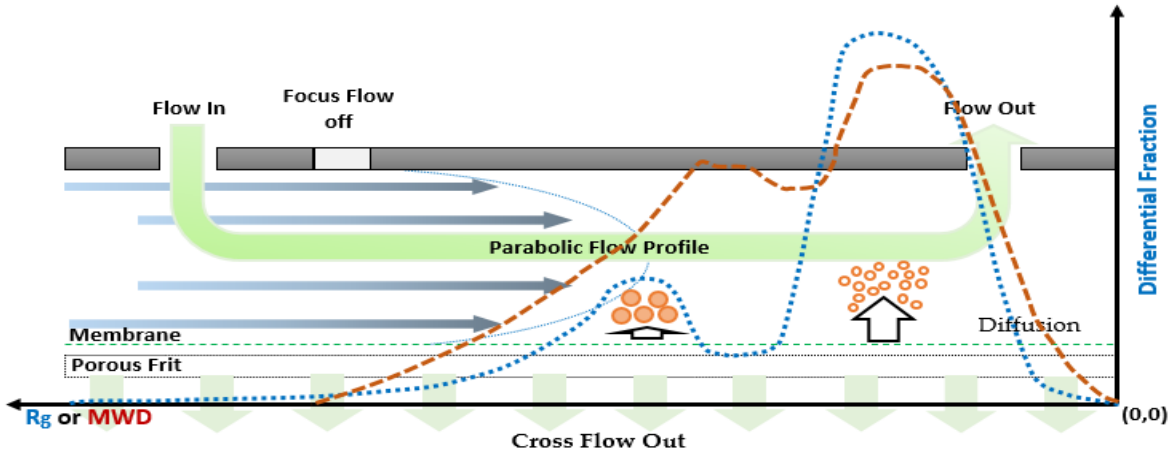

Figure 4.2. Schematic of working principle of AF4-FFF[27], [59]

A MALS detector containing a 10–50 mW laser that operates at 532 nm and has twenty-one scattering angles—7°, 12°, 20°, 28°, 36°, 44°, 52°, 60°, 68°, 76°, 84°, 90°, 100°, 108°, 116°, 132°, 140°, 148°, 156°, and 164°. A baseline or reference line was set by using the solvent or brine containing 5000 ppm NaCl in DI water. As a separation channel, a regenerated cellulose membrane with a molecular weight cut-off of 10 kDa (Postnova Analytics' Z-MEM-AQU-631) was used. The volume of the sample injected was 50 µL for each FFF experiment.

By setting the focus flow rate to 0.8 mL/min for 3 minutes, the sample accumulation and longitudinal diffusion on the membrane were permitted, and after 1 minute, the flow changeover to elution mode was enabled. The crossflow rate was held at 0.5 mL/min for 2 minutes and then allowed to decrease exponentially (with an exponent of 0.3) to 0.1 mL/min over 35 minutes. This allowed for sample elution. To prevent cross-contamination, the cross-flow rate was maintained at last at 0.1 mL/min for 15 minutes. The $\partial n/\partial c \approx 0.17$ was measured for all polymer samples to determine the number average(Mn) molar mass, the weighted average (Mw) molar mass, and the Rn using the random coil model[144].

4.3.5 Polymer injectivity Experiments

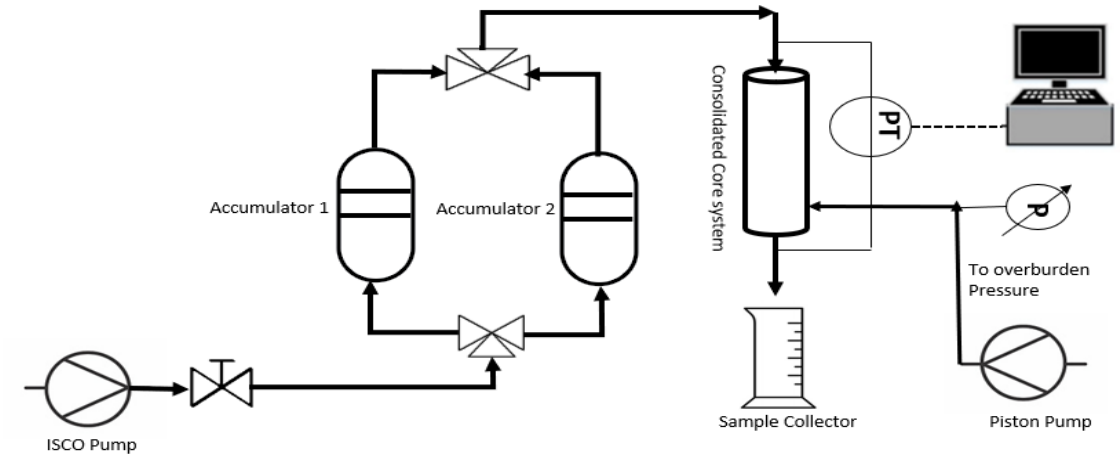

Figure 4.3 Schematic of polymer injectivity experiments

An experimental setup as shown in Figure 4.3 was used to study the flow behavior of polymer in the porous media. Bentheimer cores (supplied by Kocurek Industries Inc.) with 2 inches diameter and 6 inches length were used as a consolidated porous media. An average pore size of ~300 nm was reported for the Bentheimer core [145]. These cores were subjected to the overburden pressure of 130 psi for all experiments. Un-consolidated porous media was employed by packing the glass beads of a mesh size of 40–80, which corresponds to the 354–177 nm in to the cylindrical core holder with internal diameter of 2.86cm diameter and 15.24 cm long. The core-holder system was equipped with a differential pressure transducer connected to a computer to record the pressure profiles.

The experimental setup consisted of Teledyne ISCO 500D syringe pumps and two fluid accumulators functioning as flow injection units. These pumps were connected to the fluid accumulators, which served as storage for water and polymer solutions. From these accumulators, the fluids could be injected independently into the core holder.

The single-phase core flood experiments were performed using HPAM, C319 and D118 at fixed or variable flow rates with the objective of estimating the resistance and residual resistance factors. In the experimental process, the bulk volume of the core or sand pack is estimated by applying the formula π/4 (diameter)^2 x Length. To determine the porosity of the core, the pore volume, obtained from water injection, is divided by the bulk volume of the core.

Deionized water is then injected into the core or sand pack using an ISCO pump syringe pump to control the flow rate. During this process, the pump flow rate is recorded and compared to the time duration and the volume of collected effluent samples. Pressure drop across the core holder is measured using pressure transducers while monitoring the time with Labview. Water saturation is considered for pore volume calculations. The water flood is stopped when the steady state pressure is reached, typically after approximately 5 pore volumes, with the pressure difference estimated between the inlet transducer and the ambient outlet pressure of 1 atm.

Darcy's law is employed to estimate the water permeability of the porous media. Subsequently, polymer samples are injected at various flow rates, and the effective permeability is determined by analyzing the steady state pressure drop and volumetric flow rate. Effective polymer permeability is then estimated using Darcy's law.

A chase water injection is performed, typically around 10 pore volumes, and a steady state pressure is recorded. These recorded steady state pressure values can be utilized to estimate the resistance and residual resistance factors. Overall, this experimental procedure involves measuring bulk volume, determining porosity, water flooding, pressure monitoring, permeability estimation, polymer injection, and evaluation of resistance factors for a comprehensive understanding of the behavior of the porous media and the impact of polymer injection.

Initially, The permeability and porosity values for the porous media used in the experiments were measured by using water flooding experiments. These porous media were subjected to polymer flooding followed by chase water and secondary water injection to determine the Resistance Factor (RF) and Residual Resistance Factor (RRF) at the specific flow rate. The RF and RRF values at a specific injection rate were calculated by a ratio of pressure drops at different stages using Equations 4.5 and 4.6 subsequently.

$$RF = \frac{\Delta P_{Polymer\ Injection}\ (psi)}{\Delta P_{Initial\ Water\ Injection}\ (psi)} \tag{4.5}$$

$$RRF = \frac{\Delta P_{Chase\ Water\ Injection}\ (psi)}{\Delta P_{Initial\ Water\ Injection}\ (psi)} \tag{4.6}$$

The RF values are physically signified as the excess resistance experienced by the polymer compared to water in the porous media at a specific flow rate. Whereas, the RRF values quantify the ability of the polymer to reduce the permeability of water. More than 10 pore volumes (PV) of chase water were injected into cores to rinse out the mobile polymer phase during each experiment. Pressure stability conditions were continuously monitored for each set of experiments. A steady state condition was allowed to be achieved before switching the flow rates.

4.4 Results and Discussion

4.4.1 Rheological characterization

Figure 4.4 shows a shear rheological behavior of associating polymers as a function of concentration and hydrophobicity under saline conditions. The measured shear viscosities were found lower than the reported shear viscosities for the concerned polymer solution without salts [59]. A charge screening effect caused by mono-valent cations (Na^+) is responsible for the

viscosity reduction. As shown in Figure 4.4, all polymer solutions exhibit a shear thinning behavior due to polymer chain entanglement in the direction of shear at the higher shear rates. However, the overlapping shear profiles at 1000 ppm indicate weak inter-molecular association and the trembling of the coiled polymer chains under the direction of stress [27], [58], [59]. Hence, at the lower polymer concentration, polymer screening based on the rotational shear rheological behavior would not be an identical criterion. At 2000 ppm polymer concentration, the higher shear viscosities compared to 1000 ppm are resultant of the domination of inter-molecular interactions [146], [147]. Higher shear viscosities for D118and C319 at 2000 ppm showed higher monovalent cation tolerance due to its higher hydrophobicity compared to HPAM. However, the difference in the shear viscosities (especially for C319 and D118 at 2000 ppm) is not considerable over a wide range of shear rates. Hence, the extensional viscosity measurements may give better insights into how hydrophobicity affects the molecular interactions that are intense under the extensional field[130]–[133].

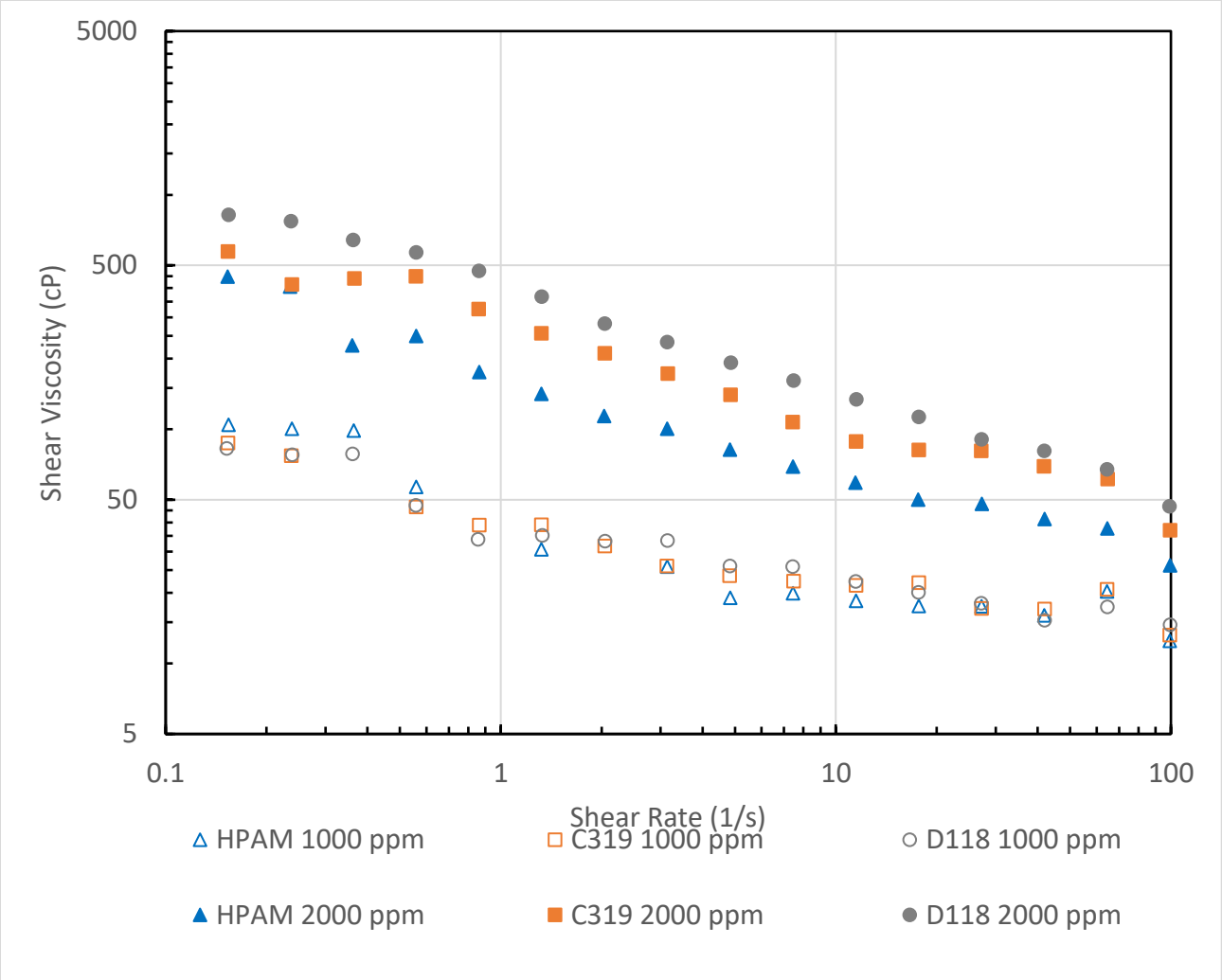

Figure 4.4: Influence of polymer concentration and hydrophobicity on the shear rheology

The results for maximum apparent extensional viscosity, relaxation time, and experimental break-up time are reported in Table 4.2. These results summarize that the above-mentioned parameters were increased with the polymer concentration. The lowest experimental break-up times of 0.61 s and 1.62 s were observed for the non-associating polymer HPAM at the concentration of 1000 ppm and 2000 ppm subsequently. Further, these lower break-up times corresponded to the lowest maximum apparent extensional viscosities of 49 and 75 Pa.s. These results prove its lowest tendency for monovalent salt resistance.

Table 4.2: maximum apparent extensional viscosity, experimental break-up time, and relaxation time of polymer samples

Polymer	Concentration (ppm)	NaCl Concentration (ppm)	Experimental Break-up time (s)	Relaxation time (s)	Maximum Apparent Extensional Viscosity (Pa·s)
C319	1000	5000	2.01	0.08	171
	2000	5000	5.06	0.255	240
D118	1000	5000	1.41	0.039	102
	2000	5000	4.43	0.2076	205
HPAM	1000	5000	0.61	0.008	49
	2000	5000	1.62	0.0100	75

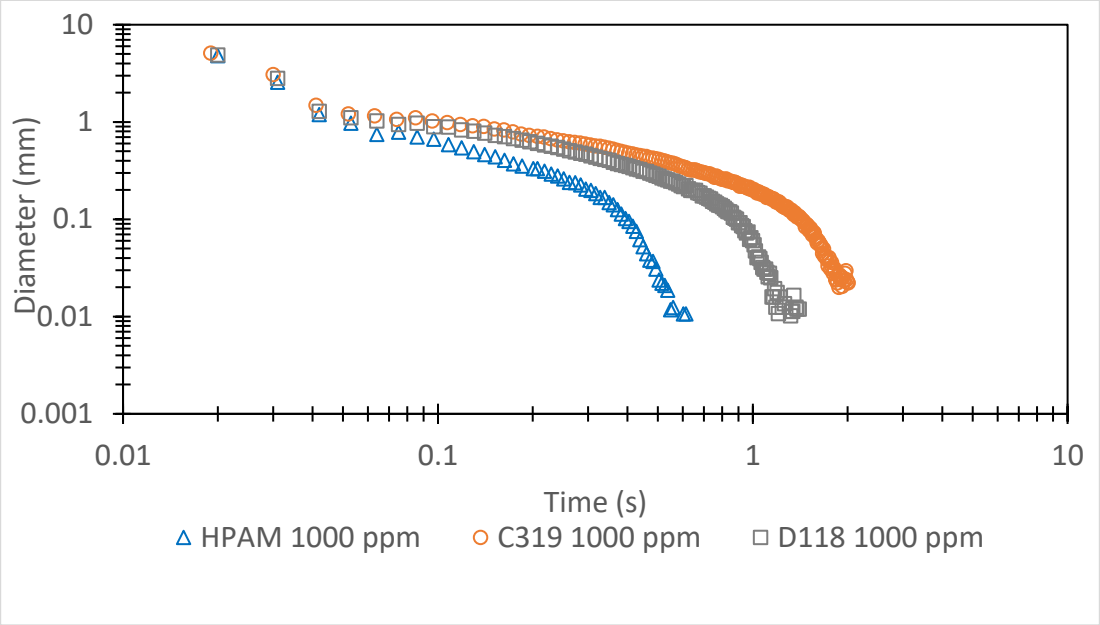

(a)

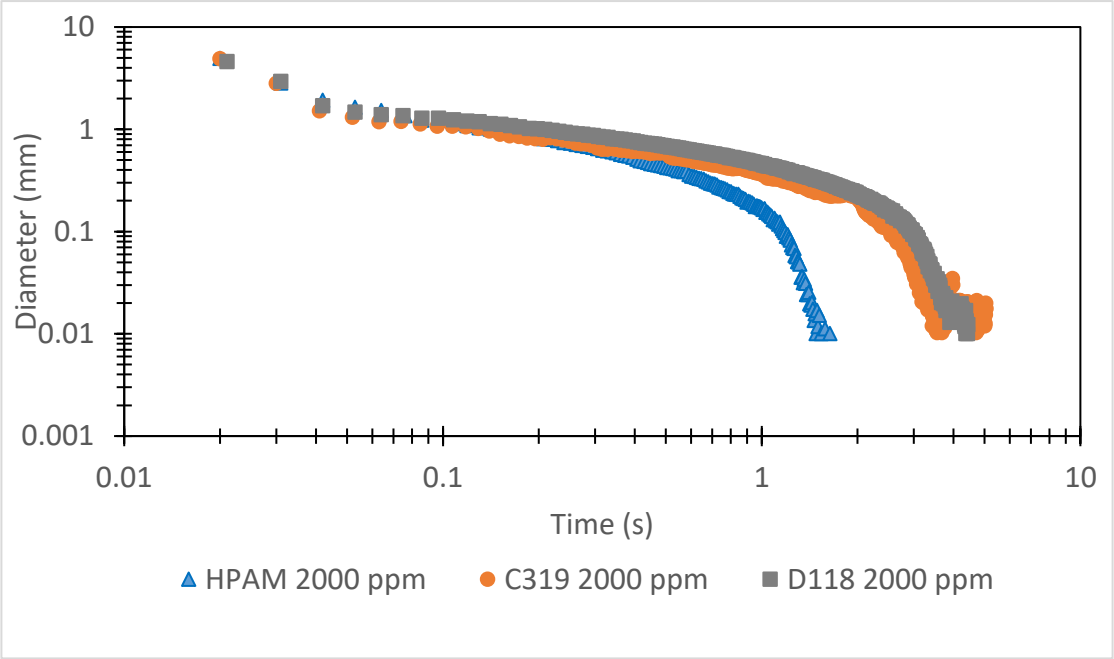

(b)

Figure 4.5 Uniaxial elongation and filament breaking for the polymer samples

Moving from HPAM to C319 having an associating characteristic due to hydrophobicity shows a higher break-up time and so a higher maximum extensional viscosity. The experimental break time of 2.01s and 5.06s were observed for C319 at 1000 ppm and 2000 ppm respectively. An order of magnitude of higher relaxation time of 0.255 for C319 at 2000 ppm shows the domination of inter-molecular association. A polymer with the highest hydrophobicity shows a lower experimental break-up time of 1.41s and 4.43s at 1000 ppm and 2000 ppm respectively. The corresponding maximum apparent extensional viscosity values, 102 Pa.s, and 205 Pa.s were lower than the concerned solution for C319. A reason behind it is the stiffness of non-hookean transformations at the higher hydrophobicity [59].

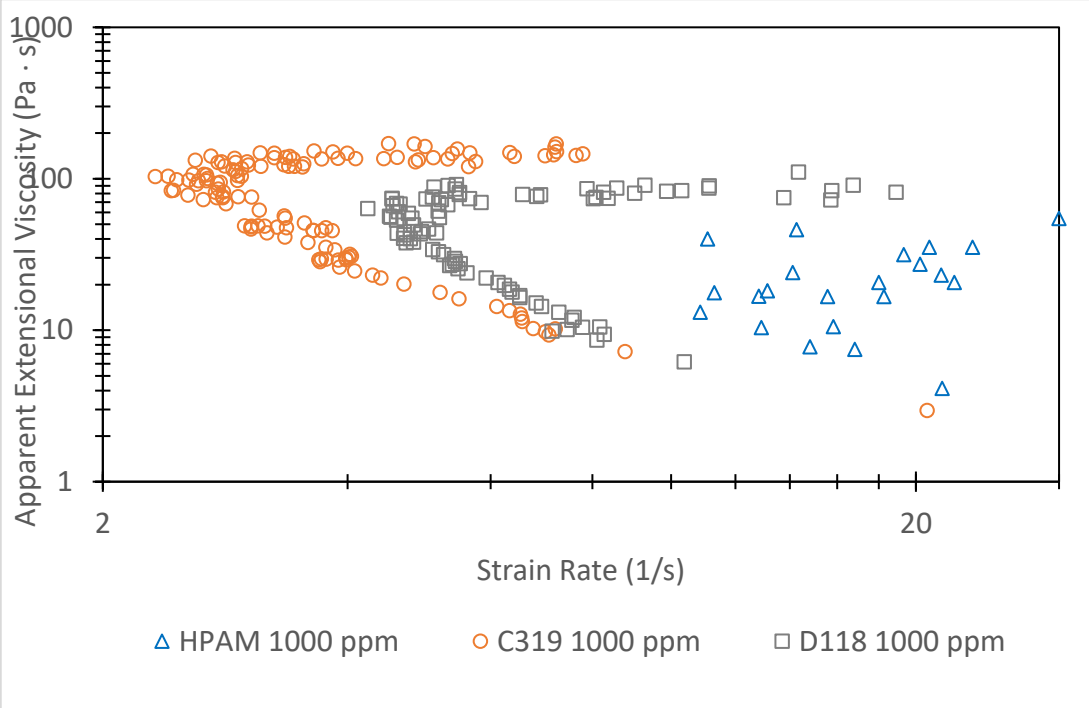

(a)

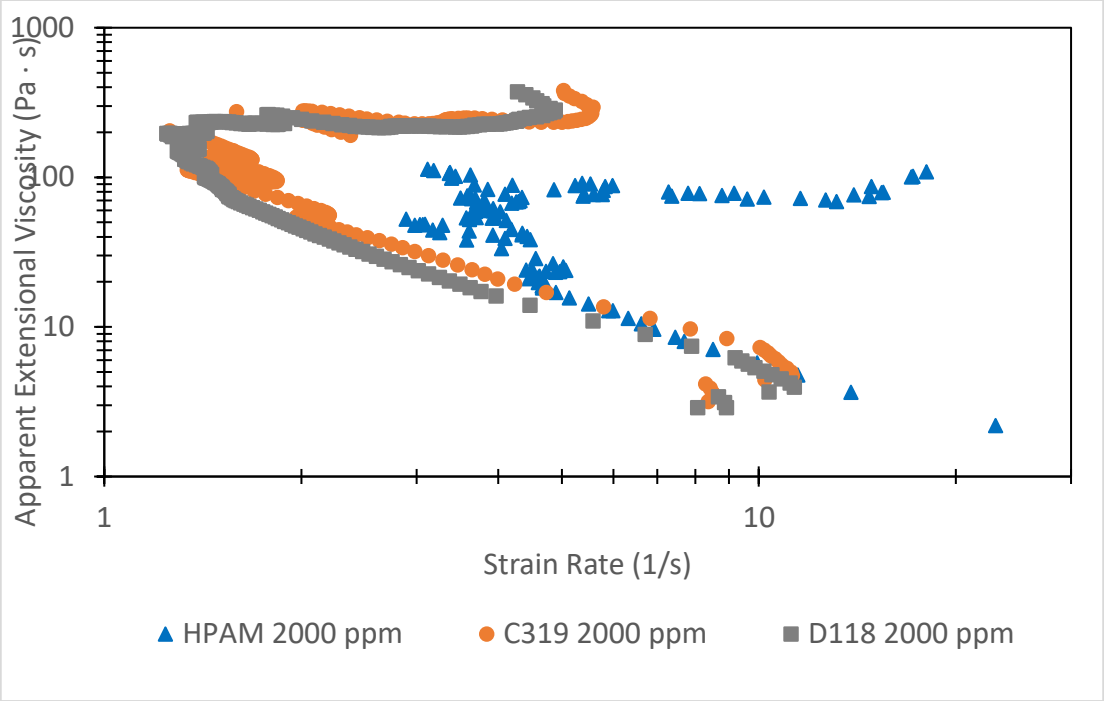

(b)

Figure 4.6: Apparent extensional viscosity as a function of strain rate

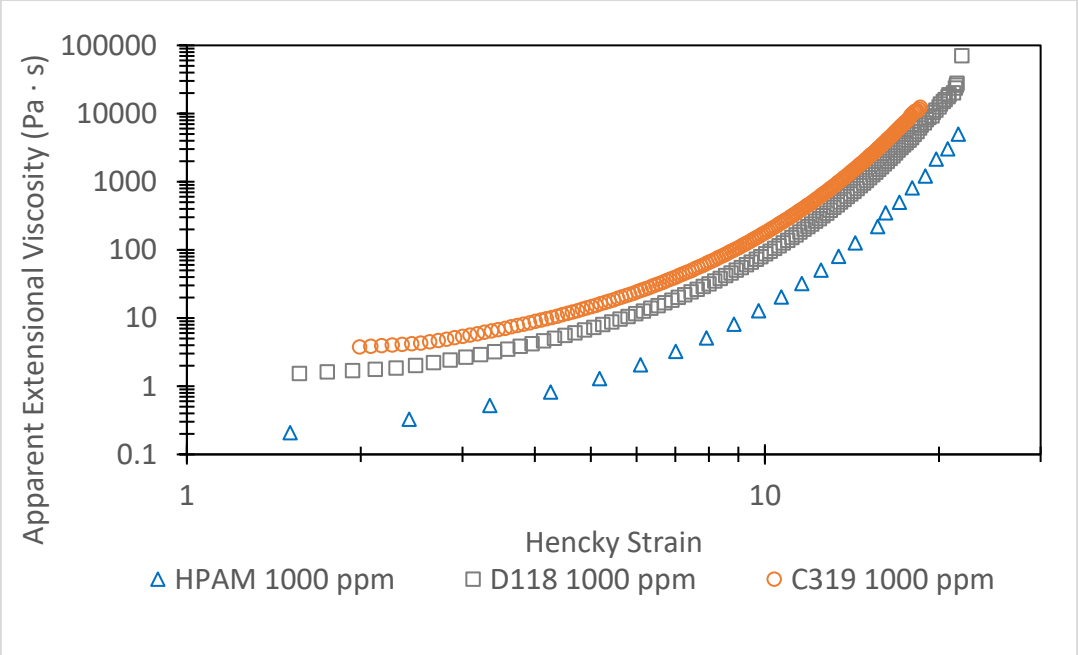

(a)

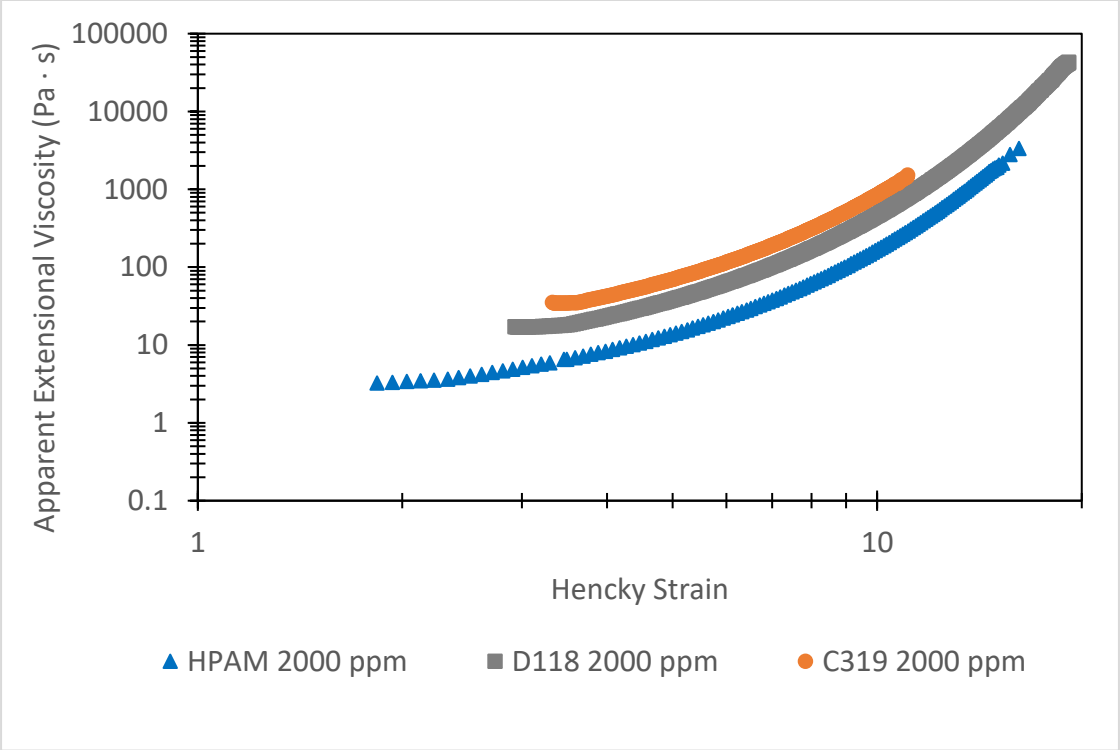

(b)

Figure 4.7 Straining hardening for polymer samples

Figures 4.5 and 4.6 show the experimental temporal evolution of mid-point diameter and extensional viscosities vs strain rate for all polymer solutions. The extended exponential decays (Figure 4.5) for the polymer concentration of 2000 ppm represent the extended coiling of polymer chains. The longest decays for C310 at 1000 ppm and 2000 ppm were observed due to Hookean transformations that formed flexible microstructures. However, the formation of rigid microstructures for D118 breaks earlier than for C319. Figure 4.6 shows the data divergence into two regimes. Firstly, the apparent extensional viscosity increases as the strain rate decreases. This is due to gravitational sagging which is not a function material characteristic. After reaching a maximum value, resultant deformations due to weak viscous resistance rises the strain rate again. These transitions were observed at the lower strain rate as the hydrophobicity increased.

However, the presence of monovalent cations favors the transition of Hookean to non-Hookean transformations. The supporting role of the cation results in the lower experimental break-up time and so the extensional viscosity compared to the concern values reported in the literature[59]. Further, the strain rate grows until unraveling polymer strands' elastic stresses form to resist the deformation caused by capillary action. Here, the inter-molecular interactions at the polymer concentration of 2000 ppm induce the higher elastic stress that results in higher apparent extensional viscosities compared to the polymer concentration of 1000 ppm.

The strain-hardening behavior caused by the mechanical disruption is shown in Figure 4.7. The results show poor strain hardening behavior for HPAM at both concentrations because of the high entanglement of polymer molecules. These entanglements may be proficient in causing stress overshoot but may not be effective enough to cause strain hardening. The hydrophobic inter and intramolecular interactions may be capable enough to make the polymer chain stiff and so the strong strain hardening was observed compared to HPAM. However, at the higher hydrophobicity, the higher entanglement of polymer chains causes poor strain hardening [32].

4.4.2 AF4-FFF characterization

AF4-MALS-dRI was used to determine the weight-average molar mass (Mw) and Radius of Gyration for the polymer solution. A summary of the results is shown in Table 4.3. Values of the recoveries for the polymer solution from the separation channels were ≥ 99%, which means that all of the injected polymer samples were eluted without any major losses of components.

Table 4.3. Average molar mass and radius of gyration for the polymer solutions

Polymer Name	Polymer (ppm)	NaCl (ppm)	Mn (MDa)	Mw (MDa)	Mz (M Da)	PDI	Rn (nm)	Rw (nm)	Rz (nm)	Slope of Conformat -ional Plot
HPAM	1000	5000	3.74	4.51	5.63	1.21	311.2	341.7	381.6	0.50
	2000	5000	6.18	8.00	9.25	1.30	413.9	462.8	488.7	0.42
C319	1000	5000	7.76	12.72	12.95	1.64	506.4	546.8	574.4	0.34
	2000	5000	9.14	17.32	16.61	1.90	499.5	576.8	603.1	0.28
D118	1000	5000	12.65	18.27	27.95	1.44	708.6	788.1	850.2	0.20
	2000	5000	20.53	31.10	54.59	1.52	738.9	804.4	885.7	0.16

Table 4.3 shows that the lowest values for the Mw ~ 3.7Mda and 6.18Mda and Radius of Gyration ~ 311.2 nm and 413.9 nm were observed for HPAM at 1000 ppm and 2000 ppm respectively. A reason behind it is the lowest or negligible hydrophobicity for HPAM. In the presence of salt, especially cations, it hardly retains its original structure due to the charge shielding effect of cation (Na^+). This charge screening effect reduces the electrostatic repulsion between two HPAM polymer chains. As a resultant domination of intramolecular interaction, the polymer chains tend to coil and reduce the Radius of gyration reported for the HPAM solution in Deionized water [144]. Also, the reported lowest Mw values are due to rapid polymer chain degradation (especially for the lower end of the weight distribution). Higher hydrophobicity for the polymers C319 and D118 result in their higher stability against NaCl compared to HPAM at

both concentrations. This is because the ionic strength of additional hydrophobes on the polymer backbone withstands against charge shielding effect and the intermolecular interaction results in higher values for Mw and Radius of gyration compared to HPAM solutions. The highest values for the Mw ~ 12.65Mda and 20.53Mda and Radius of Gyration ~ 708.6 nm and 738.9 nm were observed for D118 at 1000 ppm and 2000 ppm respectively.

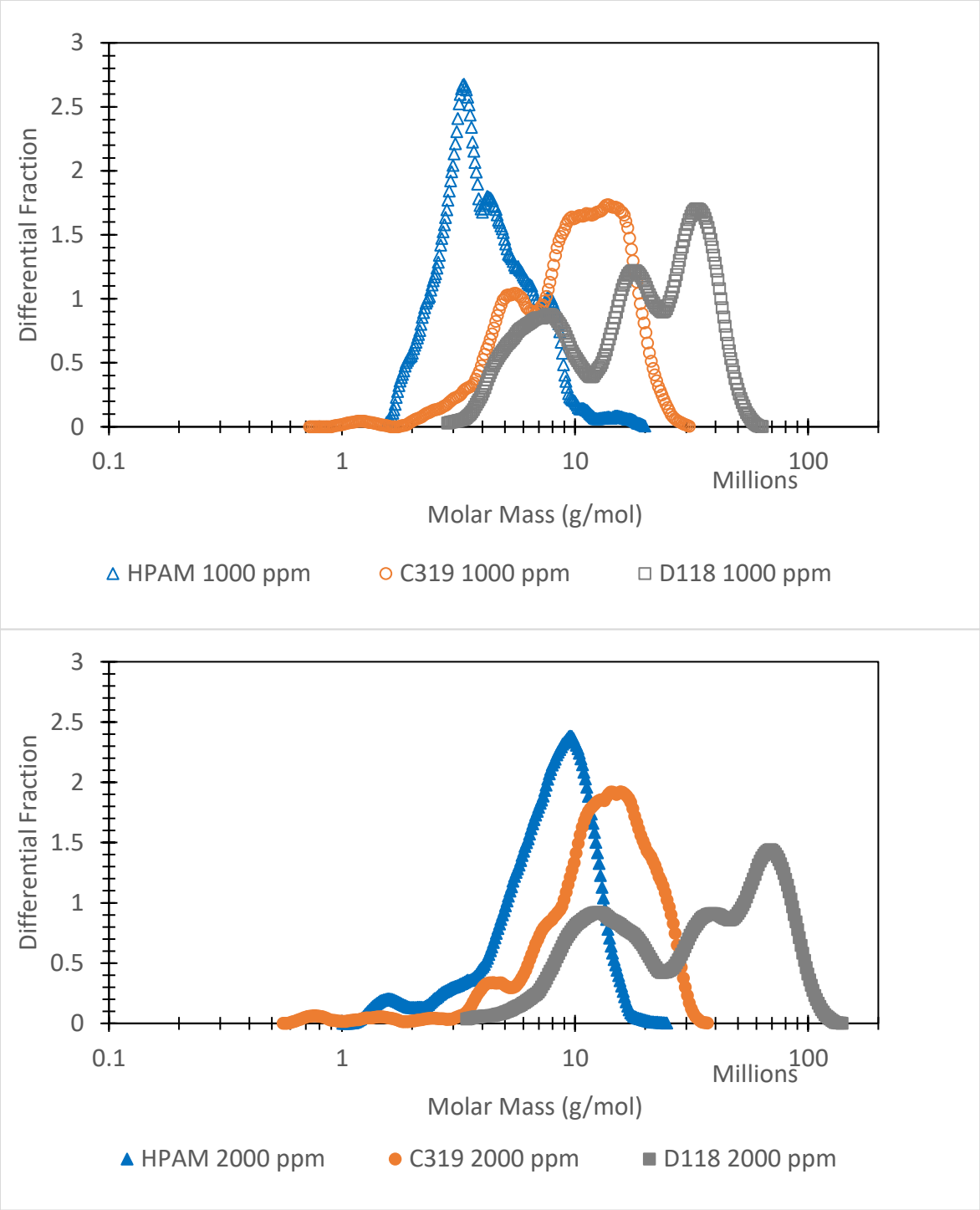

(a) Differential mass distributions for the polymer solutions

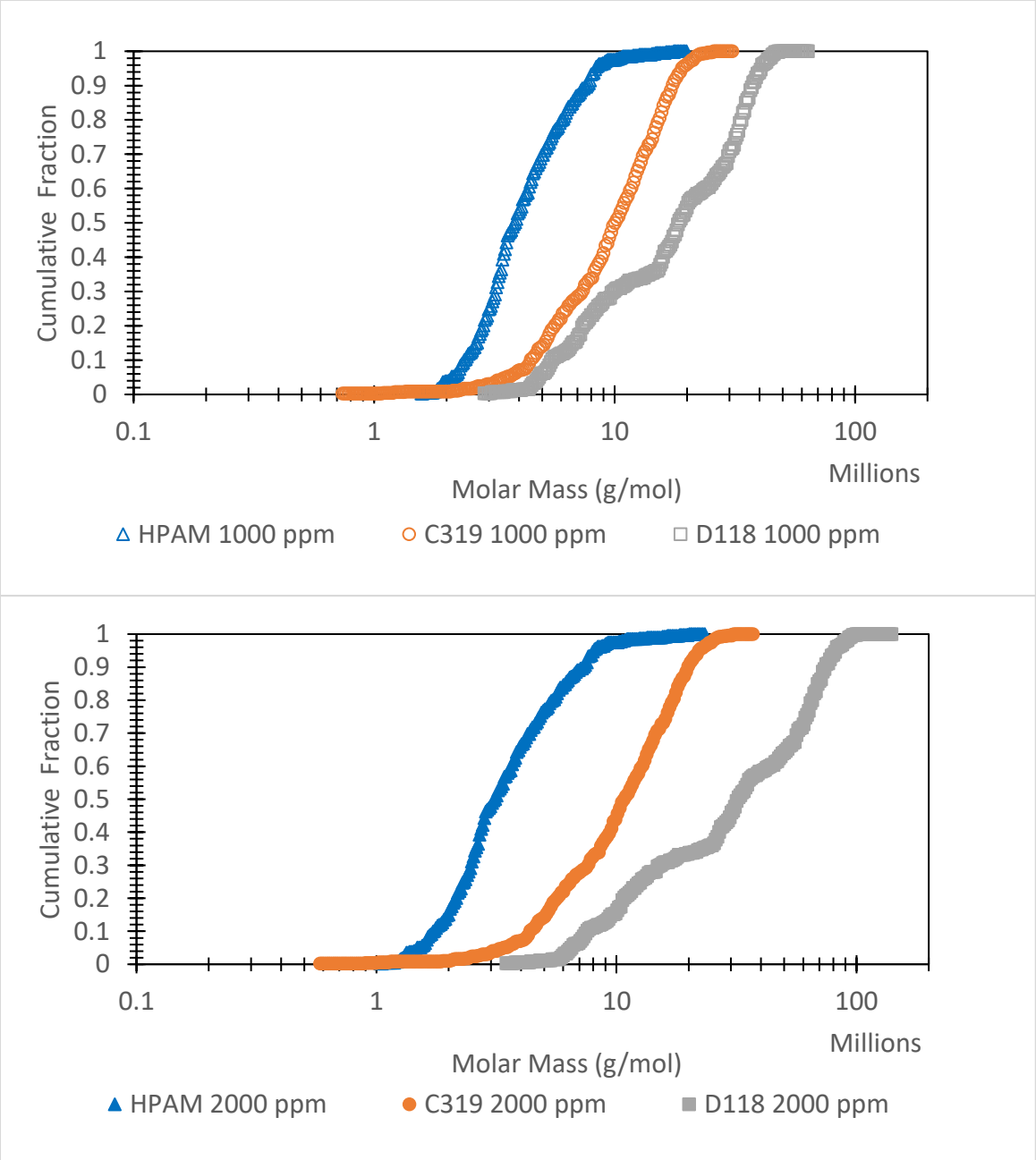

(b) Cumulative mass distributions for the polymer solutions

Figure 4.8 Mass distribution for the polymer solutions

Figure 4.8 compares measured molar mass distributions obtained from the AF4-MALS technique for the polymer solutions. The molar masses of the macromolecules range from 0.5 Mda-70Mda for the solutions with a polymer concentration of 1000 ppm and 0.5Mda- 120Mda for the ones

with a 2000 ppm polymer concentration. A negligible intensity secondary peak was observed for HPAM solutions even though the peak of the distribution curve shifts to the higher end of MWD. This is due to the domination of the intermolecular attraction between the polymer chains with the lower average molar mass at 2000 ppm polymer concentration. These inter-molecular networks are responsible for boosting up the reported viscosities (shear and extensional) for the solution with HPAM concentration of 2000 ppm.

The largest horizontal extent (≈ highest PDI) was observed for the solutions prepared with C310 with 1000 and 2000 ppm. The hydrophobic nature of the polymer showed a significant effect on the MWD even in the presence of monovalent salt. Shifting the distribution peaks at the higher ends for the polymer solutions with 2000 ppm polymer concentration indicates aggregation of polymer molecules. However, the accelerated polymer aggregation induced by its hydrophobicity resulted in the secondary peaks for the solutions with C319 and D118. The secondary spikes for the solutions containing C319 and P329 at both polymer concentrations prove their Critical Aggregation Concentration (CAC) is below 1000 ppm. This CAC is much lower than the reported CAC for polymer solutions prepared with DI water as a solvent [22]. An identical behavior for associative polymers, C319 and D118 is shifting the MWD to the higher end of the horizontal axis at 2000 ppm. For C319, the MWD peaks were shifted from 5 Mda and 15 Mda at 1000 ppm to 5 Mda and 20 Mda at 2000 ppm with a higher secondary peak intensity. Similarly, for D118, MWD peaks were shifted from 7Mda, 20 Mda, and 40 Mda at 1000 ppm to 12 Mda, 40 Mda, and 70 Mda respectively at 2000 ppm. This shows the formation of microgels due to the domination of intermolecular hydrophobic interactions withstanding against charge screening caused by cations.

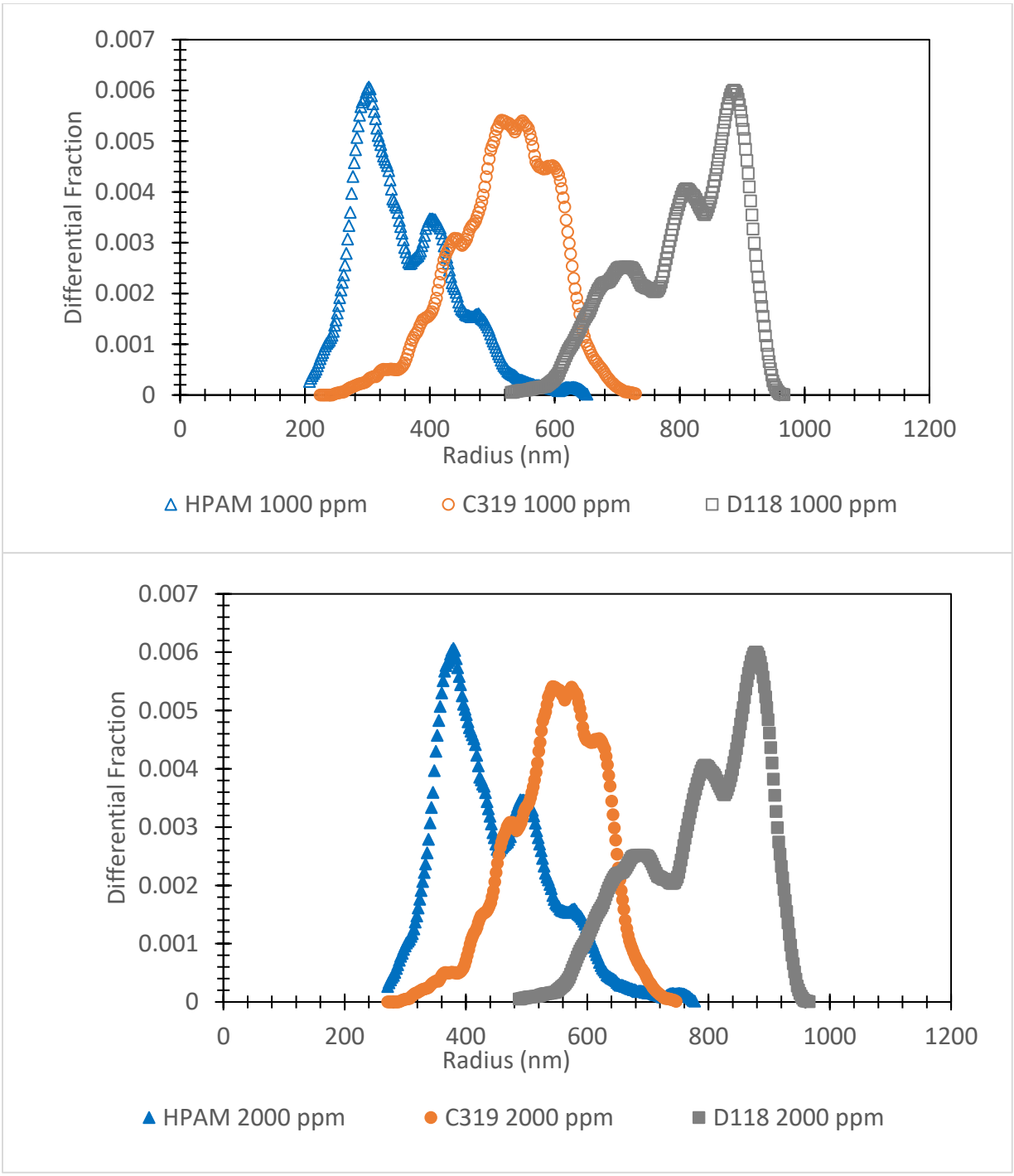

(a) Differential radius distributions for the polymer solutions

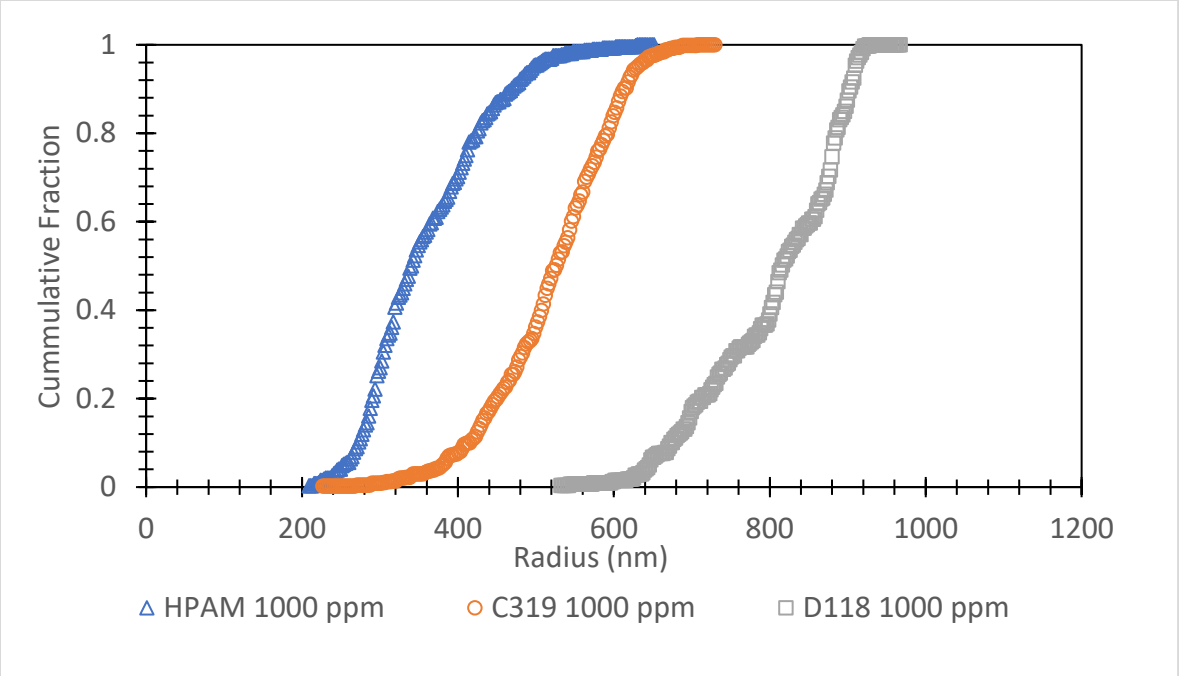

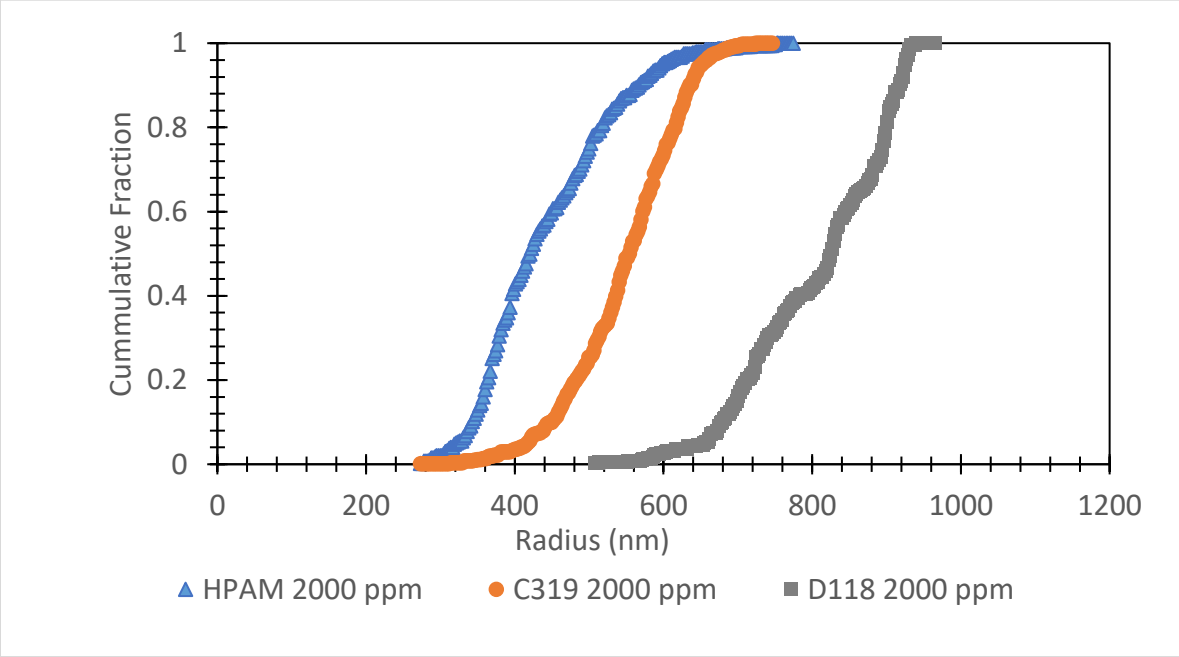

(b) Cumulative radius distributions for the polymer solutions

Figure 4.9 Radius distribution for the polymer solutions

Figure 4.9 reveals that the radius distributions for the respective polymer solutions at both concentrations were very similar except HPAM. For HPAM (non-associating polymer) the

radius distribution was shifted from a range of 200nm- 625nm to 275nm- 795nm for the polymer concentration of 1000 ppm and 2000 ppm respectively. Additionally, the slope of conformational phot (Figure 4.10) of 0.5 for 1000 ppm HPAM solution was observed to be decreased to 0.42 for the 2000 ppm HPAM solution. This shows the transformation of randomly coiled linear conformation to the cylindrical linear conformation. These confirmations are Hookean conformations that can be compacted further at the higher salinity[59]. However, once the spherical non-Hookean conformations are formed, they do not affect the radius distributions efficiently. For C319, the slope of the conformational plot changes from 0.34 for 1000 ppm to 0.28 for 2000 ppm polymer solution. The steeper cumulative radius distribution at 2000 ppm also shows a compaction of spherical conformations. However, the aggregation of the small compacted molecular species (Rn~ 200 nm) resulted in a higher average Mw without affecting the average Rn significantly. For D118 with the highest hydrophobicity, the radius distributions were observed very similar. The slope of the conformational plot of 0.2 for 1000 ppm D118 decreased to 0.16 showing the formation of compacted spherical non-Hookean conformations.

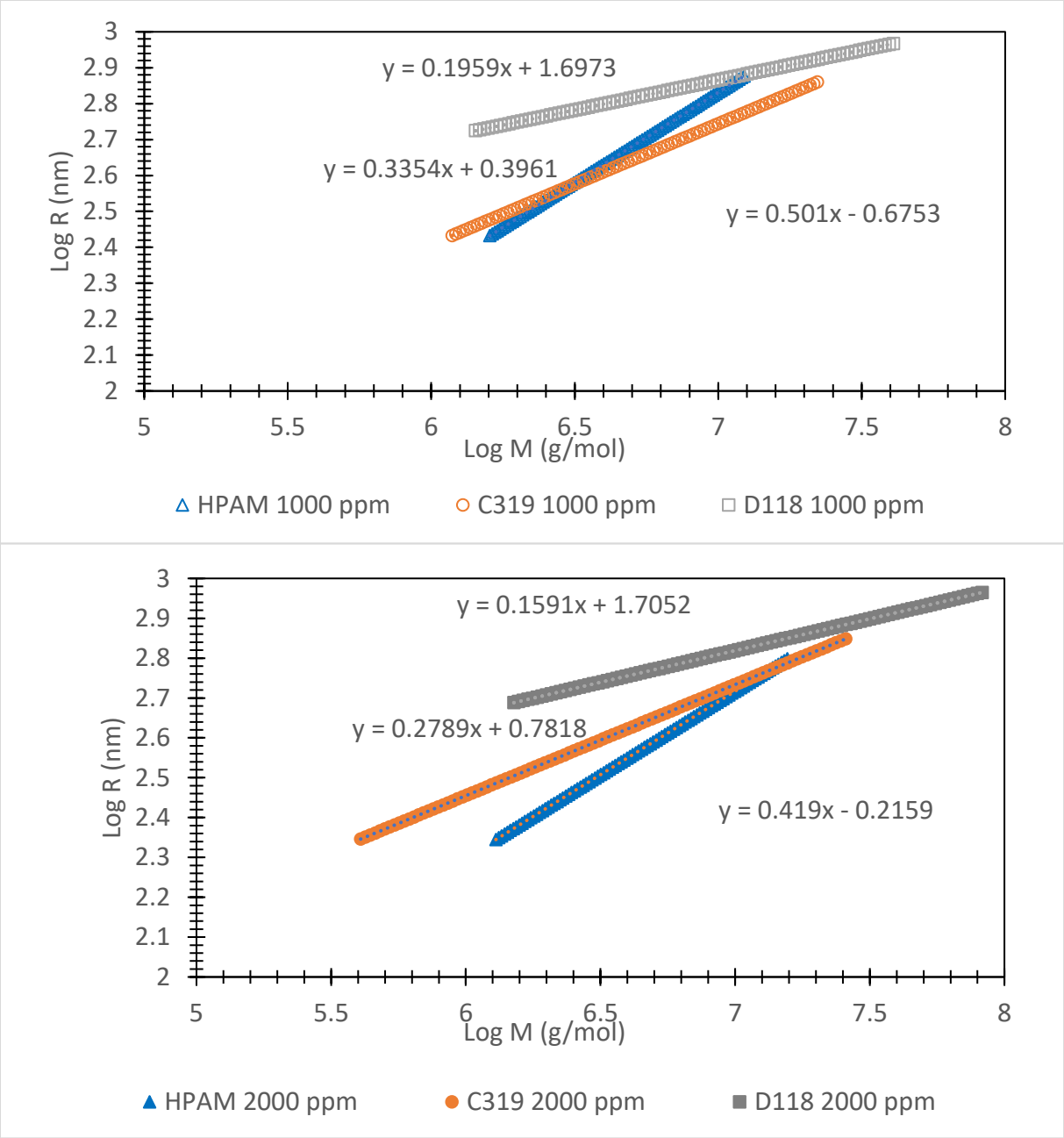

Figure 4.10 Conformational plots for the polymer solutions

4.4.3 Polymer Core floods with the consolidated cores

To determine the Resistance Factor (RF) and Residual Resistance Factor (RRF), associative polymers were used in single-phase core flood tests at various flux rates (2 ft/day, 5 ft/day, 10 ft/day, 25 feet/day, 50 ft/day). Initially, the preliminary water was injected into the Bentheimer

cores (by using the set-up shown in Figure 4.3) at the desired flux rates and the effluent was collected in the volumetric cylinder. Pressure stability was achieved at each flux rate switch over to the other higher rates. The injection flux rates vs steady state pressure data were utilized to estimate the permeability and porosity for each set of experiments. These values are reported in Table 4.4. The above-mentioned flux rates were replicated for the subsequent polymer solution flooding followed by chase water and secondary water injection. It was ensured to inject sufficient pore volume of fluid to achieve a stable pressure drop at each stage. Equations 4.5 and 4.6 were used to calculate RF and RRF for each set of experiments.

Table 4.4. Petrophysical Properties

Polymer	Concentration (ppm)	Porosity	Permeability (mD)
HPAM	1000	18%	121
	2000	17%	125
C319	1000	18%	144
	2000	19%	135
D118	1000	18%	129
	2000	19%	134

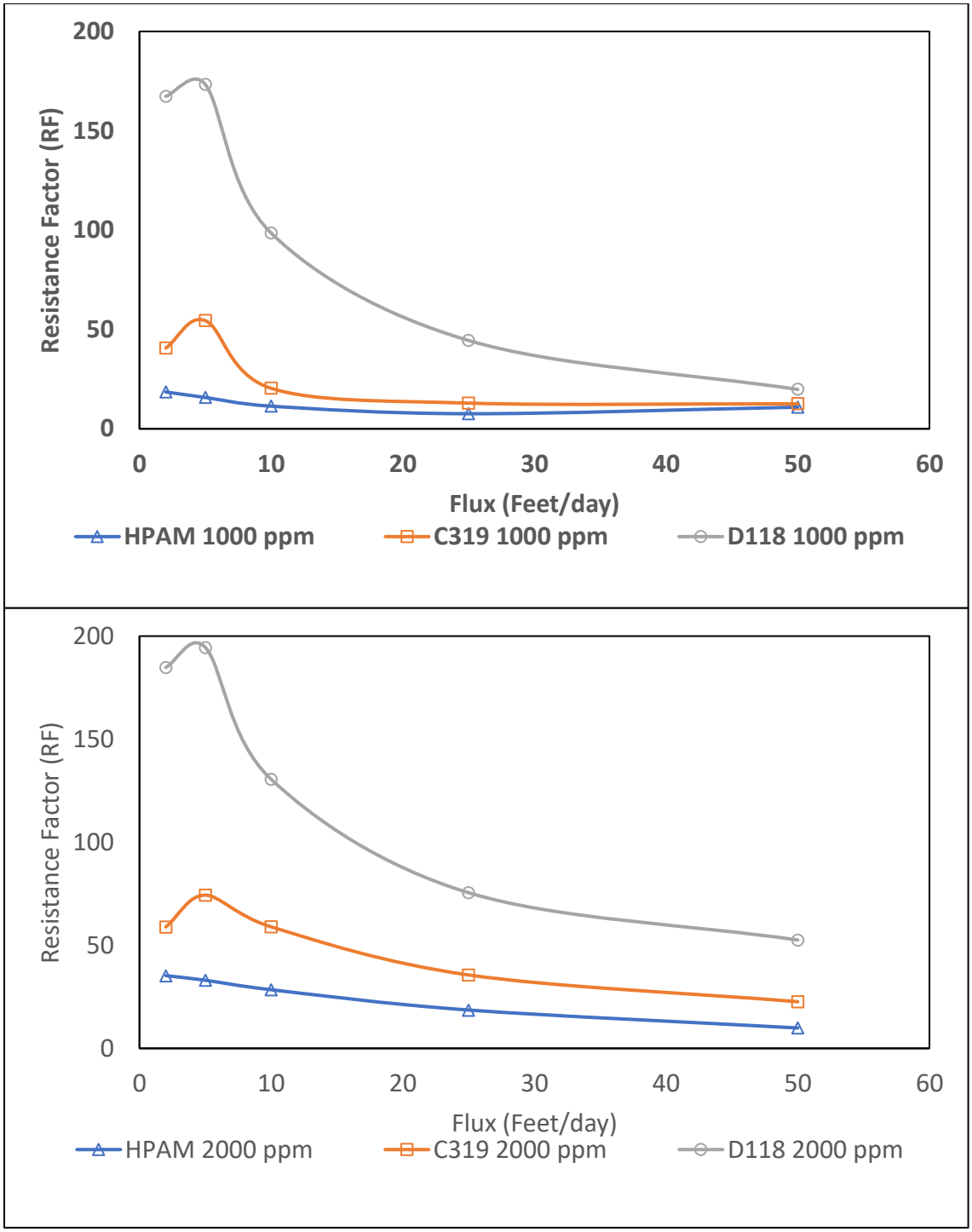

Figure 4.11 RF as a function of flux rate for polymer solutions

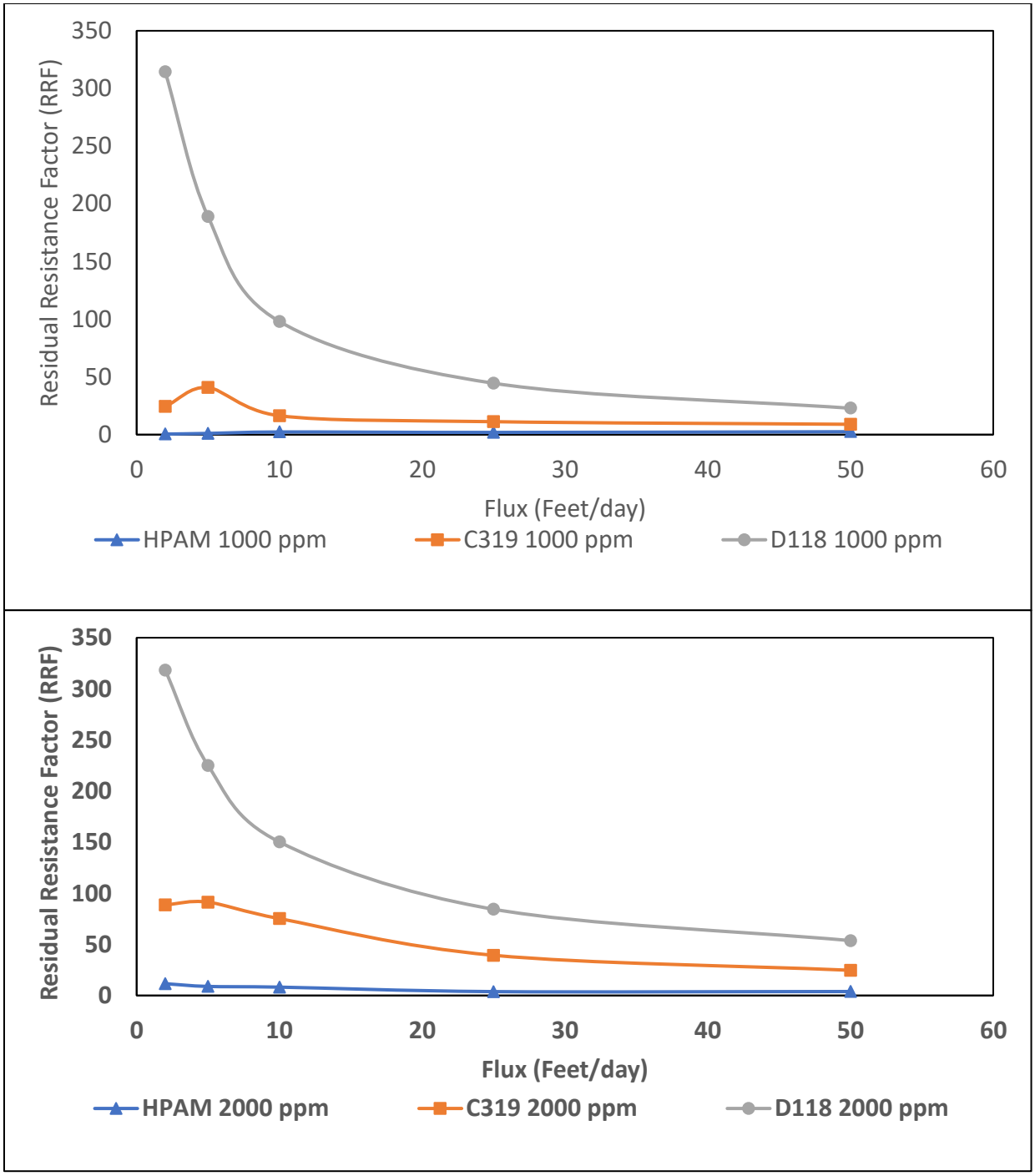

Figure 4.12 RRF as a function of flux rate for polymer solutions

By connecting the RF in accordance with the change in velocity, the flow resistance properties of the polymer solution at various speeds can be determined. These results are shown in Figure 4.11. The measurement of RRF reveals permeability reduction/polymer retention as shown in

Figure 4.12. Typically, all polymer solutions showed a declining trend for RF and RRF with increasing flux regardless of the polymer concentration. However, these curves were shifted upwards for the solutions prepared with a polymer concentration of 2000 ppm.

For HPAM solutions with 1000 ppm polymer concentration, the randomly coiled polymer structures with the smallest radius of gyration attributed to the lower RF because of a combined effect of mechanical entrapment and adsorption due to a proposed mechanism as shown in Figure 4.13(a). In this case, the whole polymer chain can be adsorbed on the rock surface, and the chances of mechanical entrapment would be lower because of the similar average pore throat size, 300 nm to the radius of gyration, 311 nm. At 2000 ppm polymer concentration, higher number density for polymer molecules with coiled conformation may result in the adsorption mechanism proposed in Figure 4.13(b). Combining this with the entrapment of aggregates with higher size (Figure 4.9(a)) seems to contribute to higher RF values. However, these flexible randomly coiled conformations for HPAM may not trigger the viscoelastic resistance that resulted in the lowest RF values for HPAM solutions.

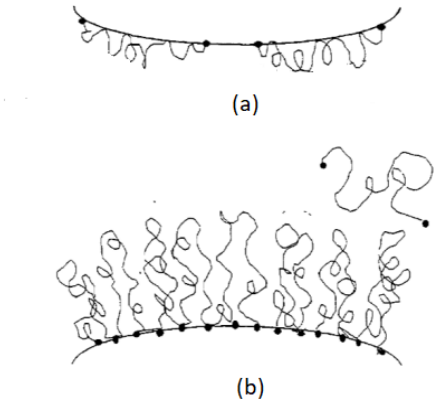

Figure 4.13 Adsorption mechanism of polymer on the rock surface [148], [149]

For the associative polymers, the compacted spherical conformations seem to create some viscoelastic resistance at a low velocity until the adsorption equilibrium is established. Additionally, the higher radius of gyration triggers mechanical entrapment. So a combined effect of these phenomena resulted in a small spike in RF at the low flux rate. Further at the higher velocity, the higher flexibility (also resulted in the higher breakup time as shown in Figure 4.5(a)) of Hookean conformations for C319 helps to overcome the viscoelastic resistance even though having a higher radius of gyration at 1000 and 2000 ppm. This might be a reason for higher RF values for C319 compared to HPAM. However, the strong domination of intermolecular networks induced by hydrophobicity resulted in higher RF values for 2000 ppm C319 solution. Further at the highest hydrophobicity, the rigid sphere conformations having a higher radius of gyration may trigger the mechanical entrapment on the top of adsorption. This could be a primary reason for having higher values of RF for D118.

Figure 4.12 shows the retention of HPAM at each flux remains constant at both 1000 and 2000 ppm polymer concentration. However, It is clear that the randomly coiled molecular chain conformations can be easily linearized to adapt to flow[148]. So the lowest values of RRF were observed for HPAM solutions. For C319 and D118 at 1000 ppm polymer concentration, the weak intermolecular structures undergo destruction, and recovery of hydrophobic association structures could not maintain dynamic equilibrium, thus causing a decrease in polymer retention at a higher flux rate. However, at the higher polymer concentrations of 2000 ppm, compacted spheres of aggregates with a higher radius of gyration increase the hydrodynamic trapping resulting in higher RRF values.

4.4.4 Molecular weight and radius distributions overcoming the limitations of rheology by explaining polymer flow in unconsolidated porous media

Table 4.5 Fluid injection sequence for the injectivity experiments using unconsolidated porous media [57]

Stage	Flux (ml/hour)	Injected Pore Volumes
Primary Water Flooding	60	2
	120	2
	180	2
	240	2
	300	2
Polymer Flooding	60	2
	120	2
	180	2
	240	2
	300	2
Chase Water	15	10.9
Secondary Water Injection	60	2
	120	2
	180	2
	240	2
	300	2

The measured porosity and permeability for all experiments were in the range of 0.35-0.39 and 1.51-1.65 D. The recorded stable (or steady-state) pressure data was used to calculate the RF and RRF for each set of experiments (Figure 4.14 and Figure 4.15) by using Equations 4.5 and 4.6.

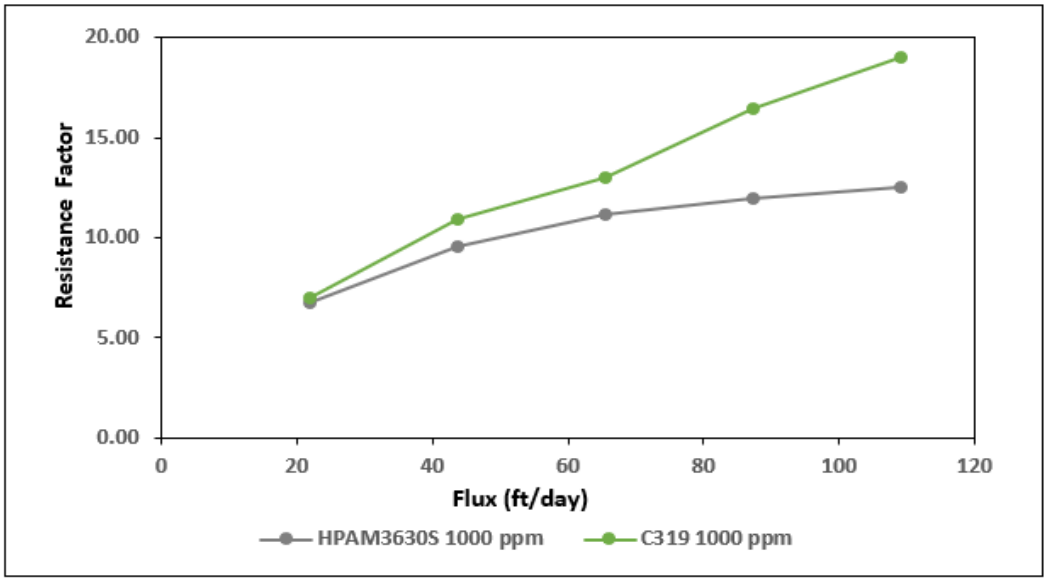

(a)

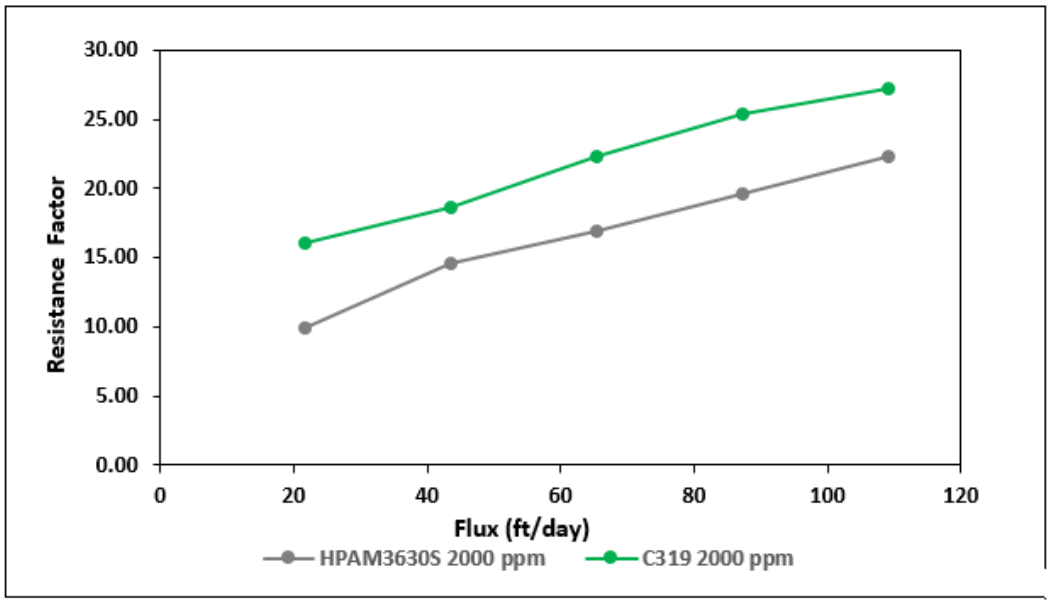

(b)

Figure 4.14 Resistance factors for the polymer solutions in unconsolidated sand-pack

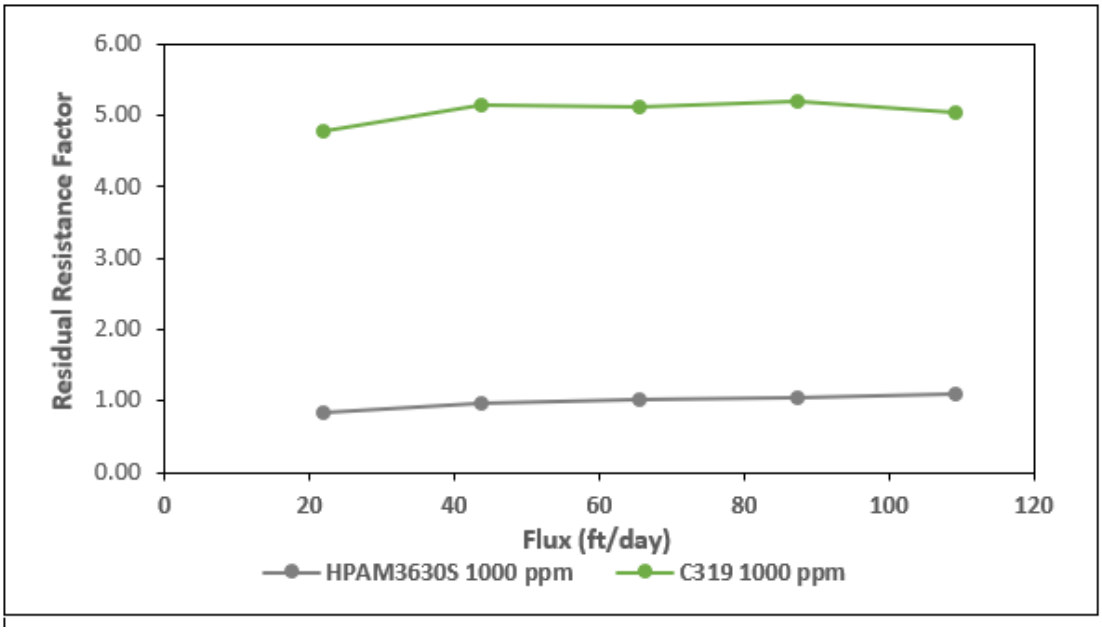

(a)

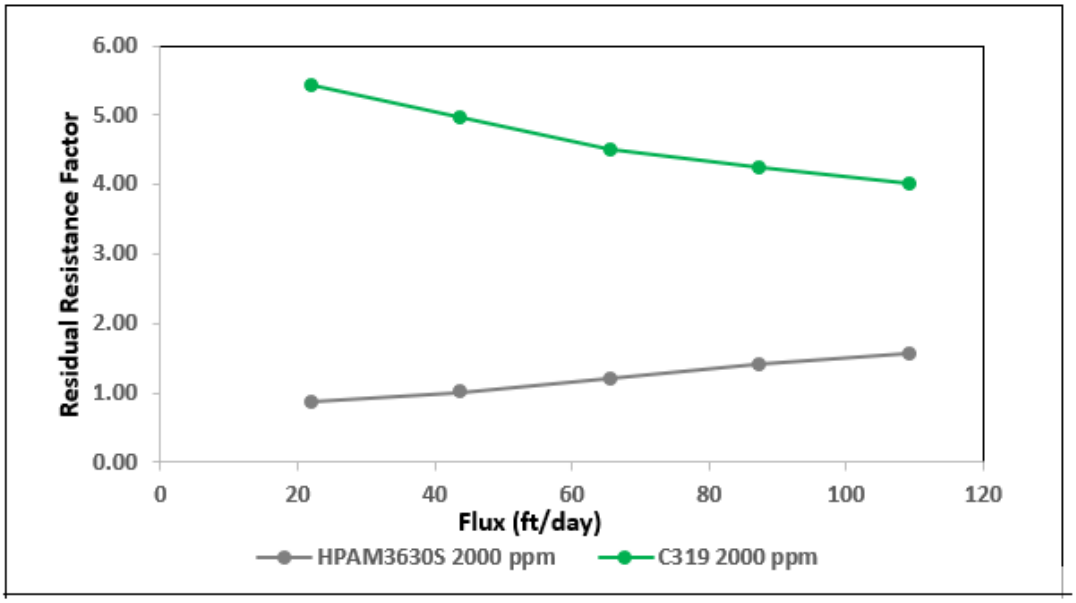

(b)

Figure 4.15 Residual Resistance factors for the polymer solutions in unconsolidated sand-pack

As both polymers, HPAM and C319 exhibit an identical rheological profile, it is important to understand how the MWD and radius distributions affect the in-situ rheology characterized by RF and RRF. The associative polymer C319 has a very similar molar mass reported by the manufacturer. However, the polymer solutions with C319 exhibit broader MWD with higher radius gyration. Also, these solutions have randomly coiled polymer conformations compared to the linear rod-like conformations for the HPAM solutions at both polymer concentrations. The injectivity results (Figures 4.14 and 4.15) indicate that the polymer solutions with the lower polydispersity and liner conformations show lower polymer retardation in the sand-pack. At 1000 ppm, below the CAC, C319 and HPAM approach similar values for RF. As the polymer chains with the higher molecular weight show pore plugin and/or adsorption results in reduced permeability and pore diameter, the RF values increase with the flux rates. However, the thickening effect pronounced for C319 indicates domination of extended higher end than the MWD for HPAM. This eventually resulted in higher RRF values compared to HPAM solutions at each flux rate. At 2000 ppm polymer concentration, which is above CAC, the domination of polymer aggregates or microgels seems to dominate the resistance. These aggregates are responsible for an additional resistance resulting in a higher value for RF than the ones at 1000 ppm. A combined effect of polymer entrapment and adsorption. However, the lower RRF values at higher flux rates for C319 indicate desorption of the microgels.

The above correlation study indicates the importance of molecular weight and radius distributions for estimating in situ rheological behavior. In addition, the polymer conformations along with the dispersity index can be used to predict the tentative pressure drop and the reduced permeability or mechanical entrapment.

4.4.5 Application of AF4-FFF technique for field application

The produced water samples were received from the polymer EOR field. These include injecting fluid (Raw Sample 3440, 2000 ppm), aerobic, and anaerobic samples. The anaerobic samples were isolated with an inert gas to prevent oxidative degradation.

(a) Aerobic-produced water samples (b) Anaerobic-produced water samples

Figure 4.16 Samples received from polymer EOR field

The concentration of polymer in the aerobic-produced water samples was measured by using the AF4-FFF system as reported in Table 1.2. A test methodology for fluid flow fractionation described in the above section was applied to characterize the produced water samples to determine molar mass distributions, radius distributions, and conformational properties. These plots were compared with the injecting fluid (Figure 1.6, Figure 1.7, and Figure 1.8) to predict the flow behavior of injecting fluid in the reservoir. Table 1.3 show the average molar mass and radius of gyration for the polymer samples.

Table 4.6 Polymer concentration in produced water

Sample ID	Polymer Concentration (ppm)
Aerobic Sample 1	1404
Aerobic Sample 2	1502
A-079 Aerobic Sample	1460

Table 4.7 Average Molar mass and radius for the produced water samples

Sample							
	Mn (M Da)	Mw (MDa)	Mz (M Da)	PDI	Rn (nm)	Rw (nm)	Rz (nm)
Anaerobic Sample 1	12.16	19.13	24.03	1.574	398.3	446.4	466.5
Aerobic Sample 1	4.681	6.446	7.087	1.377	362.3	436.3	450.9
Anaerobic Sample 2	16.82	27.95	35.42	1.861	320.4	354.6	368.6
Aerobic Sample 2	3.716	6.893	8.44	1.355	127.0	165.9	175.8
A-079 Anerobic Sample	15.26	27.27	35.3	1.787	219.6	251.9	263.6
A-079 Aerobic Sample	5.122	6.51	7.564	1.271	175	191.2	198.9
Raw Sample	32.28	47.54	57.47	1.473	505.8	556.5	577.6

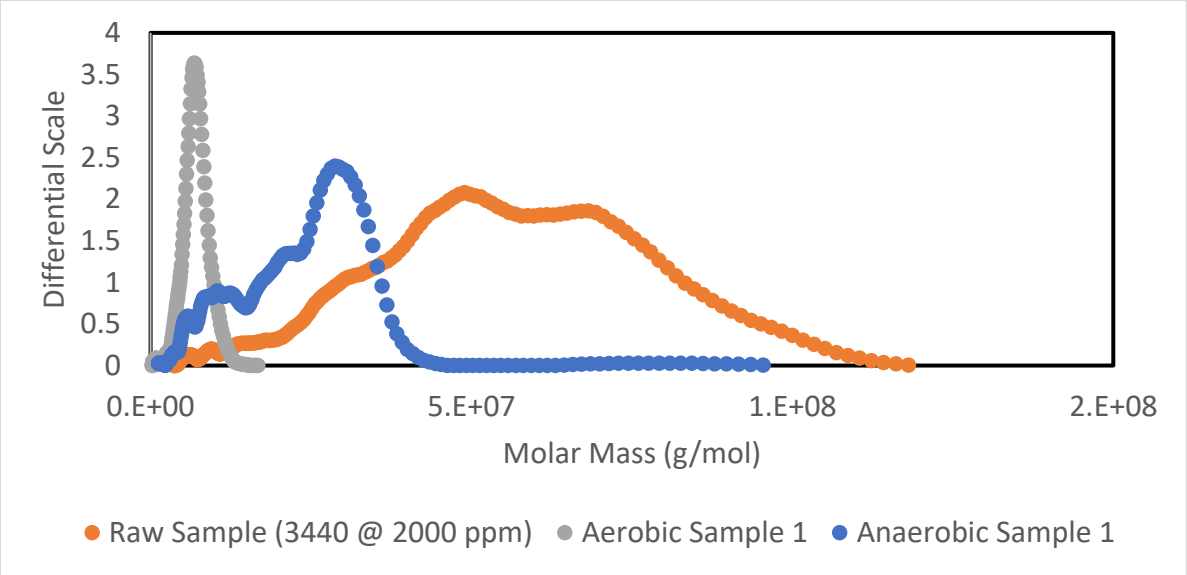

(a) Molar mass distributions for Sample 1 and Injecting Fluid

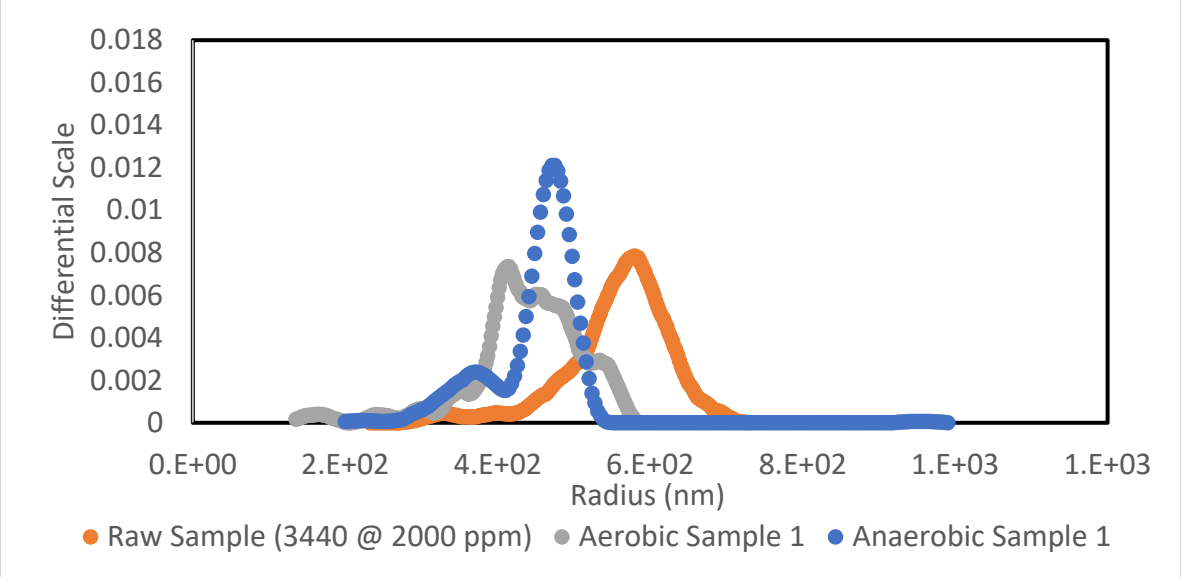

(b) Radius distributions for Sample 1 and Injecting Fluid

Figure 4.17 Comparing the distributions of sample 1 with injecting fluid

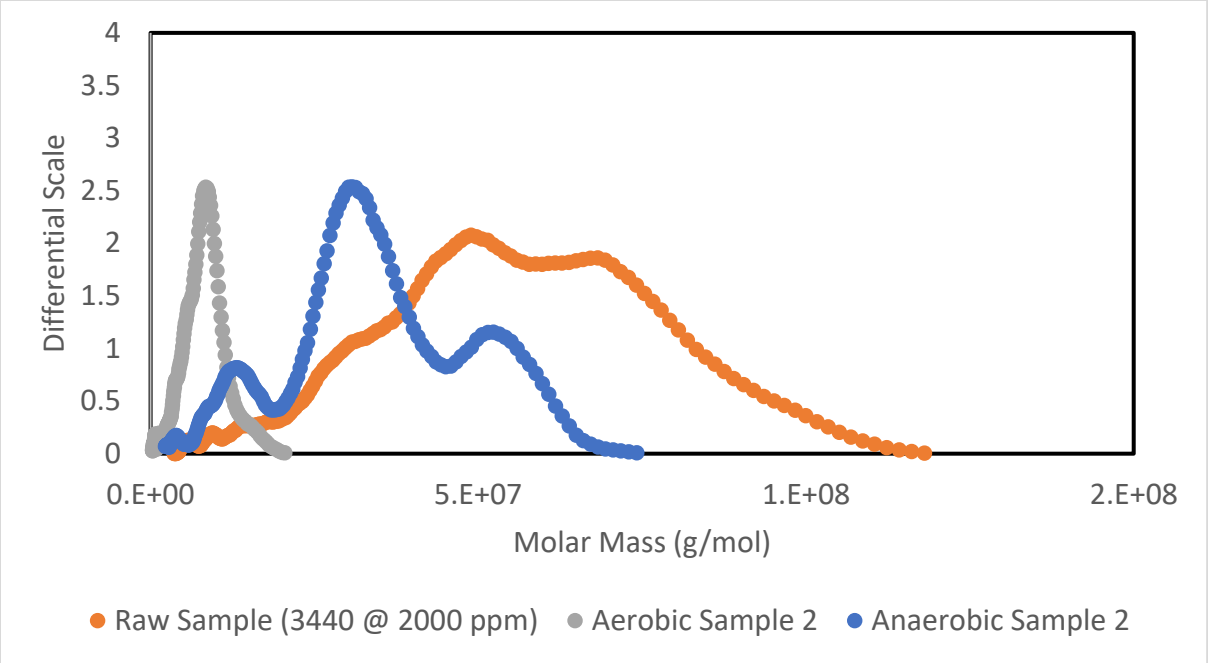

(a) Molar mass distributions for Sample 2 and Injecting Fluid

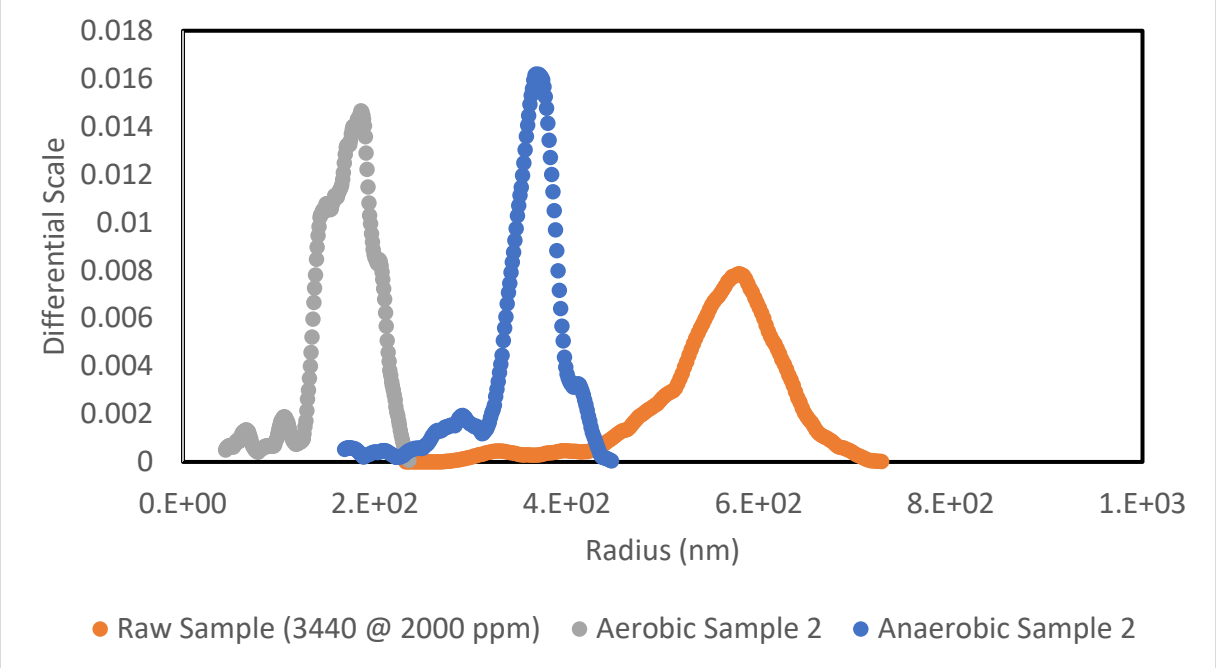

(b) Radius distributions for Sample 2 and Injecting Fluid

Figure 4.18 Comparing the distributions of sample 2 with injecting fluid

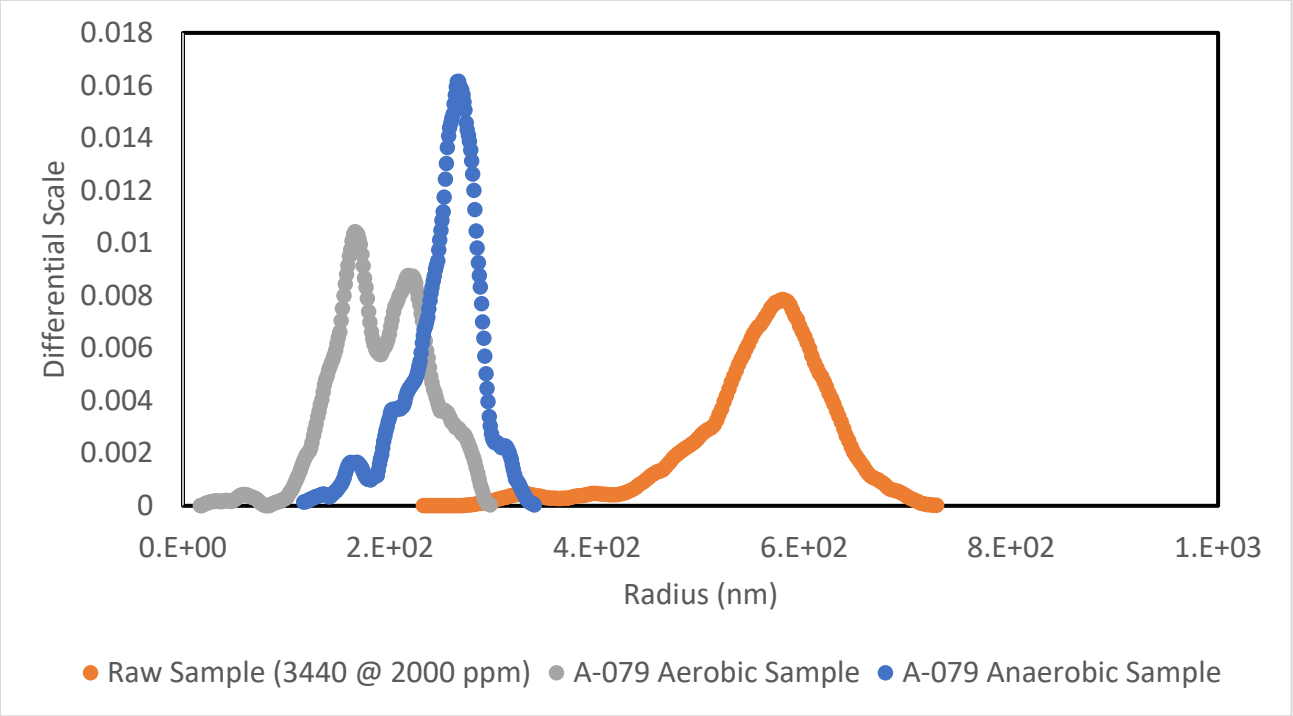

(a) Molar mass distributions for A-079 Samples and Injecting Fluid

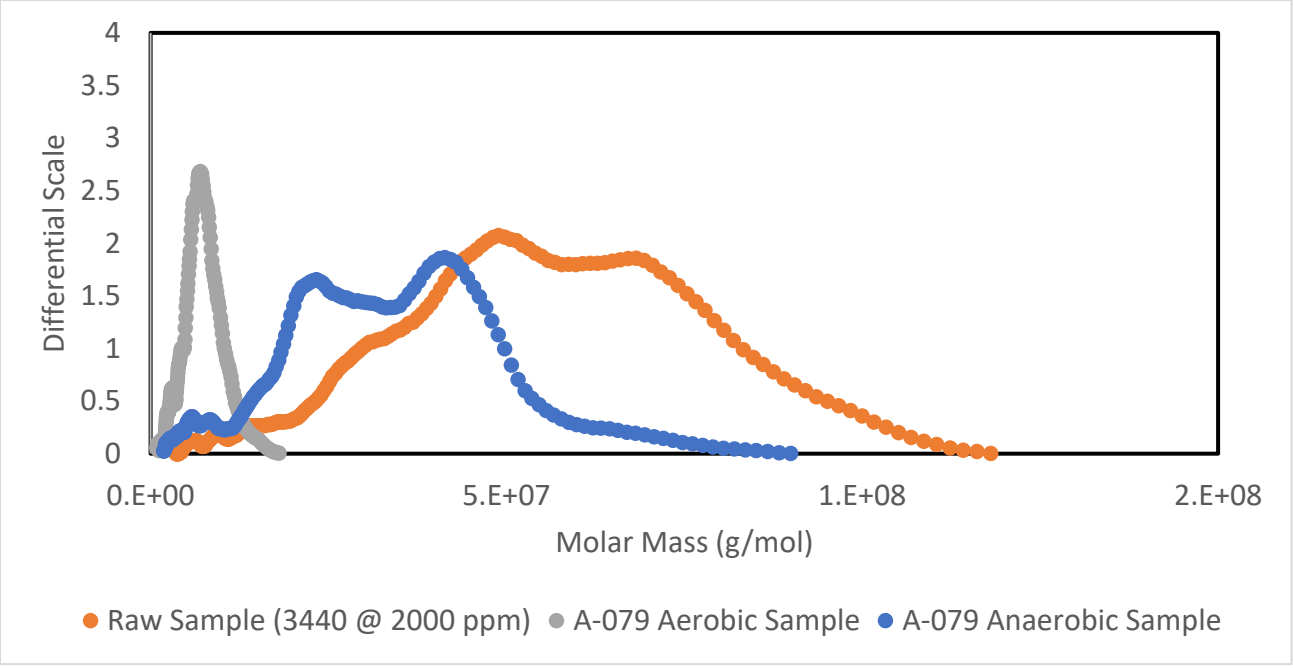

(b) Radius distributions for A-079 Samples and Injecting Fluid

Figure 4.19 Comparing the distributions of A-079 samples with injecting fluid

The results show a considerable difference in the average molar mass and radius values for the produced water samples compared to the injecting fluid. The average molar mass reduced from 47.54 MDa to a range of 19 MDa-27 MDa for the anaerobic samples. Whereas for the aerobic samples, these seem reduced further around 6MDa for all aerobic samples. A very similar trend was observed for the radius of gyration where the average molecular radius values were dropped from 556.5 nm to a range of 250-446 nm for anaerobic samples and 191-436 nm for aerobic samples. These show clear differences in the analysis or characterization performed under aerobic conditions (in the lab) vs the anaerobic conditions applied to most oil reservoirs.

The molecular weight distributions indicate that the entrapment of higher-end polymer chains is significant under anaerobic conditions. However, the crosslinking of the lower-end molecular chains (which may be due to the presence of cations in the reservoir) helps to maintain the performance of polymer flooding. Oxidative degradation due to dissolved oxygen along with cations plays a very important role in polymer success. All aerobic samples resulted in a very narrow MWD compared to injecting fluid. This indicates the redox state affects surface-charge density and potential. The injection fluid undergoes oxidative degradation, which is thought to be caused by radical species resulting from the redox cycling of transition metal ions. These radicals break the acrylic backbone of the polymer, resulting in a decrease in molecular weight and viscosity.

The injecting fluid seems quite stable under anaerobic conditions. However, the crosslinking tendency of cations may attribute to gel-forming if intermolecular interactions dominate even in the absence of oxygen. These gel particles eventually grow and no longer flow in the porous media because of having a higher radius than the average pore size. This seems a possible entrapment mechanism for polymer retention in the porous media.

4.5 Conclusions

We have investigated how hydrophobicity-dependent polymer conformations relate to the flow behavior of polymer in the porous media. The enabled polymer screen criteria explain how the hydrophobicity of polymer affects the polymer resistance and retention in the porous media, especially when shear and extensional rheology fails to pretend. The study showed that higher hydrophobic polymer was able to form non-Hookean polymer hard spherical structures that increase the hydrodynamic trapping. Whereas, at low hydrophobicity, the formation of soft randomly coiled polymer conformations offers favorable conditions even at the higher injection rates. Additionally, the polymer number density seems to be an important criterion for the prediction of polymer retention in the porous media. At the higher polymer concentration, the polymer retention in the porous media increased due to the identical rock and polymer interaction mechanism. Combining concentration and hydrophobicity-dependent structure formations allow for optimizing the operation parameters like flow rate, pre-shearing, and filtration conditions.

Chapter 5: Conclusion, Limitations, and recommendations

5.1 Conclusions

This study proposes new criteria for the polymer screening for polymer flooding. The importance of screening criteria was explained by conformational characteristics measured for the produced water samples and the injecting fluid. An explicit relationship of the polymer conformations with the flow of polymer solutions in the consolidated porous media was developed and also validated with the available literature on injectivity experiments in un-consolidated porous media.

The results show that the solutions prepared with the non-associating polymers exhibit the lowest experimental break-up time and extensional viscosity. The presence of divalent ions resulted in effective charge screening, leading to narrow molecular weight distribution (MWD) curves and lower radius of gyration (Rg) for both types of HPAMs, co-hydrolyzed and post-hydrolyzed. However, the co-hydrolyzed PAM demonstrated higher Rg values in the presence of CaCl2 brine, indicating enhanced tolerance towards divalent salts. In contrast, divalent ions more efficiently reduced the extensional viscosities of HPAM solutions compared to monovalent ions. The domination of intra-molecular forces irrespective of the polymer concentration, and solvent type results in the narrowest molecular weight and radius distributions. The average values for the radius of gyration were found close to the average pore size of the Bentheimer core. That is why the negligible viscoelastic resistance in the porous media generated by these randomly coiled polymer conformations resulted in the lowest values for RF and RRF.

For the associative polymers in the aqueous media, the domination of inter-molecular forces was observed in the semi-dilute regime (polymer concentration 2000 ppm). Hydrophobicity plays a crucial role in altering the entanglement between polymer chains, influencing the formation of rigid or flexible complex structures. Higher entanglements result in strain hardening for C319,

whereas increased hydrophobicity contributes to the rigidity and compaction of polymer complexes, resulting in lower relaxation time and extensional viscosity. Conversely, the formation of flexible polymer networks that can withstand greater extensional resistance leads to higher relaxation time and extensional viscosity in the semi-dilute regime. Very similar behavior was found for the associative polymers in brine except for the presence of cations contributed to the charge-shielding effects lowering the critical aggregation concentration below 1000 ppm of polymer in the brine. Whereas the is no direct correlation found between the extensional properties of polymer solutions and polymer retention in the porous media, the hydrophobicity-dependent polymer conformation explains this property co-relationship.

The injectivity experiments show that the resulting polymer conformation of the rigid non-Hookean type contributes to the higher polymer retention in the porous media. Additionally, the presence of higher molecular end polymer molecule chains triggers mechanical entrapment. However, the flexible Hookean polymer conformations help to overcome the visco-elastic resistance even at higher concentrations. This could be a possible reason for lower RF and RRF for C319 compared to D118.

Another side, the conformational study of the produced water samples shows considerable polymer degradation under aerobic conditions. However, the presence of cations in the reservoir can lead to the cross-linking of the lower-end molecular chains, which, in turn, helps maintain the effectiveness of polymer flooding. The success of polymer flooding is significantly influenced by oxidative degradation caused by dissolved oxygen and cations. In aerobic samples, the molecular weight distribution (MWD) becomes much narrower compared to the injecting fluid, indicating that the redox state affects the surface-charge density and potential. The injecting fluid undergoes oxidative degradation, likely due to radical species generated from the

redox cycling of transition metal ions. These radicals break the acrylic backbone of the polymer, resulting in a decrease in both molecular weight and viscosity.

Under anaerobic conditions, the injecting fluid appears to be relatively stable. However, even in the absence of oxygen, the presence of cations can lead to a tendency for crosslinking, potentially resulting in gel formation if intermolecular interactions dominate. These gel particles then grow and become immobile in porous media, as their size exceeds the average pore size. This mechanism of entrapment could explain the retention of the polymer within the porous media.

5.2 Limitations

AF4-FFF experimental set-up include using a regenerated cellulose membrane to elute the polymer sample to be tested for Mw, MWD, and radius distributions. Any chemical species reacting extensively with it limits the usage of the system. These limitations extend to the samples containing trace oil. All of the characterizations and injectivity experiments were performed at ambient temperature. However, the effect of temperature on the concerned properties can be studied and correlated with the injectivity experiments. The study could be extended to distinguish the effect of molecular weight distributions on the adsorption and hydrodynamic retention. This could be done by combining perform a separate quantitative adsorption by using the scanning electron microscopy or X-ray diffraction. The additional loss of polymer concentration along with molecular weight and radius distributions provide better insights to the mechanical retention.

5.3 Recommendations

The polydispersity index and slope of the conformational plot can be immersed in the promising rheological models to estimate the RF and RRF values. This could eliminate the requirement to perform the time-consuming core-flood experiments. Also, the Oil recovery factors can be correlated to the above-mentioned parameters to estimate the success of polymer EOR. The produced water samples could be analyzed for MWD and radius distribution determinations. Overlapping these plots with the bulk or raw sample data may give important information on the molecular species responsible for the risks associated with polymer EOR. Overlapping the radius distributions with the pore size distribution for the core enable the additional polymer screening criteria to avoid the problems associated with the polymer blockage in the porous media. The quantitative difference between polymer adsorption and mechanical entrapment could help in understanding what type of polymer chains or conformations contribute to adsorption and/or entrapment. Also, the subjected study can be expanded at various temperature conditions.

References

[1] IEA, “Oil Market Report - October 2021,” 2021. https://www.iea.org/reports/oil-market-report-october-2021 (accessed Dec. 12, 2021).

[2] E. C. Hammershaimb, V. A. Kuuskraa, and G. Stosur, “Recovery Efficiency of Enhanced Oil Recovery Methods: A Review of Significant Field Tests,” *SPE Annual Technical Conference and Exhibition*. p. SPE-12114-MS, Oct. 05, 1983, doi: 10.2118/12114-MS.

[3] A. Z. Abidin, T. Puspasari, and W. A. Nugroho, “Polymers for Enhanced Oil Recovery Technology,” *Procedia Chem.*, vol. 4, pp. 11–16, 2012, doi: https://doi.org/10.1016/j.proche.2012.06.002.

[4] S. Thomas, “Enhanced Oil Recovery – An Overview,” *Oil Gas Sci. Technol.*, vol. 63, no. 1, pp. 9–19, 2008, doi: https://doi.org/10.2516/ogst:2007060.

[5] L. Surguchev, E. Manrique, and V. Alvarado, “Improved Oil Recovery: Status And Opportunities,” *18th World Petroleum Congress*. p. WPC-18-0886, Sep. 25, 2005.

[6] L. Romero-Zerón, *Introduction to enhanced oil recovery (EOR) processes and bioremediation of oil-contaminated sites*. BoD–Books on Demand, 2012.

[7] R. C. Aadland *et al.*, “High-Temperature Core Flood Investigation of Nanocellulose as a Green Additive for Enhanced Oil Recovery,” *Nanomaterials*, vol. 9, no. 5. 2019, doi: 10.3390/nano9050665.

[8] B. Wei, “Advances in Polymer Flooding,” in *Viscoelastic and Viscoplastic Materials*, M. F. El-Amin, Ed. Rijeka: IntechOpen, 2016.

[9] A. Mohsenatabar Firozjaii and H. R. Saghafi, “Review on chemical enhanced oil recovery using polymer flooding: Fundamentals, experimental and numerical simulation,” *Petroleum*, vol. 6, no. 2, pp. 115–122, 2020, doi: https://doi.org/10.1016/j.petlm.2019.09.003.

[10] Oil & Gas Authority United Kingdom, “Polymer Enhanced Oil Recovery,” no. October, p. 44, 2017.

[11] L. SUN, X. WU, W. ZHOU, X. LI, and P. HAN, “Technologies of enhancing oil recovery by chemical flooding in Daqing Oilfield, NE China,” *Pet. Explor. Dev.*, vol. 45, no. 4, pp. 673–684, 2018, doi: https://doi.org/10.1016/S1876-3804(18)30071-5.

[12] G. Zhu *et al.*, “Enhanced Oil Recovery by Seawater Flooding in Halfaya Carbonate Reservoir, Iraq: Experiment and Simulation,” *SPE EOR Conference at Oil and Gas West Asia*. p. D031S020R004, Mar. 21, 2016, doi: 10.2118/179843-MS.

[13] A. M. Handhal, F. R. Ettensohn, A. M. Al-Abadi, and M. J. Ismail, “Spatial assessment of gross vertical reservoir heterogeneity using geostatistics and GIS-based machine-learning classifiers: A case study from the Zubair Formation, Rumaila oil field, southern Iraq,” *J. Pet. Sci. Eng.*, vol. 208, p. 109482, 2022, doi: https://doi.org/10.1016/j.petrol.2021.109482.

[14] C. Ekweribe *et al.*, “Tengiz Well Performance Forecasting Using Wellbore Transient Flow Modeling,” *SPE Annual Caspian Technical Conference and Exhibition*. p. SPE-172266-MS, Nov. 12, 2014, doi: 10.2118/172266-MS.

[15] P. Kumar, R. Raj, N. Koduru, S. Kumar, and A. Pandey, “Field Implementation of Mangala Polymer Flood: Initial Challenges, Mitigation and Management,” *SPE EOR Conference at Oil and Gas West Asia*. p. D011S001R003, Mar. 21, 2016, doi: 10.2118/179820-MS.

[16] R. S. Seright, “How Much Polymer Should Be Injected During a Polymer Flood? Review of Previous and Current Practices,” *SPE J.*, vol. 22, no. 01, pp. 1–18, Jun. 2016, doi: 10.2118/179543-PA.

[17] T. Kopač, A. Ručigaj, and M. Krajnc, “Effect of polymer-polymer interactions on the flow behavior of some polysaccharide-based hydrogel blends,” *Carbohydr. Polym.*, vol. 287, p. 119352, Mar. 2022, doi: 10.1016/j.carbpol.2022.119352.

[18] D. Wang, J. Cheng, Q. Yang, W. Gong, and Q. Li, “Viscous-Elastic Polymer Can Increase Microscale Displacement Efficiency in Cores,” *SPE Annual Technical Conference and Exhibition*. p. SPE-63227-MS, Oct. 01, 2000, doi: 10.2118/63227-MS.

[19] S. Rodriguez, C. Romero, M. L. Sargenti, A. J. Müller, A. E. Sáez, and J. A. Odell, “Flow of polymer solutions through porous media,” *J. Nonnewton. Fluid Mech.*, vol. 49, no. 1, pp. 63–85, 1993, doi: https://doi.org/10.1016/0377-0257(93)85023-4.

[20] J. Cao, S. Zhu, Z. Shu, and L. Shi, “Effects of residual resistance factor in the mobility control of the polymer flooding,” *J. Appl. Polym. Sci.*, vol. 139, no. 48, p. e53217, Dec. 2022, doi: https://doi.org/10.1002/app.53217.

[21] C. A. Finch, “Polymer-improved oil recovery. K. S. Sorbie Blackie & Son, Glasgow, 1991. pp. xii + 359, price £59.00. ISBN 0–216–92693–9,” *Polym. Int.*, vol. 28, no. 3, p. 256, Jan. 1992, doi: https://doi.org/10.1002/pi.4990280317.

[22] A. J. Mu¨ller *et al.*, “Mechanical Degradation of Polymers in Flows Through Porous Media: Effect of Flow Path Length and Particle Size,” *Appl. Mech. Rev.*, vol. 50, no. 11S, pp. S149–S155, Nov. 1997, doi: 10.1115/1.3101827.

[23] H. A. Larsen and H. G. Drickamer, “Mechanical Degradation and Cross Linking of Polymers by Plastic Deformation at High Pressure,” *J. Phys. Chem.*, vol. 61, no. 12, pp. 1643–1646, Dec. 1957, doi: 10.1021/j150558a019.

[24] F. Bueche, “Mechanical degradation of high polymers,” *J. Appl. Polym. Sci.*, vol. 4, no. 10, pp. 101–106, Jul. 1960, doi: https://doi.org/10.1002/app.1960.070041016.

[25] S. Ray and R. P. Cooney, “7 - Thermal Degradation of Polymer and Polymer Composites,” M. B. T.-H. of E. D. of M. (Second E. Kutz, Ed. Oxford: William Andrew Publishing, 2012, pp. 213–242.

[26] J. J. Maurer and G. D. Harvey, “Thermal degradation characteristics of poly(acrylamide-co-acrylic acid) and poly(acrylamide-co-sodium acrylate) copolymers,” *Thermochim. Acta*, vol. 121, pp. 295–306, 1987, doi: https://doi.org/10.1016/0040-6031(87)80180-6.

[27] V. Patel, Y. Dalsania, M. Azad, and J. Trivedi, “Characterization of co- and post-hydrolyzed polyacrylamide molecular weight and radius distribution under saline environment,” *J. Appl. Polym. Sci.*, vol. 138, 2021, doi: 10.1002/app.50616.

[28] Y. Dalsania, A. Doda, and J. Trivedi, “Characterization of Ultrahigh-Molecular-Weight Oilfield Polyacrylamides Under Different pH Environments by Use of Asymmetrical-Flow Field-Flow Fractionation and Multiangle-Light-Scattering Detector,” *SPE J.*, vol. 23, no. 01, pp. 48–65, Oct. 2017, doi: 10.2118/174624-PA.

[29] D. Levitt and G. A. Pope, “Selection and Screening of Polymers for Enhanced-Oil Recovery,” *SPE Symposium on Improved Oil Recovery*. p. SPE-113845-MS, Apr. 20, 2008, doi: 10.2118/113845-MS.

[30] N. Willenbacher, Y. Matter, I. Gubaydullin, and V. Schädler, “Effect of aggregation on shear and elongational flow properties of acrylic thickeners,” *Korea Aust. Rheol. J.*, vol. 20, 2008.

[31] H. Chen, Z. Ye, L. Han, and P. Luo, “Studies on the self-assembly behavior of the hydrophobically associating polyacrylamide,” *J. Appl. Polym. Sci.*, vol. 123, no. 4, pp. 2397–2405, Feb. 2012, doi: https://doi.org/10.1002/app.34756.

[32] J.-S. Sun, D. Weichao, X.-L. Pu, Z.-Z. Zou, and B.-B. Zhu, “Synthesis and evaluation of a novel hydrophobically associating polymer based on acrylamide for enhanced oil recovery,” *Chem. Pap.*, vol. 69, Dec. 2015, doi: 10.1515/chempap-2015-0185.

[33] Y. Bai, X. Shang, Z. Wang, and X. Zhao, “Experimental Study on Hydrophobically Associating Hydroxyethyl Cellulose Flooding System for Enhanced Oil Recovery,” *Energy & Fuels*, vol. 32, no. 6, pp. 6713–6725, Jun. 2018, doi: 10.1021/acs.energyfuels.8b01138.

[34] K. C. Taylor and H. A. Nasr-El-Din, “Water-soluble hydrophobically associating polymers for improved oil recovery: A literature review,” *J. Pet. Sci. Eng.*, vol. 19, no. 3, pp. 265–280, 1998, doi: https://doi.org/10.1016/S0920-4105(97)00048-X.

[35] M. Rubinstein and A. Dobrynin, “Solutions of Associative Polymers,” *Trends Polym. Sci.*, vol. 5, pp. 181–186, Jun. 1997.

[36] A. Rock, R. E. Hincapie, M. Tahir, N. Langanke, and L. Ganzer, “On the Role of Polymer Viscoelasticity in Enhanced Oil Recovery: Extensive Laboratory Data and Review,” *Polymers* , vol. 12, no. 10. 2020, doi: 10.3390/polym12102276.

[37] H. Dong, S. Fang, D. Wang, J. Wang, Z. L. Liu, and W. Hou, “Review of Practical Experience & Management by Polymer Flooding at Daqing,” *SPE Symposium on Improved Oil Recovery*. p. SPE-114342-MS, Apr. 20, 2008, doi: 10.2118/114342-MS.

[38] A. Alquraishi and F. Alsewailem, “Xanthan and guar polymer solutions for water shut off in high salinity reservoirs,” *Carbohydr. Polym.*, vol. 88, pp. 859–863, Apr. 2012, doi: 10.1016/j.carbpol.2012.01.022.

[39] P. E. F. Terapane, “United States Patent (19),” no. 19, 1989.

[40] Berdugo-Clavijo, C.; Scheffer, G.; Sen, A.; Gieg, L.M. Biodegradation of Polymers Used in Oil and Gas Operations: Towards Enzyme Biotechnology Development and Field Application. Polymers 2022, 14, 1871. https://doi.org/10.3390/polym14091871.

[41] T. Dow, C. Company, S. Evani, and P. E. B. Guynn, "United States Patent (19)," no. 19, 1984.

[42] G. Dupuis, D. Rousseau, R. Tabary, and B. Grassl, "Hydrophobically Modified Sulfonated Polyacrylamides for IOR: Correlations between Associative Behavior and Injectivity in the Diluted Regime," *Oil Gas Sci. Technol.*, vol. 67, pp. 903–919, Nov. 2013, doi: 10.2516/ogst/2012016.

[43] R. Reichenbach-Klinke, A. Stavland, D. Strand, B. Langlotz, and G. Brodt, "Can Associative Polymers Reduce the Residual Oil Saturation?," *SPE EOR Conference at Oil and Gas West Asia*. p. D031S018R002, Mar. 21, 2016, doi: 10.2118/179801-MS.

[44] E. C. Vermolen, M. J. van Haasterecht, S. K. Masalmeh, M. J. Faber, D. M. Boersma, and M. Gruenenfelder, "Pushing the Envelope for Polymer Flooding Towards High-temperature and High-salinity Reservoirs with Polyacrylamide Based Ter-polymers," *SPE Middle East Oil and Gas Show and Conference*. p. SPE-141497-MS, Sep. 25, 2011, doi: 10.2118/141497-MS.

[45] C. L. McCormick and C. B. Johnson, "Structurally Tailored Macromolecules for Mobility Control in Enhanced Oil Recovery BT - Water-Soluble Polymers for Petroleum Recovery," G. A. Stahl and D. N. Schulz, Eds. Boston, MA: Springer US, 1988, pp. 161–180.

[46] A. Moradi-Araghi and P. H. Doe, "Hydrolysis and Precipitation of Polyacrylamides in Hard Brines at Elevated Temperatures," *SPE Reserv. Eng.*, vol. 2, no. 02, pp. 189–198, May 1987, doi: 10.2118/13033-PA.

[47] F. L. McCrackin, "Relationship of intrinsic viscosity of polymer solutions to molecular weight," *Polymer (Guildf).*, vol. 28, no. 11, pp. 1847–1850, 1987, doi: https://doi.org/10.1016/0032-3861(87)90289-8.

[48] M. Guaita, O. Chiantore, A. Munari, P. Manaresi, F. Pilati, and M. Toselli, "A general intrinsic viscosity-molecular weight relationship for linear polydisperse polymers—3. Applicability to the evaluation of the mark-houwink-sakurada k and a constants," *Eur. Polym. J.*, vol. 27, no. 4, pp. 385–388, 1991, doi: https://doi.org/10.1016/0014-3057(91)90193-R.

[49] D. Hunkeler, "Synthesis and characterization of high molecular weight water-soluble polymers," *Polym. Int.*, vol. 27, no. 1, pp. 23–33, Jan. 1992, doi: https://doi.org/10.1002/pi.4990270105.

[50] M. R. Kasaai, J. Arul, and G. Charlet, "Intrinsic viscosity–molecular weight relationship for chitosan," *J. Polym. Sci. Part B Polym. Phys.*, vol. 38, no. 19, pp. 2591–2598, Oct. 2000, doi: https://doi.org/10.1002/1099-0488(20001001)38:19<2591::AID-POLB110>3.0.CO;2-6.

[51] B. Gampert and P. Wagner, “The Influence of Molecular Weight and Molecular Weight Distribution on Drag Reduction and Mechanical Degradation in Turbulent Flow of Highly Dilute Polymer Solutions BT - The Influence of Polymer Additives on Velocity and Temperature Fields,” 1985, pp. 71–85.

[52] J. Wang, H. Huang, and X. Huang, “Molecular weight and the Mark-Houwink relation for ultra-high molecular weight charged polyacrylamide determined using automatic batch mode multi-angle light scattering,” *J. Appl. Polym. Sci.*, vol. 133, no. 31, Aug. 2016, doi: https://doi.org/10.1002/app.43748.

[53] H. Chen, Y. Ding, and C. Tan, “Rheological behaviour of nanofluids,” *New J. Phys.*, vol. 9, no. 10, p. 367, 2007.

[54] V. G. Kulichikhin and A. Y. Malkin, “The Role of Structure in Polymer Rheology: Review,” *Polymers*, vol. 14, no. 6. 2022, doi: 10.3390/polym14061262.

[55] K. Xie, X. Lu, Q. Li, W. Jiang, and Q. Yu, “Analysis of Reservoir Applicability of Hydrophobically Associating Polymer,” *SPE J.*, vol. 21, May 2015, doi: 10.2118/174553-PA.

[56] M. S. Azad and J. J. Trivedi, “Extensional Effects during Viscoelastic Polymer Flooding: Understanding Unresolved Challenges,” *SPE J.*, vol. 25, no. 04, pp. 1827–1841, Aug. 2020, doi: 10.2118/201112-PA.

[57] S. Chissonde, M. S. Azad, and J. Trivedi, “Flow of hydrophobically associating polymers through unconsolidated sand pack: Role of extensional rheology and degree of association,” *J. Mol. Liq.*, vol. 344, p. 117643, 2021, doi: https://doi.org/10.1016/j.molliq.2021.117643.

[58] M. Azad, Y. Dalsania, and J. Trivedi, “Understanding the Flow Behaviour of Copolymer and Associative Polymers in Porous Media Using Extensional Viscosity Characterization: Effect of Hydrophobic Association,” *Can. J. Chem. Eng.*, vol. 96, Feb. 2018, doi: 10.1002/cjce.23169.

[59] V. Patel, J. Trivedi, and T. Sharma, “Influence of hydrophobic association in the aqueous media on the rheology and polymer conformation of associative polymers,” *Polym. Bull.*, 2022, doi: 10.1007/s00289-022-04484-9.

[60] T. Chevalier *et al.*, “Darcy’s law for yield stress fluid flowing through a porous medium,” *J. Nonnewton. Fluid Mech.*, vol. 195, pp. 57–66, 2013, doi: https://doi.org/10.1016/j.jnnfm.2012.12.005.

[61] R. H. Pelton and L. H. Allen, “The effects of some electrolytes on flocculation with a cationic polyacrylamide,” *Colloid Polym. Sci.*, vol. 261, no. 6, pp. 485–492, 1983, doi: 10.1007/BF01419832.

[62] Y.-Y. Wang *et al.*, “Hydrophobically Modified Associating Polyacrylamide Solutions: Relaxation Processes and Dilational Properties at the Oil−Water Interface,” *Macromolecules*, vol. 37, no. 8, pp. 2930–2937, Apr. 2004, doi: 10.1021/ma049923v.

[63] L. Castle, “Determination of acrylamide monomer in mushrooms grown on

polyacrylamide gel," *J. Agric. Food Chem.*, vol. 41, no. 8, pp. 1261–1263, Aug. 1993, doi: 10.1021/jf00032a019.

[64] C.-Y. Li *et al.*, "The biofilm property and its correlationship with high-molecular-weight polyacrylamide degradation in a water injection pipeline of Daqing oilfield," *J. Hazard. Mater.*, vol. 304, pp. 388–399, 2016, doi: https://doi.org/10.1016/j.jhazmat.2015.10.067.

[65] Q. Wen, Z. Chen, Y. Zhao, H. Zhang, and Y. Feng, "Biodegradation of polyacrylamide by bacteria isolated from activated sludge and oil-contaminated soil," *J. Hazard. Mater.*, vol. 175, no. 1, pp. 955–959, 2010, doi: https://doi.org/10.1016/j.jhazmat.2009.10.102.

[66] B. J. Lee and M. A. Schlautman, "Effects of Polymer Molecular Weight on Adsorption and Flocculation in Aqueous Kaolinite Suspensions Dosed with Nonionic Polyacrylamides," *Water*, vol. 7, no. 11. pp. 5896–5909, 2015, doi: 10.3390/w7115896.

[67] B. Xiong *et al.*, "Polyacrylamide degradation and its implications in environmental systems," *npj Clean Water*, vol. 1, no. 1, p. 17, 2018, doi: 10.1038/s41545-018-0016-8.

[68] D. K. Ramsden and K. McKay, "The degradation of polyacrylamide in aqueous solution induced by chemically generated hydroxyl radicals: Part II—Autoxidation of Fe2+," *Polym. Degrad. Stab.*, vol. 15, no. 1, pp. 15–31, 1986, doi: https://doi.org/10.1016/0141-3910(86)90003-0.

[69] U. Gröllmann and W. Schnabel, "Free radical-induced oxidative degradation of polyacrylamide in aqueous solution," *Polym. Degrad. Stab.*, vol. 4, no. 3, pp. 203–212, 1982, doi: https://doi.org/10.1016/0141-3910(82)90027-1.

[70] P. Chen, L. Yao, Y. Liu, J. Luo, G. Zhou, and B. Jiang, "Experimental and theoretical study of dilute polyacrylamide solutions: effect of salt concentration.," *J. Mol. Model.*, vol. 18, no. 7, pp. 3153–3160, Jul. 2012, doi: 10.1007/s00894-011-1332-9.

[71] Q. Zhang, J. Zhou, Y. Zhai, F. Liu, and G. Gao, "Effect of salt solutions on chain structure of partially hydrolyzed polyacrylamide," *J. Cent. South Univ. Technol.*, vol. 15, no. 1, pp. 80–83, 2008, doi: 10.1007/s11771-008-0319-x.

[72] S. Rezaei Gomari, K. Uranta, P. Russell, and F. Hamad, "Determining Safe Maximum Temperature Point (SMTP) for Polyacrylamide Polymer (PAM) in Saline solutions," *J. Oil , Gas Petrochemical Sci.*, vol. 1, Jan. 2018, doi: 10.30881/jogps.00004.

[73] R. G. Ryles, "Chemical Stability Limits of Water-Soluble Polymers Used in Oil Recovery Processes," *SPE Reserv. Eng.*, vol. 3, no. 01, pp. 23–34, Feb. 1988, doi: 10.2118/13585-PA.

[74] P. S. Carman and K. E. Cawiezel, "Successful Breaker Optimization for Polyacrylamide Friction Reducers Used in Slickwater Fracturing," *SPE Hydraulic Fracturing Technology Conference*. p. SPE-106162-MS, Jan. 29, 2007, doi: 10.2118/106162-MS.

[75] J. M. Maerker, "Shear Degradation of Partially Hydrolyzed Polyacrylamide Solutions," *Soc. Pet. Eng. J.*, vol. 15, no. 04, pp. 311–322, Aug. 1975, doi: 10.2118/5101-PA.

[76] S. Ghoniem, G. Chauveteau, M. Moan, and C. Wolff, "Mechanical degradation of semi-

dilute polymer solutions in laminar flows," *Can. J. Chem. Eng.*, vol. 59, no. 4, pp. 450–454, Aug. 1981, doi: https://doi.org/10.1002/cjce.5450590406.

[77] A. R. Al Hashmi, R. S. Al Maamari, I. S. Al Shabibi, A. M. Mansoor, A. Zaitoun, and H. H. Al Sharji, "Rheology and mechanical degradation of high-molecular-weight partially hydrolyzed polyacrylamide during flow through capillaries," *J. Pet. Sci. Eng.*, vol. 105, pp. 100–106, 2013, doi: https://doi.org/10.1016/j.petrol.2013.03.021.

[78] A. Keller and J. A. Odell, "The extensibility of macromolecules in solution; A new focus for macromolecular science," *Colloid Polym. Sci.*, vol. 263, no. 3, pp. 181–201, 1985, doi: 10.1007/BF01415506.

[79] T. T. Perkins, D. E. Smith, and S. Chu, "Single Polymer Dynamics in an Elongational Flow," *Science (80-.).*, vol. 276, no. 5321, pp. 2016–2021, Jun. 1997, doi: 10.1126/science.276.5321.2016.

[80] R. S. Seright, "The Effects of Mechanical Degradation and Viscoelastic Behavior on Injectivity of Polyacrylamide Solutions," *Soc. Pet. Eng. J.*, vol. 23, no. 03, pp. 475–485, Jun. 1983, doi: 10.2118/9297-PA.

[81] M. Deckers, T. Clemens, M. Kornberger, T. Gumpenberger, and M. Zechner, "Polymer Solution Injection - Near Wellbore Dynamics and Displacement Efficiency, Pilot Test Results, Matzen Field, Austria - (SPE-164904)," Jun. 2013, doi: 10.3997/2214-4609.20130546.

[82] C. Puls, T. Clemens, C. Sledz, R. Kadnar, and T. Gumpenberger, "Mechanical Degradation of Polymers During Injection, Reservoir Propagation and Production - Field Test Results 8 TH Reservoir, Austria," *SPE Europec featured at 78th EAGE Conference and Exhibition*. p. SPE-180144-MS, May 30, 2016, doi: 10.2118/180144-MS.

[83] K. Godwin Uranta, S. Rezaei-Gomari, P. Russell, and F. Hamad, "Studying the Effectiveness of Polyacrylamide (PAM) Application in Hydrocarbon Reservoirs at Different Operational Conditions," *Energies*, vol. 11, no. 9. 2018, doi: 10.3390/en11092201.

[84] M. Kurata, "Effect of molecular weight distribution on viscoelastic properties of polymers. 2. Terminal relaxation time and steady-state compliance," *Macromolecules*, vol. 17, no. 4, pp. 895–898, Apr. 1984, doi: 10.1021/ma00134a061.

[85] R. L. Combs, D. F. Slonaker, and H. W. Coover, "Effects of molecular weight distribution and branching on rheological properties of polyolefin melts," *J. Appl. Polym. Sci.*, vol. 13, no. 3, pp. 519–534, Mar. 1969, doi: https://doi.org/10.1002/app.1969.070130312.

[86] J. F. Rudd, "The effect of molecular weight distribution on the rheological properties of polystyrene," *J. Polym. Sci.*, vol. 44, no. 144, pp. 459–474, Jun. 1960, doi: https://doi.org/10.1002/pol.1960.1204414417.

[87] A. Samanta, A. Bera, K. Ojha, and A. Mandal, "Effects of Alkali, Salts, and Surfactant on Rheological Behavior of Partially Hydrolyzed Polyacrylamide Solutions," *J. Chem. Eng. Data*, vol. 55, no. 10, pp. 4315–4322, Oct. 2010, doi: 10.1021/je100458a.

[88] B. Al-Shakry, T. Skauge, B. Shaker Shiran, and A. Skauge, “Polymer Injectivity: Investigation of Mechanical Degradation of Enhanced Oil Recovery Polymers Using In-Situ Rheology,” *Energies*, vol. 12, no. 1. 2019, doi: 10.3390/en12010049.

[89] K. C. Tam and C. Tiu, “Role of ionic species and valency on the viscoelastic properties of partially hydrolyzed polyacrylamide solutions,” *Colloid Polym. Sci.*, vol. 272, no. 5, pp. 516–522, 1994, doi: 10.1007/BF00653215.

[90] A. V Shenoy, “Extensional flow properties BT - Rheology of Filled Polymer Systems,” A. V Shenoy, Ed. Dordrecht: Springer Netherlands, 1999, pp. 395–415.

[91] B. H. Bersted, “Effect of molecular weight distribution on elongational viscosity of undiluted polymer fluids,” *J. Appl. Polym. Sci.*, vol. 24, no. 3, pp. 671–682, Aug. 1979, doi: https://doi.org/10.1002/app.1979.070240305.

[92] M. S. Azad and J. J. Trivedi, “Quantification of the Viscoelastic Effects During Polymer Flooding: A Critical Review,” *SPE J.*, vol. 24, no. 06, pp. 2731–2757, Jul. 2019, doi: 10.2118/195687-PA.

[93] M. S. Azad, Y. K. Dalsania, and J. J. Trivedi, “Capillary breakup extensional rheometry of associative and hydrolyzed polyacrylamide polymers for oil recovery applications,” *J. Appl. Polym. Sci.*, vol. 135, no. 22, p. 46253, Jun. 2018, doi: https://doi.org/10.1002/app.46253.

[94] S. Akbari, S. M. Mahmood, I. M. Tan, H. Ghaedi, and O. L. Ling, “Assessment of Polyacrylamide Based Co-Polymers Enhanced by Functional Group Modifications with Regards to Salinity and Hardness,” *Polymers*, vol. 9, no. 12. 2017, doi: 10.3390/polym9120647.

[95] M. S. Azad and J. J. Trivedi, “Does Polymer’s Viscoelasticity Influence Heavy-Oil Sweep Efficiency and Injectivity at 1 ft/D?,” *SPE Reserv. Eval. Eng.*, vol. 23, no. 02, pp. 446–462, May 2020, doi: 10.2118/193771-PA.

[96] K. Lewandowska, “Comparative studies of rheological properties of polyacrylamide and partially hydrolyzed polyacrylamide solutions,” *J. Appl. Polym. Sci.*, vol. 103, no. 4, pp. 2235–2241, Feb. 2007, doi: https://doi.org/10.1002/app.25247.

[97] P. Sagbana and A. Abushaikha, “A comprehensive review of the chemical-based conformance control methods in oil reservoirs,” *J. Pet. Explor. Prod. Technol.*, vol. 11, Apr. 2021, doi: 10.1007/s13202-021-01158-6.

[98] “Applications in Inorganic Chemistry,” in *Infrared and Raman Spectra of Inorganic and Coordination Compounds*, 2008, pp. 149–354.

[99] S. Papageorgiou, E. Kouvelos, E. Favvas, A. Sapalidis, G. Romanos, and F. Katsaros, “Metal–Carboxylate Interactions in Metal–Alginate Complexes Studied with FTIR Spectroscopy,” *Carbohydr. Res.*, vol. 345, pp. 469–473, Feb. 2010, doi: 10.1016/j.carres.2009.12.010.

[100] N. Pal, K. Babu, and A. Mandal, “Surface Tension, Dynamic Light Scattering and Rheological studies of a new Polymeric Surfactant for application in enhanced oil

recovery," *J. Pet. Sci. Eng.*, vol. 146, pp. 591–600, Jul. 2016, doi: 10.1016/j.petrol.2016.07.023.

[101] N. Pal, M. Vajpayee, and A. Mandal, "Cationic/Nonionic Mixed Surfactants as Enhanced Oil Recovery Fluids: Influence of Mixed Micellization and Polymer Association on Interfacial, Rheological, and Rock-Wetting Characteristics," *Energy & Fuels*, vol. 33, no. 7, pp. 6048–6059, Jul. 2019, doi: 10.1021/acs.energyfuels.9b00671.

[102] A. Cesàro, "The role of conformation on the thermodynamics and rheology of aqueous solutions of carbohydrate polymers," *J. Food Eng.*, vol. 22, no. 1, pp. 27–42, 1994, doi: https://doi.org/10.1016/0260-8774(94)90023-X.

[103] D. Levitt and G. A. Pope, "Selection and Screening of Polymers for Enhanced-Oil Recovery," SPE Symposium on Improved Oil Recovery. p. SPE-113845-MS, Apr. 20, 2008, doi: 10.2118/113845-MS.

[104] R. O. Afolabi, G. F. Oluyemi, S. Officer, and J. O. Ugwu, "Hydrophobically associating polymers for enhanced oil recovery – Part B: A review of modelling approach to flow in porous media," *J. Mol. Liq.*, vol. 293, p. 111495, 2019, doi: https://doi.org/10.1016/j.molliq.2019.111495.

[105] D. Kawale *et al.*, "Polymer conformation during flow in porous media," *Soft Matter*, vol. 13, no. 46, pp. 8745–8755, 2017, doi: 10.1039/C7SM00817A.

[106] yabin Niu, jian Ouyang, zhuoyan Zhu, guijiang Wang, guanghua Sun, and lijun Shi, "Research on Hydrophobically Associating Water-Soluble Polymer Used for EOR," *SPE Int. Oilf. Chem. Symp. Proc.*, Feb. 2001, doi: 10.2118/65378-MS.

[107] M. E. Zeynali, A. Rabii, and H. Baharvand, "Synthesis of partially hydrolyzed polyacrylamide and investigation of solution properties (Viscosity Behaviour)," *Iran. Polym. J. (English Ed.*, vol. 13, pp. 479–484, Nov. 2004.

[108] Y. Lin, K. Luo, and H. Ronghua, "Study on P(AM-DMDA) hydrophobically associating water-soluble copolymer," *Eur. Polym. J.*, vol. 36, pp. 1711–1715, Aug. 2000, doi: 10.1016/S0014-3057(99)00227-X.

[109] M. I. Romero, "Flow of Emulsions in Porous Media," *SPE Annual Technical Conference and Exhibition*. p. SPE-129519-STU, Oct. 04, 2009, doi: 10.2118/129519-STU.

[110] S. Gou *et al.*, "A novel water-soluble hydrophobically associating polyacrylamide based on oleic imidazoline and sulfonate for enhanced oil recovery," *New J. Chem.*, vol. 39, Jul. 2015, doi: 10.1039/C5NJ01153A.

[111] A. El-hoshoudy, S. Dessouky, A. Al-Sabagh, M. Betiha, M. El-Kady, and S. Mahmoud, "Evaluation of solution and rheological properties for hydrophobically associated polyacrylamide copolymer as a promised enhanced oil recovery candidate," *Egypt. J. Pet.*, vol. 26, Oct. 2016, doi: 10.1016/j.ejpe.2016.10.012.

[112] S. Chissonde, M. S. Azad, and J. Trivedi, "Flow of hydrophobically associating polymers

through unconsolidated sand pack: Role of extensional rheology and degree of association," J. Mol. Liq., vol. 344, p. 117643, 2021, doi: https://doi.org/10.1016/j.molliq.2021.117643.

[113] R. Haas and F. Durst, "Viscoelastic flow of dilute polymer solutions in regularly packed beds," *Rheol. Acta*, vol. 21, no. 4, pp. 566–571, 1982, doi: 10.1007/BF01534349.

[114] M. Delshad, O. Magbagbeola, C. Huh, G. Pope, and F. Tarahhom, "Mechanistic Interpretation and Utilization of Viscoelastic Behavior of Polymer Solutions for Improved Polymer-Flood Efficiency," *SPE - DOE Improv. Oil Recover. Symp. Proc.*, vol. 2, Apr. 2008, doi: 10.2118/113620-MS.

[115] M. S. Azad and J. J. Trivedi, "Injectivity Behavior of Copolymer and Associative Polymers Decoded Using Extensional Viscosity Characterization: Effect of Hydrophobic Association," *SPE Western Regional Meeting*. p. D031S006R004, Apr. 23, 2017, doi: 10.2118/185668-MS.

[116] M. Azad and J. Trivedi, *Does Polymer's Viscoelasticity Influence Heavy Oil Sweep Efficiency and Injectivity at 1ft/Day?* 2018.

[117] M. Azad and J. Trivedi, "Novel Viscoelastic Model for Predicting the Synthetic Polymer's Viscoelastic Behavior in Porous Media using Direct Extensional Rheological Measurements," *Fuel*, vol. 235, Jul. 2018, doi: 10.1016/j.fuel.2018.06.030.

[118] M. Erincik, P. Qi, M. Balhoff, and G. Pope, "New Method To Reduce Residual Oil Saturation by Polymer Flooding," *SPE J.*, vol. 23, Jun. 2018, doi: 10.2118/187230-PA.

[119] G. McKinley, "Visco-Elasto-Capillary Thinning and Break-Up of Complex Fluids," *Rheol. Rev.*, vol. 3, Jun. 2005.

[120] D. W. Bousfield, R. Keunings, G. Marrucci, and M. M. Denn, "Nonlinear analysis of the surface tension driven breakup of viscoelastic filaments," *J. Nonnewton. Fluid Mech.*, vol. 21, no. 1, pp. 79–97, 1986, doi: https://doi.org/10.1016/0377-0257(86)80064-7.

[121] V. M. Entov and E. J. Hinch, "Effect of a spectrum of relaxation times on the capillary thinning of a filament of elastic liquid," *J. Nonnewton. Fluid Mech.*, vol. 72, no. 1, pp. 31–53, 1997, doi: https://doi.org/10.1016/S0377-0257(97)00022-0.

[122] A. Rozhkov, "Dynamics and Breakup of Viscoelastic Liquids (A Review)," *Fluid Dyn.*, vol. 40, Nov. 2005, doi: 10.1007/s10697-006-0001-7.

[123] M. Azad, V. Patel, N. Shah, T. Sharma, and J. Trivedi, "Extensional Rheological Measurements of Surfactant–Polymer Mixtures," *ACS Omega*, vol. 5, pp. 30787–30798, Dec. 2020, doi: 10.1021/acsomega.0c00481.

[124] C. Zhong, W. Wang, and M. Yang, "Synthesis and solution properties of an associative polymer with excellent salt-thickening," *J. Appl. Polym. Sci.*, vol. 125, Sep. 2012, doi: 10.1002/app.36743.

[125] E. K. Perttamo, “Characterization of Associating Polymer (AP) Solutions. Influences on flow behavior by the degree of hydrophobicity and salinity,” 2013.

[126] A. LøbøViken, T. Skauge, and K. Spildo, “Rheological properties of a hydrophobically modified anionic polymer: Effect of varying salinity and amount of hydrophobic moieties,” *J. Appl. Polym. Sci.*, vol. 133, 2016.

[127] A. Zell, S. Gier, S. Rafaï, and C. Wagner, “Is there a relation between the relaxation time measured in CaBER experiments and the first normal stress coefficient?,” *J. Nonnewton. Fluid Mech.*, vol. 165, no. 19, pp. 1265–1274, 2010, doi: https://doi.org/10.1016/j.jnnfm.2010.06.010.

[128] A. Thomas, N. Gaillard, and C. Favero, “Some Key Features to Consider When Studying Acrylamide-Based Polymers for Chemical Enhanced Oil Recovery,” *Oil Gas Sci. Technol.*, vol. 67, pp. 887–902, Nov. 2013, doi: 10.2516/ogst/2012065.

[129] C. Clasen *et al.*, “How Dilute are Dilute Solutions in Extensional Flows?,” *J. Rheol. (N. Y. N. Y).*, vol. 50, pp. 849–881, Jun. 2013, doi: 10.1122/1.2357595.

[130] J. Ferguson, K. Walters, and C. Wolff, “Shear and extensional flow of polyacrylamide solutions,” *Rheol. Acta*, vol. 29, no. 6, pp. 571–579, 1990, doi: 10.1007/BF01329303.

[131] C. Stoltz, J. J. de Pablo, and M. D. Graham, “Concentration dependence of shear and extensional rheology of polymer solutions: Brownian dynamics simulations,” *J. Rheol. (N. Y. N. Y).*, vol. 50, no. 2, pp. 137–167, Feb. 2006, doi: 10.1122/1.2167468.

[132] V. Sharma *et al.*, “The rheology of aqueous solutions of ethyl hydroxy-ethyl cellulose (EHEC) and its hydrophobically modified analogue (hmEHEC): extensional flow response in capillary break-up, jetting (ROJER) and in a cross-slot extensional rheometer,” *Soft Matter*, vol. 11, no. 16, pp. 3251–3270, 2015, doi: 10.1039/C4SM01661K.

[133] J. C. Kennedy, J. Meadows, and P. A. Williams, “Shear and extensional viscosity characteristics of a series of hydrophobically associating polyelectrolytes,” *J. Chem. Soc. Faraday Trans.*, vol. 91, no. 5, pp. 911–916, 1995, doi: 10.1039/FT9959100911.

[134] C. Bria, F. Violleau, and S. Williams, “Field-Flow Fractionation for Biological, Natural, and Synthetic Polymers: Recent Advances and Trends,” *LC GC Eur.*, vol. 26, pp. 660–671, Dec. 2013.

[135] S. Rellegadla, G. Prajapat, and A. Agrawal, “Polymers for enhanced oil recovery: fundamentals and selection criteria,” *Appl. Microbiol. Biotechnol.*, vol. 101, no. 11, pp. 4387–4402, 2017, doi: 10.1007/s00253-017-8307-4.

[136] A. Anand, H. Al Sulaimani, O. Riyami, and A. AlKindi, “Success and Challenges in Ongoing Field Scale Polymer Flood in Sultanate of Oman - A Holistic Reservoir Simulation Case Study for Polymer Flood Performance Analysis & Prediction,” *SPE EOR Conference at Oil and Gas West Asia*. p. D021S014R002, Mar. 26, 2018, doi: 10.2118/190431-MS.

[137] E. Delamaide, “Is Chemical EOR Finally Coming of Age?,” *SPE Asia Pacific Oil & Gas*

Conference and Exhibition. p. D033S025R002, Nov. 17, 2020, doi: 10.2118/202276-MS.

[138] J. Sheng, *Enhanced oil recovery field case studies*. Gulf Professional Publishing, 2013.

[139] J. J. Sheng, B. Leonhardt, and N. Azri, "Status of polymer-flooding technology," *J. Can. Pet. Technol.*, vol. 54, no. 02, pp. 116–126, 2015.

[140] W. Demin, W. Gang, and X. Huifen, "Large Scale High Viscous-Elastic Fluid Flooding in the Field Achieves High Recoveries," *SPE Enhanced Oil Recovery Conference*. p. SPE-144294-MS, Jul. 19, 2011, doi: 10.2118/144294-MS.

[141] D. Wang, G. Wang, W. Wu, H. Xia, and H. Yin, "The Influence of Viscoelasticity on Displacement Efficiency—From Micro- to Macroscale," *SPE Annual Technical Conference and Exhibition*. p. SPE-109016-MS, Nov. 11, 2007, doi: 10.2118/109016-MS.

[142] D. Wang, P. Han, Z. Shao, J. Chen, and R. S. Seright, "Sweep Improvement Options for the Daqing Oil Field," *SPE/DOE Symposium on Improved Oil Recovery*. p. SPE-99441-MS, Apr. 22, 2006, doi: 10.2118/99441-MS.

[143] D. Wang, H. Xia, Z. Liu, and Q. Yang, "Study of the Mechanism of Polymer Solution With Visco-Elastic Behavior Increasing Microscopic Oil Displacement Efficiency and the Forming of Steady 'Oil Thread' Flow Channels," *SPE Asia Pacific Oil and Gas Conference and Exhibition*. p. SPE-68723-MS, Apr. 17, 2001, doi: 10.2118/68723-MS.

[144] Y. K. Dalsania, "Characterization of Oilfield High Molar Mass Polymers Under Different pH and Mono-Di Valent Ion Environment Using Asymmetrical Flow Fluid Flow Fractionation," University of Alberta, 2017.

[145] B. Najafiazar *et al.*, "Polymer Gels Made with Functionalized Organo-Silica Nanomaterials for Conformance Control," *Energies*, vol. 12, p. 3758, Sep. 2019, doi: 10.3390/en12193758.

[146] A. Løbø Viken, T. Skauge, and K. Spildo, "Rheological properties of a hydrophobically modified anionic polymer: Effect of varying salinity and amount of hydrophobic moieties," *J. Appl. Polym. Sci.*, vol. 133, no. 23, Jun. 2016, doi: https://doi.org/10.1002/app.43520.

[147] D. N. Schulz and J. Bock, "Synthesis and Fluid Properties of Associating Polymer Systems," *J. Macromol. Sci. Part A - Chem.*, vol. 28, no. 11–12, pp. 1235–1243, Nov. 1991, doi: 10.1080/00222339108054096.

[148] C. Ligoure and L. Leibler, "Thermodynamics and kinetics of grafting end-functionalized polymers to an interface," *J. Phys.*, vol. 51, no. 12, pp. 1313–1328, 1990.

[149] P. G. de Gennes, "Polymers at an interface; a simplified view," *Adv. Colloid Interface Sci.*, vol. 27, no. 3, pp. 189–209, 1987, doi: https://doi.org/10.1016/0001-8686(87)85003-0.